FACULTY OF ENGINEERING AND THE BUILT ENVIRONMENT
School of Chemical and Metallurgical Engineering

Characterizing flotation processes of Platreef PGM ores: The applicability of models based on the Weibull and γ rate constant distributions.

by

SITHANDOKUHLE FORTUNE NGEMA

A dissertation submitted to the faculty of Engineering and the Built Environment University of Witwatersrand, Johannesburg, in fulfilment of the requirements for the degree of Master of Science in Engineering

Supervisor - Prof Vusumuzi Sibanda
Co-Supervisor - Dr Mehdi Safari

June 2024

DECLARATION

I declare that the research project is my own work and that each source of information used has been acknowledged by means of a complete reference. This thesis has not been submitted before for any other research project, degree or examination at any university.

Sithandokuhle Ngema

……
(Signature of the student)

…… 27 June 2024……
(Date)

……Midrand……., South Africa
(Signed at)

ACKNOWLEDGEMENTS

I would like to express my sincerest appreciation to the following individuals/organizations:

Firstly, to my supervisor, Prof Vusumuzi Sibanda, for providing me with patience, encouragement, guidance, and unwavering support throughout my research. Your invaluable insights and helpful suggestions were instrumental in the success of this project.

Secondly, to Dr Mehdi Safari for overseeing the laboratory and technical research work. Your assistance in understanding technical report writing was highly appreciated.

I am also grateful to Mintek for the financial support and equipment provided for my research. I extend my thanks to Senmin (Pty) Ltd and Chemquest (Pty) Ltd for supplying the necessary reagents and to Anglo American Platinum for the ore material used in this study.

Last but not least, to my mother Ngenzeni Ngema, I cannot express my gratitude enough for your unwavering support and encouragement throughout my studies.

LIST OF PUBLICATIONS AND PRESENTATIONS

Ngema, S. F., Sibanda, V., & Safari, M., 2023. Characterizing flotation processes of Platreef PGM ores- The applicability of models based on the Weibull and γ rate constant distributions: Flotation 23' Poster Presentation

Ngema, S. F., Sibanda, V., & Safari, M., 2024. Characterizing flotation processes of Platreef PGM ores- The applicability of models based on the Weibull and γ rate constant distributions: A review. Journal of Metallurgy

ABSTRACT

This dissertation delves into a comprehensive examination of the flotation behaviour of Platreef Platinum Group Metal ores, with a specific focus on the applicability of two widely used distribution models, the Weibull and Gamma distributions. The primary objective of this study was to demonstrate the effectiveness of these models in characterizing the flotation response of the ore under varying grind sizes, ranging from 80% passing 150 µm down to 38 µm, and under varying collector dosages.

In this research, a series of meticulous experiments that involved the collection of samples from Platreef PGM ore were conducted. These samples were characterized based on their mineralogical composition, and their flotation behaviour across specified particle size distributions and varying collector dosages. The gathered data were then subjected to analysis using the Weibull and Gamma models. This allowed the assessment of the flotation performance of the ore and the description of the intricate flotation sub-processes involved to be possible. The parameters for both the Weibull and Gamma distributions were determined through a rigorous statistical method known as regression. This method involved fitting the experimental data to the models and iteratively adjusting the model parameters until convergence to their most accurate estimates was achieved.

The results from the research reveal that both the Weibull and Gamma models demonstrate a commendable ability to describe the flotation process of Platreef PGM ores. However, the study also highlights certain limitations of these models, especially when dealing with coarser grind sizes, where the Weibull model shows a slight decrease in effectiveness. The investigation also points to the significant impact of liberation and grinding time on the accuracy of these models. These findings underscore the importance of understanding the nuances of particle interactions and liberation at different grind sizes in floatation processes.

Furthermore, the effect of varying collector dosages on the performance of the models was explored. It was observed that the accuracy of the models diminishes with longer residence times, particularly when collector dosages are changed. This sensitivity to longer residence times and grind characteristics underscores the need for a holistic approach to model development. Another intriguing aspect of the study was the relationship between collector dosage and grind characteristics. It became apparent that increasing collector dosage has a more

pronounced positive effect on recoveries for both coarser and finer grinds, while the intermediate grinds exhibit a less substantial improvement. This discovery challenges the convention of a near-linear relationship between collector dosage and recovery.

In conclusion, the research provides valuable insights into the complexities of the flotation process for Platreef PGM ores and underscores the significance of selecting the most appropriate distribution models based on specific ore characteristics and grind sizes. The dissertation also highlights the need for a nuanced approach to process optimization, acknowledging the interplay of factors such as liberation, grind characteristics, and collector dosage. This understanding can be applied to enhance recovery rates and efficiency in flotation processes, offering valuable contributions to the field of mineral processing and chemical engineering. Findings of this work shed light on the intricate nature of chemical processes, emphasizing the importance of a holistic approach to model development and practical applications.

1. TABLE OF CONTENTS

LIST OF FIGURES

List of Tables

List of Equations

Nomenclature

x_C	Concentrate mass fraction
x_F	Feed mass fraction
F_C	Concentrate flowrate
F_F	Feed flowrate
R	Recovery
ER	Enrichment ratio
w_R	Mass recovery
$\gamma_{s/a}$	Adhesion forces between solid-air interfaces
$\gamma_{s/w}$	Adhesion forces between solid-water interfaces
$\gamma_{w/a}$	Adhesion forces between solid-air interfaces
θ	Contact angle formed due to adhesion forces
t	Corresponds to the flotation time
k	Rate constant for the flotation process
C	Mineral concentration at a specific time
C_∞	Concentration at equilibrium (or at $t \rightarrow \infty$).
$R(t)$	Flotation recovery as a function of time
R_∞	Maximum achievable recovery
n	Reaction order
E_K	Collection efficiency

E_C	Collision efficiency
E_A	Adhesion efficiency
E_S	Stability factor
P_C	Probability of collision
P_A	Probability of adhesion
F_S	Stability factor
θ^*	Parameter describing detachment processes
v	Relative velocity of bubbles to particles
λ	Particle-bubble adhesion induction period
R_B	Bubble radius
r_P	Particle radius
N_O	Initial particle concentration per unit volume of pulp
n'	Bubble concentration per unit volume of pulp
ρ_S	Particle density
$\zeta(\lambda)$	Density function
φ	Particle size constant
β	Gas dispersion constant
$f(k)$	Flotation rate distribution or a variety of rate constants
δ	Delta function
w_i	Weights that determine the contribution of each delta function to the overall sum

$\xi(t)$	Residence time distribution
α	Gamma shape parameter
β	Gamma scale parameter
Γ	Gamma normalization constant
n	Weibull shape parameter
k_m	Weibull scale paramter
$\mathcal{L}[f\ (k)]$:	Laplace Transform of the flotation rate distribution

1. INTRODUCTION

The introduction section for this work will provide an overview of several key aspects related to Platinum Group Metals (PGMs) mining and processing. It starts by introducing PGMs and their importance in modern industries such as automotive, electronic, and chemical industries. It then discusses the significant role played by South Africa in the world's PGMs supply chain, particularly from the Bushveld Igneous Complex. The section also highlights the challenges faced in mining and processing PGMs, including the complex nature of PGM reefs, the presence of other minerals, and the need for sustainable and efficient extraction methods. The introduction further emphasizes the importance of mineral processing in extracting PGMs and other valuable minerals from ore. The problem statement and research questions are also included in this section, followed by research objectives and the layout of the dissertation. Overall, the introduction serves as an essential background to the study, laying out the context and setting the stage for the subsequent sections.

1.1. Background

PGMs i.e. Platinum, Palladium, Rhodium, Ruthenium, Iridium and Osmium are highly valued in various industries because of their unique properties. They are used in numerous industrial applications, including the manufacture of catalytic converters that decrease vehicle emissions and in chemical production. PGMs are also vital in the manufacture of hydrogen fuel cells, which generate sustainable energy. In addition, PGMs are frequently used to manufacture jewellery, especially platinum, which is favoured because of its durability and rarity. As a major source of revenue for many countries, PGMs provide job opportunities and economic growth. Due to the ability to retain their value over time, PGMs, specifically platinum and palladium, are also well-known investment assets and act as a hedge against inflation (Jones, 2005). In total, there are six elements which occur as PGMs, i.e platinum (Pt), palladium (Pd), rhodium (Rh), ruthenium (Ru), iridium (Ir), and osmium (Os). They exist together with other metals such as gold (Au), nickel (Ni), cobalt (Co), and copper (Cu).

The Bushveld Igneous Complex (BIC) located in South Africa hosts the world's largest known deposit of PGMs and chrome. The BIC is a large layered mafic to ultramafic igneous intrusion, and is approximately 2 billion years old and covers an area of over 66,000 square kilometres, see Figure 1.1. It is divided into several different zones or “reefs”, namely, the Merensky Reef, the UG2 chromitite reef, and the Platreef. These zones are characterized by their distinct geology and mineralization, with the Merensky Reef being the most economically significant.

The Merensky Reef is a thin layer of sulfide-rich rock that contains the highest grades of PGMs and is the primary source of PGMs in the BIC. South Africa is the largest producer of PGMs in the world, and the BIC accounts for over 70% of the country's PGM production and 40% of the world's palladium (Kraemer, et al., 2017).

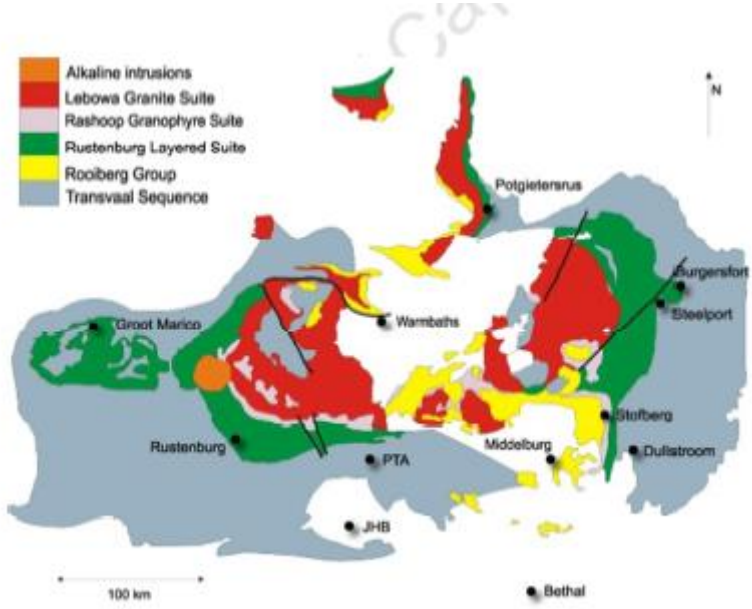

Figure 1.1: The Bushveld Igneous Complex (University of Witwatersrand, School of Geosciences, 2009).

The UG2 reef exhibits a PGM content similar to that of the Merensky, however with a notable presence of chromite, alongside lower levels of nickel and copper. Conversely, the Platreef showcases diminished PGM values but boasts abundance in palladium and base metals. Pure PGM ores, typically rich in sulphides, demonstrate concentrations ranging from 3 to 10 ppm. Comminution processes are employed to liberate Base Metal Sulphide (BMS) grains associated with PGM minerals, succeeded by froth flotation to separate liberated sulphide mineral and PGM grains from unwanted gangue minerals (Crundwell et al., 2011). The resultant concentrate from froth flotation typically holds a PGM content of about 70 to 100 ppm, comprising BMS minerals like pyrrhotite, pentlandite, and chalcopyrite, with over 85% Pt recovery. The efficacy of froth flotation in processing pristine PGM ores is attributed to the strong association between BMS and PGM minerals in the pristine ores, with the sulphide minerals being readily floatable (Oberthur et al., 2013; Kraemer et al., 2017).

Interest in near-surface or open-pit non-sulphide PGM ores has surged due to the rapid depletion of pristine PGM ores and escalating mining costs linked to deeper-level mining. Nonetheless, endeavours to process such ores have yielded inconsistent results, with flotation stages consistently delivering recoveries lower than 50%, exemplified by the experiences at the Hartley mine (1997-1999) and Old Wedza mine (1926-1928) (Oberthur et al., 2013; Vermaak, 2005). Efforts to process non-sulphide PGM ores at the Impala Platinum mine in the western Bushveld, the Pilanesburg Platinum Mine (PPM), and Bushveld Complex UG2 Reef at Smokey Hills mine, have been made, but conventional metallurgical processes have consistently resulted in low recoveries across all instances (Becker et al., 2014; Oberthur et al., 2013).

The Platreef layer has garnered significant attention, yet it also presents several challenges as the ore is typically mined underground and is processed using conventional flotation techniques to recover the valuable metals. One of the main difficulties in flotation of Platreef ore is its complex mineralogy. The ore contains a variety of minerals, including pyroxenes, amphiboles, feldspars, apatite, and various sulphide minerals. This complex mineralogy can make it challenging to separate the valuable minerals from the gangue minerals, which can negatively impact the overall recovery of the ore. Another challenge in processing Platreef ore is the presence of talc, which can interfere with the flotation process. Talc is a naturally occurring mineral that is often found in association with the PGMs in the ore. Talc can adsorb onto the surface of the PGM minerals, preventing them from being recovered in the flotation process. As a result, it is important to carefully control the addition of talc depressants during flotation to ensure optimal recovery of the PGM minerals.

In minerals processing, the kinetics of flotation are often studied for various purposes, such as scaling up metallurgical results, investigating the effects of different operational parameters, and simulating flotation processes to determine the maximum achievable recoveries and grades. A first-order model, originally introduced by Garcia-Zuniga in 1935, is commonly employed for batch-scale flotation kinetics characterization. This model represents the cumulative recovery (R) as a function of flotation time (t) and the flotation rate constant (k), with the maximum recovery achievable (R_∞) as t approaches infinity. It is widely recognized that the heterogeneous responses of flotation by size, ore composition or liberation, and ore association justify the distributed nature of flotation rate constants (Trahar, 1981; Morris, 1952; Sutherland, 1989). As a result, fractionation of solids or particles based on a physical property,

such as particle size, has become a common method for characterizing each fraction or class with a single rate constant (Runge et al, 2003).

In minerals processing, the kinetics of flotation are commonly modelled using rate constant distributions. Two commonly used rate constant distributions are the Gamma and the Weibull distributions. The Gamma distribution is a two-parameter distribution that is often used to describe flotation rate constant data for a single particle size or size fraction. The parameters of the Gamma distribution are the shape parameter, α, and the scale parameter, β. The shape parameter controls the shape of the distribution, while the scale parameter controls the location and spread of the distribution. The Weibull distribution is a three-parameter distribution that can describe the flotation rate constants for multiple particle sizes or size fractions. The parameters of the Weibull distribution are the shape parameter, n, the scale parameter, k_m, and the location parameter, δ. The shape parameter controls the shape of the distribution, the scale parameter controls the location of the distribution, and the location parameter controls the shift of the distribution.

Extensive literature on flotation kinetics studies, using various commodities, analysis tools, and flotation techniques has been reported in the minerals processing field (Polat and Chander, 2000; Trahar, 1981; Jameson, 2012; Morris, 1952). Nonetheless, there has been limited extensive reporting on the utilization of size-by-size flotation kinetics employing the Weibull and Gamma rate distributions to characterize Platreef ores. The complex nature of Platreef ores, with their irregular microscopic distribution of palladium (Pd) nuggets or grains, presents challenges in product grade and recovery variability during chemical analysis of sub-samples, which can be influenced by the presence of Pd nuggets. Despite these challenges, this study aims to demonstrate that the Weibull and Gamma models provide good fits to time-recovery and grade-recovery curves, estimate flotation rate constant distributions for different particle sizes, and illustrate how the Weibull and Gamma model parameters change with particle size.

1.2. Problem Statement and Research Questions

Conventional methods and reagent regimes face challenges in processing Platreef PGM ores, often resulting in inadequate flotation recoveries of less than 50%. Various factors contribute to this poor response, as highlighted by different researchers. These factors include high contents of naturally floating gangue, such as talc, poor association of BMS with PGMs, and the remobilization of Pd, leading to alterations in the Pt:Pd ratio (Becker et al., 2014; Bulatovic, 2003; Kraemer et al., 2017). Moreover, the intricate nature of Platreef ores, characterized by irregular microscopic distribution of Pd nuggets or grains, poses challenges in maintaining consistent product grade and recovery during analysis and modelling.

This study aims to demonstrate that, despite the complex nature of Platreef ores, it is possible to estimate the flotation rate constant distributions at various particle sizes and collector dosages by fitting the Weibull and Gamma models to the time-recovery curves. Furthermore, the study aims to show how particle size and collector dosages regimes affects the model parameters for each model.

The following research questions were explored in this study:

i. What is the bulk modal mineralogical composition of the Platreef PGM ore?

ii. Which statistical methodology can be used to find the parameters of the Weibull and Gamma models?

iii. What are the optimum particle size and collector dosage, based on the highest recovery?

iv. How does particle size and varying collector dosages influence the model parameters?

1.3. Research Aim

To demonstrate that the Gamma and Weibull models can be used to estimate the flotation rate constant distributions at different particle sizes and collector dosages, despite the complex nature of Platreef ores.

1.4. Research Objectives

The study has the following specific research objectives;

- Conduct chemical and mineralogical analysis of Platreef ore: To gain a better understanding of this PGM ore's complex nature.
- Perform rougher flotation rate experiments: Collect data needed for flotation rate constants estimation.
- Perform numerical integration to evaluate $R(t)$ for the Gamma model: Assess the time-recovery relationship using the Gamma model.
- Fit Gamma and Weibull models to time-recovery curves: Estimate rate distributions at different particle sizes and collector dosages.
- Determine the effect of particle size and collector dosages on the Gamma and Weibull model parameters: Analyse how particle size and varying collector dosages influences the model parameters.

1.5. Dissertation Layout

The dissertation is structured into five chapters. Chapter 1 offers a background of the research problem and delineates the study objectives. Chapter 2 constitutes the literature review, commencing with an examination of comminution and the fundamental froth flotation principles. It delves into previous research on processing complex PGM ores using froth flotation and hydrometallurgical processing routes, while also discussing flotation rate constant distribution models.

Chapter 3 elaborates on the methods employed for sample preparation, the analytical techniques utilized for ore material characterization, and the experimental design adopted for conducting the experiments. Chapter 4 presents the results and discussion pertaining to the impact of particle size on the Weilbull and γ model parameters, drawing from the rougher flotation experiments. This section encompasses statistical analysis, optimization studies, and kinetic studies.

Finally, Chapter 5 concludes the dissertation and furnishes recommendations based on the research findings.

2. LITERATURE REVIEW

The literature review section of this dissertation will provide a comprehensive overview of the relevant research related to froth flotation. The section is organized into several key subsections, each covering specific topics related to the subject matter. The comminution subsection discusses the critical role of comminution in PGMs processing and describes the method essential for reducing ore size. The subsection of principles of froth flotation provides an in-depth explanation of the froth flotation process and the basic principles behind it. The mechanical factors subsection highlights the different mechanical factors that influence flotation, such as the hydrodynamics and turbulence. The kinetics of flotation subsection delves into the mathematical models used to describe the rate and efficiency of flotation, including the first-order, second-order, and mixed-order kinetics models. Finally, the $f(k)$ flotation model structures subsection explores the different models developed to define the complex interactions between the various factors involved in flotation. Overall, the literature review section provides a detailed and comprehensive overview of the existing research on froth flotation, serving as a foundation for the subsequent sections of this work.

2.1. Comminution

The application of metal production processes is widespread. Metals are often found in two forms: as native elements, such as copper, or as minerals found in ore in the Earth's crust. The mined ore is a mix of rich minerals such as galena and chalcopyrite e.t.c, as well as gangue minerals like silica and calcium carbonate. Metals can be extracted from these ores using two methods: pyrometallurgical and hydrometallurgical approaches. Yet, due to the high leaching agent consumption of gangue materials during metal leaching in the hydrometallurgical processes and the high energy required to smelt both metals and gangue materials in the pyrometallurgical processes, reducing the amount of gangue materials in the ore is economically essential. As a result, the ore must be concentrated prior to undergoing chemical extraction methods.

The technology in mineral processing or concentration involves two distinct types of processes, namely liberation and separation. The primary objective in mineral processing is to produce a concentrate that contains the majority of the valuable minerals (Weimeng Hu, 2014). Adequate liberation is a crucial prerequisite for a successful mineral beneficiation operation. When the degree of liberation is inadequate, the mineral particles must be broken down into smaller fragments to improve the liberation. This is accomplished via the comminution or size

reduction process. Comminution in mineral beneficiation generally has two primary goals. The first goal is liberation, which is the procedure used to break up composite minerals in the raw ore into independent particles to allow collection of the desired components. The ore from the mine undergoes a series of crushing processes in order to achieve better liberation of the valuable minerals, as depicted in Figure 2.1, and to obtain appropriate sizes for subsequent downstream processes.

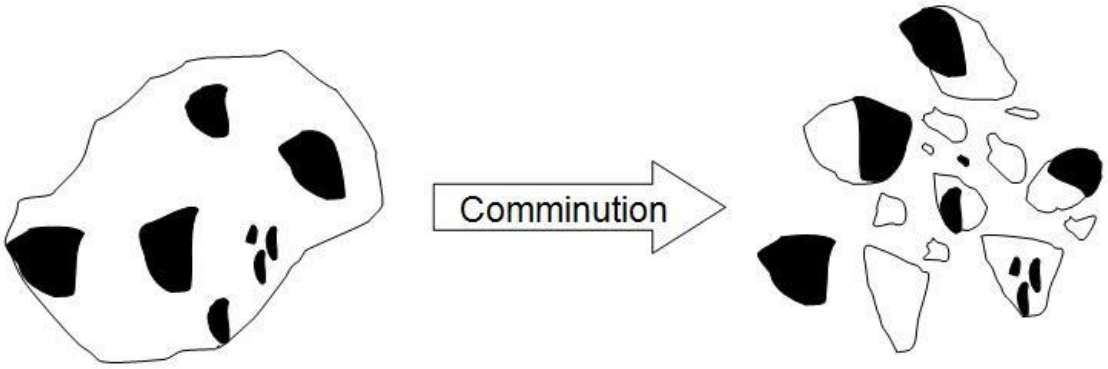

Figure 2.1: Comminution process: The shaded surface area in the figure (Weimeng, 2014) represents the valuable mineral particles after the ore has been crushed into smaller particles.

The secondary goal of comminution is altering the size of mineral particles to fit the size requirements of the subsequent separation process. After crushing, the ore is combined with water to make a pulp, which is subsequently milled to achieve a specified Particle Size Distribution (PSD), such as minus 100µm. The ideal size distribution for flotation is pre-defined to enable a suitable separation process, for example, 80% of the milled ore should be finer than a specified size. This can be accomplished through the introduction of classification techniques such as hydro-cyclones or a succession of screens.

2.2. Principles of Froth Flotation

In the mineral processing industry, froth flotation is the most commonly employed method for mineral beneficiation, which is vital for the recovery of valuable minerals like gold, platinum, copper, and other base metals. The flotation preparation phase involves comminution, wherein the mined ore is pulverized in the vicinity of water, forming a slurry containing ore particles with a suitable size distribution to effectively liberate the valuable minerals. Flotation is a sub-process of mineral recovery that utilizes the hydrophobic or hydrophilic properties of particles to separate the desired minerals from unwanted materials. Hydrophobic particles attach to air bubbles and coalesce into particle-bubble aggregates that rise to the froth layer, whereas the hydrophilic particles stay in the pulp zone, as illustrated in Figure 2.2;

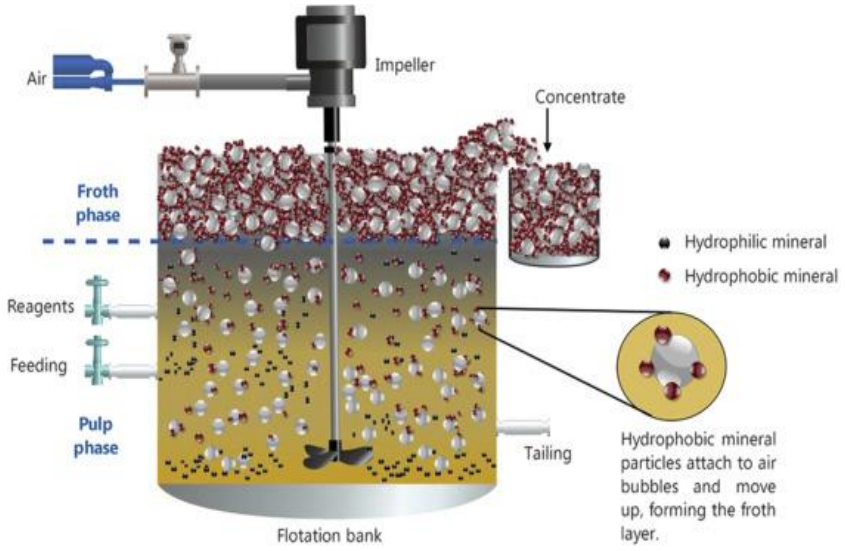

Figure 2.2: Schematic diagram depicting the froth flotation process in a mechanical flotation cell (Li et al., 2019).

The overall efficiency of the flotation process is influenced by several internal parameters, including mineral liberation, PSD, pulp viscosity, pulp density, chemical environment, bubble size distribution (BSD), turbulence level, froth stability, and froth transport distances. Macroscopically, the efficiency is assessed by the recovery R, defined as the ratio of a component's flow into the concentrate to its flow in the feed. The recovery of a mineral or metal in a flotation system is mathematically described by Equation 2.2.1.

$$\mathrm{R} = \frac{\mathrm{x_C\ F_C}}{\mathrm{x_F\ F_F}} = \mathrm{ER} \cdot \mathrm{w_R} \qquad \text{(Equation 2.2.1)}$$

whereby,

- x_C represents the concentrate grade,
- x_F represents the feed grade,
- F_C and F_F indicate the total solid flow rates in the concentrate and feed, respectively.
- $ER = x_C/x_F$ is the enrichment ratio and $w_R = F_C/F_F$ is the mass recovery or mass yield.

In froth flotation, the two main areas of focus for the recovery and upgrading of PGMs are:

1. Pulp phase
2. Froth phase

2.2.1 Pulp Phase

According to Wiese et al. (2011) and Bradshaw et al. (2005), the primary aim of the pulp phase is to extract valuable minerals by establishing a physicochemical setting conducive to effective bubble-particle collision, attachment of hydrophobic particles, and subsequent transportation of these particles to the froth phase. This phase comprises two sub-processes:

- Bubble-particle collision and attachment and
- Transportation of attached particles to the froth phase.

To ensure selective attachment of PGMs to air bubbles, it is essential to have favourable chemical and hydrodynamic conditions. As observed by Van der Westhuizen and Deglon (2007), chemical conditions facilitate particle aggregation, while hydrodynamic conditions support optimal suspension of solids within the pulp. This is accomplished by introducing reagents into the pulp that can alter the mineral surface properties or modify the slurry characteristics, as outlined in Fuerstenau et al. (2007). The reagent chemicals are typically classified into three categories: collectors, frothers and modifiers (such as depressants, regulators, and activators), each with a specific effect on the behaviour of a particular mineral or the slurry properties.

2.2.1.1 Collectors

Wills and Napier-Munn (2005) state that chemicals known as collectors react with the surfaces of valuable minerals to give them a water-resistant coating. Ionizing compounds, which completely dissolve in water, and non-ionizing compounds, which do not dissolve in water, can be used to categorize these collectors. The collector and the mineral surface can connect chemically or physically, and the process usually takes some time. When the concentration of the collector in the solution drops, it will separate from the mineral surface in cases of weak and reversible bonding. As indicated by Jan (1982), Crozier (1992) characterizes irreversible bonding as restricted to particular active spots on the mineral surface, such as kinks, ledges, dislocations, and lattice defects.

Collectors include both non-polar and polar groups, as seen in Figure 2.3. According to Lotter and Bradshaw (2010), the non-polar groups repel water and interact with the mineral surface to form a hydrophobic surface.

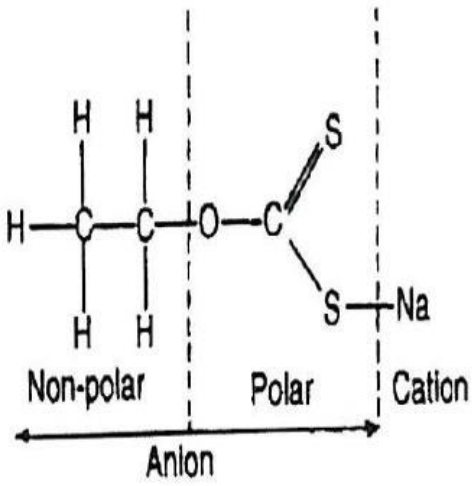

Figure 2.3: The collector known as sodium ethyl xanthate's composition as described by Wills and Napier-Munn (2005).

Lotter and Bradshaw (2010) claim that sulfide minerals can provide or receive electrons in an electrochemically active environment, exhibiting semi-conductor characteristics. As previously indicated, collectors cling to the solid surface through their polar groups, which can create chemical, physical, or electrical interactions. The collector's non-polar group faces the solution, which enables it to form a hydrophobic surface on the mineral (Wills and Napier-Munn, 2005).

Anionic collectors, which are categorized as oxyhydral or sulphyhydral depending on the structure of their polar group, are frequently employed in mineral flotation (Wills and Napier-Munn, 2005). Sodium Isobutyl Xanthate (SIBX) is one of the most widely used thiol collectors and is essential for the flotation of sulphide minerals. Since thiol collectors have bivalent sulfur in their molecular structure, they are by nature sulphyhydral. The non-polar hydrocarbon group "R," which includes hydrocarbon groups with carbon atom counts ranging from one to six, is responsible for the names of these xanthates, including ethyl, isopropyl, isobutyl, and hexyl (Wills and Napier-Munn, 2005).

According to Lotter and Bradshaw (2010), the length of the "R" group affects the collector's behavior, with the collector's stability growing as the chain lengthens. Additionally, as the chain lengthens, less collector concentration is needed for efficient flotation. Lotter and Bradshaw (2010) state that the length of the "R" groups determines how collector molecules are oriented on the mineral surface, with longer chains being positioned horizontally and shorter chains perpendicular to the surface.

2.2.1.2 Frothers

Frothers are heterophilic surface active reagents that can be distinguished based on their solubility in water, as noted by Wills and Napier-Munn (2005) and Crozier (1992). One category consists of low solubility frothers, such as alkoxy paraffins, natural oils, and aliphatic alcohols. The other category consists of frothers that are completely soluble in water, such as polyglycol and polyglycerol ethers. According to Crozier (1992), these glycols can create "compact, long-lasting froths" that quickly dissipate upon agitation. Compared to the frothers that have low solubility in water, glycols are capable of producing more selective froths.

A few examples of the molar weights of the frothers manufactured by The Dow Chemical Co. are Dowfroth 200 (DOW200), which has a molar weight of 206 g/mol (Crowier, 1992). As noted by Wills and Napier-Munn (2005), these polyglycol frothers are well known for their durability and effectiveness in handling bigger particles and high-grade feed materials. Wills and Napier-Munn (2005) underline that a high-performing frother must not have any major collecting qualities. When frothers have characteristics similar to ionic collectors, they produce very stable froths that impede the appropriate movement of precious minerals and may even complicate processing. The ideal froth should be stable enough to transfer important minerals to the launder but quickly decompose thereafter. Frothers are essential to the flotation process because they help to selectively drain entrained gangue minerals from the pulp, stabilize the froth phase to some extent, and maintain bubble formation inside the pulp (Wills and Napier-Munn, 2005).

2.2.1.3 Depressants

According to Bradshaw et al. (2005), depressants work to reduce the recovery of particular gangue minerals that would otherwise be present in the concentrate in a selective manner. This is accomplished by making those particles hydrophilic, which prevents them from adhering to the surface of the air bubble and increases the process's overall selectivity. There are many different kinds of depressants, both organic and inorganic (Wills and Napier-Munn, 2005). A collector cannot preferentially adsorb onto the surface of the targeted valuable particle when two or more particles have qualities so comparable. In such cases, inorganic depressants such as sulfuric acid, zinc sulfate, and sodium cyanide are used. According to Crozier (1992), two frequently utilized inorganic depressants are lime and cyanide. In an alkaline environment, cyanide interacts with the majority of sulphide minerals to generate a persistent metal-cyanide layer that inhibits the precipitation of metal xanthate on the particle surface. Furthermore,

cyanide has the ability to remove a mineral's preexisting xanthate layer. But as noted by Wills and Napier-Munn (2005), cyanide is extremely poisonous and can dissolve gold and silver.

Natural sources of polysaccharides, such as starch, tannic acid, and glues, together with artificially generated polyglycols, are utilized to depress minerals that are inherently hydrophobic. Because polymeric organic depressants have fewer risks than some inorganic depressants, their use is becoming more and more common. Polymeric depressants that are frequently used in the PGM business in South Africa include modified guar gum (guar) and carboxymethyl cellulose (CMC) (Corin and Harris, 2010). The structural components for each kind of depressant are shown in Figure 2.4.

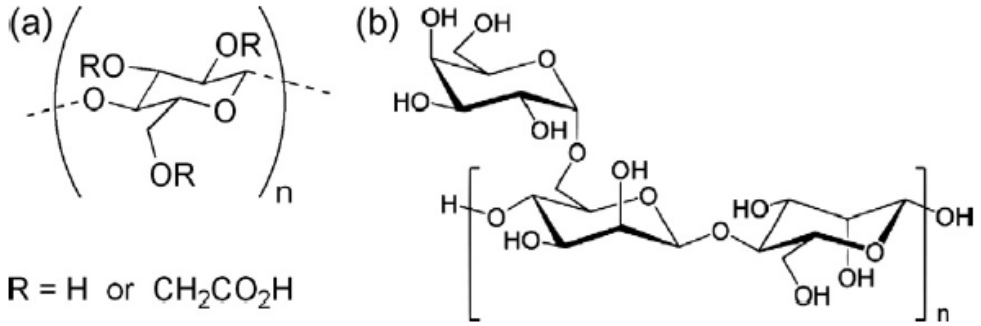

Figure 2.4: Structure of (a) carboxymethyl cellulose and (b) guar as denoted by (Corin and Harris, 2010)

According to Wills and Napier-Munn (2005), a particle's surface wettability, or hydrophobicity, is a critical factor in the adsorption of particles onto bubble surfaces. Furthermore, Muganda et al. (2011) clarified that the contact angle—which is determined on the liquid phase side—affects a particle's attachment to a bubble. The contact angle is the angle between the solid surface and the tangent to the liquid surface at the point where the three interfaces (solid, liquid, and air) meet, as described by Jan (1982). The interfacial tensions of the solid-air, solid-water, and water-air interfaces, as illustrated in Figure 2.5, determine the contact angle, as explained by Ives (1984). The magnitude of these tensions, represented as $\gamma_{s/a}$, $\gamma_{s/w}$, and $\gamma_{w/a}$, respectively, influences the adhesion forces between the bubble and the solid, solid and water, and lastly water and air, respectively. According to Wills and Napier-Munn (2005), hydrophobic particles produce higher contact angles than hydrophilic particles, resulting in their selective recovery in the froth phase while leaving behind the hydrophilic particles.

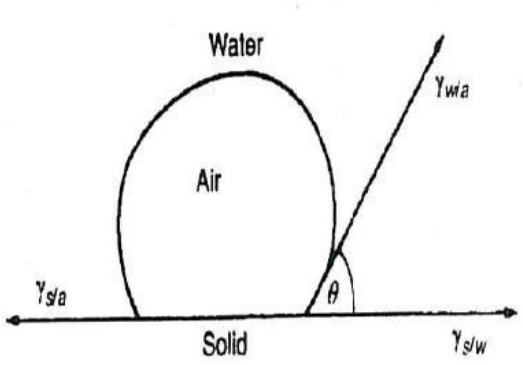

Figure 2.5: The contact angle formed between a bubble and a particle in a watery environment, as discussed in Wills and Napier-Munn's 2005 publication.

The force balance at equilibrium for the figure mentioned above is;

$$\gamma_{s/a} = \gamma_{s/w} + \gamma_{w/a} cos\theta \qquad \text{(Equation 2.2.2)}$$

Important mineral surfaces are chemically changed to become hydrophobic, which makes it easier for them to adhere to air bubbles and move to the froth phase's surface. It is a procedure called "true flotation," and it is the preferred way for pulp transport. However, non-selective phenomena such as entrainment and entrapment, which occur within and between the streamlines of rising bubbles, respectively, greatly increase the probability of recovering undesirable gangue and valuable minerals in the output concentrate. The 2005 publication by Wills and Napier-Munn discusses this information.

2.2.2 Froth Phase

According to Bradshaw et al. (2005), "upgrading of the valuable materials reporting to the concentrate without loss of valuable materials" is made possible in mainly by the froth phase. The film between bubbles thins as they move through the mineral-rich froth, causing coalescence and changes in the size and amount of water in the bubbles. The froth has varying heights at which these dynamics change. Rising bubble distortion is usually caused by a higher liquid percentage at the froth-pulp interface than in the top layers of the froth. Ata (2012) found that bubbles can start out spherical at the froth-pulp interface and change to polyhedral shapes at the froth's top layer.

Coalescence is more likely when water drains because the distance between bubble Plateau boundaries gets smaller. The viscosity of the liquid affects the pace of froth drainage; as Jan's 1982 study found, less viscous liquids allow the liquid layers surrounding the bubbles to drain more quickly.

2.2.1.1 Froth Drainage Mechanisms

Plateau boundaries are the curved areas that separate the thin films of bubbles from the bulk pulp, as Ives (1984) pointed out. According to Jan (1982), the liquid's mobility within the film and gravity drainage are the main causes of the liquid film's thinning. As noted by Crozier in 1992, these films can drain quickly or slowly, depending on the properties of the air-water contact. Figure 2.6 shows the boundaries of the Plateau.

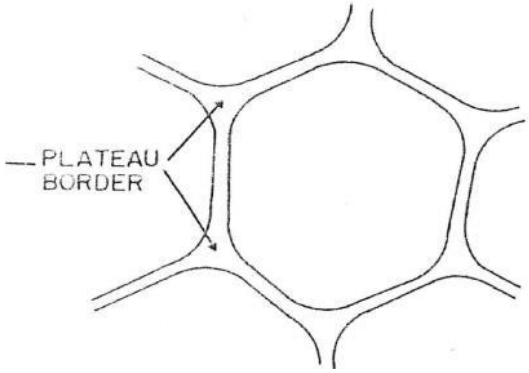

Figure 2.6: Plateau borders (Jan, 1982)

The processes of bubble coalescence, bursting, and froth overloading are crucial in the separation of hydrophobic particles that were initially attached to the bubbles. According to Ross's 1997 study, the wake of the bubbles can entrain some of these hydrophobic and gangue particles into the froth. Bubbles burst only at the surface of the froth layer. These broken particles could leak back into the pulp phase or reattach to additional ascending bubbles. With hydrophilic particles being less likely to re-attach than hydrophobic ones, it is thought that the amount of detached particles recovered in the froth phase is significantly higher than those recovered by rising bubbles in the pulp phase. Moreover, there is a considerable amount of entrained gangue minerals in the interstitial liquid that drains continually. Consequently, a well-drained froth enhances the overall selectivity of the flotation process, leading to a higher recovery of hydrophobic and valuable minerals compared to gangue minerals.

Both the liquid portion of the froth and hydrophobic particles have the ability to cause bubble rupture and coalescence. A particle will travel to the center of the space created by two neighboring bubbles until it satisfies a particular contact angle requirement. It is possible to evaluate whether a particle will cause bubble coalescence by looking for a crucial wetting angle. The contact angle that the bubble forms tells us this essential angle. The bubbles will not coalesce, as seen in Figure 2.7(a), if the contact angle (θ) is less than 90°, indicating that it is below the critical wetting angle. Nevertheless, as shown in Figure 2.7(b), if the contact angle

is greater than 90°, the particle will penetrate both sides of the liquid layers, resulting in bubble coalescence.

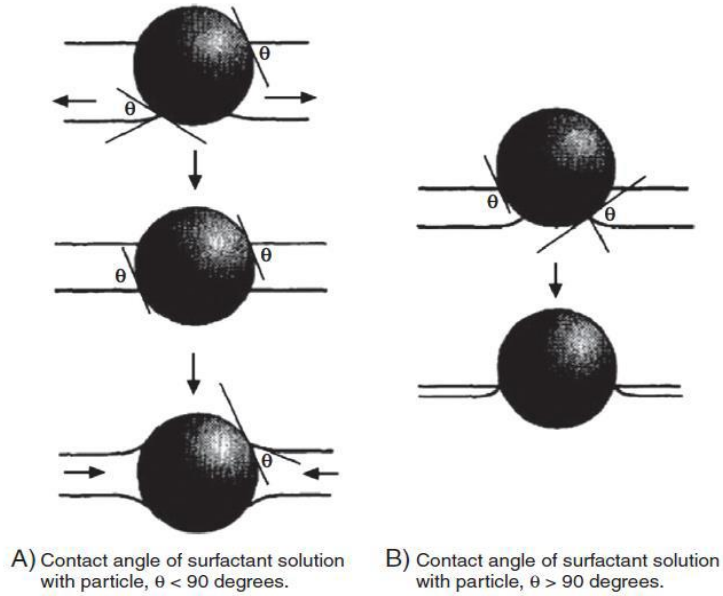

Figure 2.7*:* The behaviour of particles during bubble coalescence (Ata, 2012).

Particles having contact angles larger than 90° are particularly hydrophobic and, as a result of bubble coalescence and rupture, are difficult to recover in the flotation concentrate. Particles with contact angles of 30° to 50°, on the other hand, are anticipated to cling to and be conveyed through the froth without entering the lamella, and so constitute the majority of particles recovered in the flotation concentrate as reported by Ata (2012). The maximum capacity for particles in the froth, also known as froth loading, is reached when bubble coalescence occurs. The limit that can be reached before no more particle recovery is possible is known as the saturation point. Particle detachment can occur when bubbles merge because of the oscillations between them; larger particles are more susceptible because of their mass and momentum. Studies have shown that covering bubbles with more particles before to coalescence, which produces a high particle loading, decreases the amount of particles that detach later on during coalescence (Ross, 1997).

2.3. Mechanical Factors

Efficient dispersion of gas, suspension of particles, and flotation within the cell are attributed to mechanical impellers and induced air flow (Deglon, 2005). According to Yang and Aldrich (2006), controlling the aeration rate and impeller speed is crucial in improving the flotation performance. The impeller is responsible for imparting energy to the pulp, which creates movement and flow within the float cell.

2.3.1 Flotation Hydrodynamics

As reported by Deglon (2005), hydrodynamics pertains to the movement of the pulp in the flotation cell as a whole. The impeller's rotation produces a specific flow pattern in the cell, which is also known as the average path of the bulk pulp flow. The dimensions of the flotation cell, such as its size and shape, and the impeller's properties, such as its geometry and rotational speed, influence these flow patterns. The impeller disperses the fluid in three directions: radially, axially, and tangentially. These directions create fluid jets that disseminate into the pulp's bulk. These fluid jets carry kinetic energy, which is transformed into turbulence within the cell. The fluid is then recycled back to the impeller, where it is redistributed to the pulp. This way, the fluid flow patterns in the cell are constant.

2.3.2 Turbulence in Flotation

Deglon (2005) reported that turbulence plays a crucial role in fundamental sub processes such as "bubble-breakup, particle dispersion and bubble-particle contacting." The conversion of kinetic energy to turbulence is achieved through "vortex stretching," which is responsible for generating physical vortices within the cell volume (Deglon, 2005). Modelling of this turbulence is accomplished by applying Navier Stokes equations (Deglon, 2005). Two types of eddies have been identified as the main contributors to flotation sub processes, namely "inertial sub-range eddies" and "viscous dissipation eddies." However, this project will not include modelling of the turbulence in the cell.

According to Çilek and Yılmazer (2003), the hydrodynamics in the flotation cell can be characterized using dimensionless groups such as Reynolds number, Froude number, and Air Flow Number (AFN), which are based on physical variables such as aeration rate, impeller speed, and pulp density. These physical variables have a direct impact on gangue entrainment and water recovery in the concentrate. Increasing the air flow rate and impeller speeds can improve drainage by increasing the number of bubbles in the system, which causes them to push against each other and decrease the thickness of the plateau borders. This squeezing effect,

combined with the natural gravity of the draining liquid, leads to an increase in the velocity of the draining liquid (Jan, 1982).

2.4. Kinetics of Flotation

Mineral recoveries and overall enrichment ratios are critical parameters for assessing flotation system performance and selectivity. These metallurgical indices are often calculated at certain flotation residence durations. However, some applications necessitate the continuous monitoring of these performance parameters during the entire flotation process. The analysis, called kinetic response, has been used for a number of purposes, including sizing flotation circuits, simulating flotation processes, scaling up metallurgical results, comparing flotation machines, and determining the maximum recoveries that can be achieved. A drop in mineral concentrations over time or an increase in cumulative recovery as a function of time are common characteristics of kinetic response.

In theoretical terms, the collection process has been likened to a chemical reaction. In this analogy, bubbles and particles are regarded as reactants, while the particle-bubble aggregate represents the final product. This concept is illustrated in Figure 2.8;

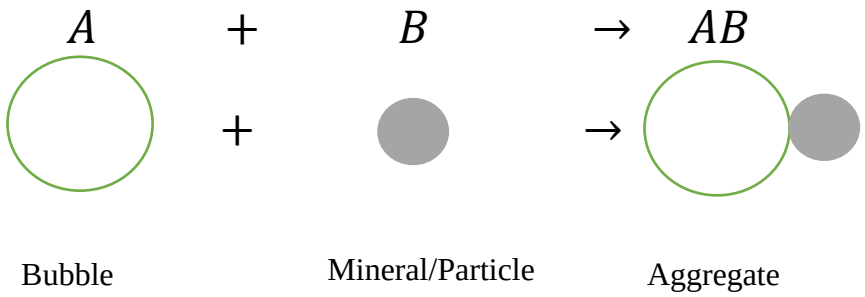

Figure 2.8*:* A schematic diagram illustrating a flotation process akin to a chemical reaction. In this depiction, A (depicted as a bubble) and B (depicted as a hydrophobic particle) represent the reactants, while AB (shown as an aggregate) symbolizes the product.

Previous studies by Laskowski (2001), Hernáinz and Calero (2001), Polat and Chander (2000) and Mendez et al. (2009), and have commonly assumed an excess of bubbles in batch flotation processes, resulting in the mineral concentration (C) varying based on a first-order reaction described by Equation 2.4.1 (Garcia-Zuñiga, 1935).

$$\frac{dC}{dt} = -k(C - C_{\infty}) \qquad \text{(Equation 2.4.1)}$$

Whereby,

- t corresponds to the flotation time,
- k represents the rate constant for the flotation process,
- C is the mineral concentration at a specific time,
- C_∞ is the concentration at equilibrium (or at $t \rightarrow \infty$).

Equation 2.4.1 can be integrated to give the flotation recovery as a function of time as;

$$R(t) = R_\infty(1 - e^{-kt}) \qquad \text{(Equation 2.4.2)}$$

where R_∞ is the maximum achievable recovery of a valuable mineral in a specific experimental setting (Garcia-Zuñiga, 1935). Essentially, it is the upper theoretical limit of the recovery that can be achieved. Several factors, including the ore type, mineralogy, and chemical and physical conditions of the flotation process, contribute to the determination of R_∞. R_∞ is not a fixed value and can change based on particular process conditions. It is also commonly used as a benchmark for measuring the effectiveness of a flotation process. If the actual recovery rate is close to R_∞, it is an indication that the process is efficient and successful in separating the valuable mineral from the ore. The idea of R_∞ is frequently applied in literature to determine the optimal flotation time. Studies have found that there is an ideal flotation duration, beyond which the recovery rate does not improve significantly. This is because R_∞, the maximum recovery rate, has been attained, and further flotation time does not have any additional advantages (King, 2012; Agante et al., 2007; Trahar and Warren, 1976). The specific ideal flotation time may differ depending on the ore type and flotation process conditions.

Equation 2.4.2 was established by Garcia-Zuñiga (1935) to evaluate the flotation of five different ores: silver, copper oxide, gold from a feed stream, gold from a tail stream, and copper sulphide. With the use of this technique, different flotation rates and maximum recoveries could be assessed under the same experimental settings, which included solid percentage, reagent conditioning, and grinding duration. Conversely, Schuhmann Jr. (1942) created a first-order system-based laboratory instrument for determining the particular flotation rate in a continuous operation. This rate, which is directly connected to particle-bubble attachment kinetics, was computed by dividing the recovery rate of a mineral by the weight of the ingredient in the pulp zone. The highest recovery rate of 100% was considered in the study.

Numerous factors associated with solid properties and process variables significantly influence the intricate flotation process. Since the groundbreaking studies conducted by Schuhmann Jr

(1942) and Garcia-Zuñiga (1935), extensive endeavours have been undertaken to establish a correlation between rate constants and critical flotation parameters.

2.4.1. Reaction Order of a Flotation Process

Kinetic characterizations and process modelling have widely accepted first-order models (Agar et al., 1980; Albijanic et al., 2015b; Asghar et al., 2015; Bu et al., 2017b; Harris and Chakravarti, 1970; Imaizumi and Inoue, 1963; Klimpel, 1980; Mehrotra and Kapur, 1974; Polat and Chander, 2000; Welsby et al., 2010; Xu, 1998). Nonetheless, higher-order models have also been documented in the literature, based on an expansion of Equation (2.4.1), as shown in works by Tewari and Biswas (1969), Ek (1992), Bu et al. (2017b), and Horst (1958).

$$\frac{dC}{dt} = -k(C - C_\infty)^n \qquad \text{(Equation 2.4.3)}$$

The Equation 2.4.3 provides the instantaneous rate of change of the mineral concentration (C) in a batch flotation machine, where the reaction order is represented by n. The recovery for a batch process with a single rate constant (k_n) and reaction order (n_*) can be determined using the equation provided by Tewari and Biswas (1969), Ek (1992), and Bu et al. (2017b) below.

$$R(t) = R_\infty \left(1 - \frac{1}{\left(1 + (n-1)\, R_\infty^{n-1}\, k_n\, t\right)^{\frac{1}{n-1}}}\right) \qquad \text{(Equation 2.4.4)}$$

A second-order model, Equation 2.4.5, with a single rate constant k_2, was proposed by Arbiter (1951) to fit six independent data sets, arguing that the dependence of recovery rate on the initial mineral concentration supported the use of a higher-order model. Equation (2.4.5) is a specific case of Equation (2.4.4) with $n = 2$.

$$R(t) = \frac{R_\infty^2\, k_2\, t}{1 + R_\infty\, k_2\, t} \qquad \text{(Equation 2.4.5)}$$

Various studies (Yuan et al., 1996; Bu et al., 2017a; Dowling et al., 1985; 2016; Chaves and Ruiz, 2009; Zhang et al., 2013 Bahrami et al., 2019a; Ek, 1992; Ni et al.,) have included Equation (2.4.5) in their comparisons of various kinetic models for laboratory-scale flotation processes. Different findings are obtained from these comparisons, however, indicating that no one deterministic model is sufficiently flexible to capture every possible scenario involving flotation.

De Bruyn and Modi (1956) established an empirical model between the reaction order and flotation rate for quartz at varied particle sizes, where R_∞ was assumed to be 100%. For particle sizes smaller than 65 µm, continuous flotation tests were performed on pure minerals, yielding an approximate reaction order of $n = 1$, while for larger fractions, the values of n increased. Holland-Batt (1971) evaluated batch flotation tests using arbitrary reaction orders and assumed R_∞ values of 100% for the two components (valuable and gangue) that were assessed. The kinetic response orders were examined by Bu et al. (2017) with respect to particle size, and it was found that they ranged from $n = 1$ to 2. The intermediate-coarse size class was observed to have the highest value of n, which was thought to be due to the typical concave relationship between flotation performance and particle size.

2.4.2. The Flotation Rate Constant and its Relationship with Process Variables

When it comes to the formation of stable particle-bubble aggregates by adhesion and collision, the flotation rate constant has been intimately associated with the effectiveness of the collecting process. Studies by Ahmed and Jameson (1989), Duan et al. (2003), Karimi et al. (2014), and Pyke et al. (2003) have presented Equation 2.4.6, which demonstrates the relationship between the collection efficiency E_K, collision E_C and adhesion E_A efficiencies, and a stability factor E_S, indicative of the strength of the particle-bubble attachment.

$$E_K = E_C\, E_A\, E_S \qquad \text{(Equation 2.4.6)}$$

The relationship between the flotation rate constant and the efficiency of particle-bubble aggregate formation has been expressed through Equation 2.4.6. This equation has been modified by various researchers to simplify certain efficiencies or probabilities and relate the flotation rate constant to E_K. In several instances, froth factors and other parameters have been added to the apparent rate constant in order to account for separation process inefficiencies. As an example, Schuhmann Jr (1942) incorporated a froth stability factor (F_S) in addition to the probabilities of collision (P_C) and adhesion (P_A) in Equation 2.4.7 to derive the rate constant.

$$k = P_C\, P_A\, F_S \qquad \text{(Equation 2.4.7)}$$

Sutherland (1948) included such particles in a potential flow by extending the simplified relationship, which was initially meant for particles without inertia. This led to the development of a closed formula for the rate constant that depended on a number of variables, such as pulp characteristics, induction period, bubble and particle sizes. The particles had to follow the liquid streamlines and interact with rising bubbles as they passed over a critical zone, which was specified by a critical diameter of the bubble's equator, which controlled the likelihood of collision. The model assumed a non-viscous and incompressible fluid. The adhesion process was considered as well, and it depended on the particle's journey distance on the bubble surface over time (t_C). Only if the induction period was less than or equal to (t_C) would there be a successful adhesion. Equation 2.4.8 then provided the expression for the rate of flotation.

$$k = 4\pi^2\theta^* \, sech^2\left(\frac{3v\lambda}{4R_B}\right) R_B \, r_P^2 \, N_O \, n' \, v \, \rho_S \qquad \text{(Equation 2.4.8)}$$

The model comprises the following variables: θ^*, which characterizes the processes of detachment; v, the bubbles' velocity in relation to the particles; λ, the induction period needed for particle-bubble adhesion; R_B, the bubbles' radius; r_P, the particles' radius; N_O, the initial particle concentration per pulp volume; n' , the bubble concentration per pulp volume; and ρ_s , the particle density. A first-order equation that accounts for the heterogeneous environments of bubble size, particle size, and induction time is used to explain the flotation kinetics. Equation 2.4.9 is presented as an example of modeling a distributed induction period with density function ζ(λ).

$$R(t) = [1 - \int_0^\infty e^{-\varphi t sech^2(\beta\lambda)} \, \zeta(\lambda) d\lambda] \qquad \text{(Equation 2.4.9)}$$

In Equation 2.4.9, the constants φ and β relate to particle size, gas dispersion, and drop-back terms in Equation 2.4.8. Sutherland (1948) recommended utilizing the Inverse Laplace Transform of $[1 - R(t)]$ to determine the density function $\zeta(\lambda)$ in cases where an analytical form of $R(t)$ was obtainable.

2.4.3. Flotation Rate Distributions

The heterogeneous nature of the process is highlighted by the variability in flotation performance based on size (Trahar, 1981; & Morris, 1952), liberation, or composition (Sutherland, 1989) and association (Sutherland, 1989). Deterministic rate parameters and maximum recoveries are frequently used to characterize flotation kinetics. Sutherland's groundbreaking theoretical work from 1948 evaluated how recovery rates and flotation performance were affected by dispersed process factors. The first-order model of Equation 2.4.2 was expanded by Imaizumi and Inoue (1963) to account for the range of recorded recovery rates as per Equation 2.4.10;

$$R(t) = R_{\infty}\,(1 - \int_0^{\infty} e^{-kt} f(k) dk) \qquad \text{(Equation 2.4.10)}$$

Equation 2.4.10 denotes a continuous sum of exponentials that accounts for flotation rate heterogeneity, where $f(k)$ denotes a flotation rate distribution or a variety of rate constants. The integration of $f(k)$ from 0 to infinity equals 1. Imaizumi and Inoue (1963) examined the impact of changes in particle size, pulp density, and collector concentration, as well as the association level pyrite and chalcopyrite grains on Equation 2.4.10 using a Gamma distribution to describe $f(k)$. Their study assumed R_{∞} to be 100%.

A version of Equation 2.4.10 has been utilized to describe the kinetics of flotation, resulting in a discrete distribution for $f(k)$. This approach has resulted in Equation 2.4.11, which describes the recovery of a batch flotation process undergoing a first-order reaction with N discrete rate constants (where $\sum_{i=1}^{N} w_i = 1$).

$$R(t) = R_{\infty}(1 - \sum_{i=1}^{N} w_i\, e^{-k_{1,i}t}) \qquad \text{(Equation 2.4.11)}$$

According to Equation 2.4.12, the function $f(k)$ can be expressed as a summation of N Dirac delta functions (δ) centered at $(k - k_{1,i})$, with weights given by the values w_i
Mathematically, this can be written as follows:

$$f(k) = \Sigma_{i=1}^{N} w_i\, \delta(k - k_{1,i}) \qquad \text{(Equation 2.4.12)}$$

This equation essentially means that the function $f(k)$ is a weighted sum of N individual Dirac delta functions, each of which is centered at a different location $(k_{1,i})$. The weights w_i determine the contribution of each delta function to the overall sum. Equations 2.4.10 and 2.4.11 provide a more comprehensive approach compared to the first-order method outlined

in Equation 2.4.2 by incorporating a continuous or discrete sum of exponentials. Furthermore, Klimpel's work in 1980 shows that Equation 2.4.13 can be utilized to generalize any reaction order into a distributed system.

$$R(t) = R_\infty(1 - \int_0^\infty \gamma(k,t) f(k) dk) \qquad \text{(Equation 2.4.13)}$$

The function $\gamma(k,t)$ is a function of both k and t and is calculated using the solution of Equation 2.4.3, depending on the reaction order. For example, in a first-order reaction, $\gamma(k,t)$ would be equal to $e^{-k\,t}$, while in a second-order reaction, it would be equal to $1/[R_\infty\, k\, t + 1]$. Equations 2.4.10 to 2.4.13 have broad applicability in batch flotation systems, as they can accommodate various reaction orders with distributed rate constants. In continuous flotation systems, the characterization of the system is typically based on the residence time distribution (RTD), which is measured for a particular flotation machine or a sequence of machines. In a study by Woodburn and Loveday (1965), Equation 2.4.14 was employed to evaluate the flotation performance of different flotation arrangements.

$$R(t) = R_\infty(1 - \int_0^\infty \int_0^\infty e^{-kt} f(k) \xi(t) dk dt) \qquad \text{(Equation 2.4.14)}$$

Equation 2.4.14 incorporates the residence time distribution, denoted as $\xi(t)$, which was observed to resemble that of a perfect mixer. The performance of various circuit configurations was evaluated by utilizing a Gamma distribution to describe $f(k)$. It was assumed that each individual flotation machine exhibited perfect mixing. However, studies conducted by Yianatos et al. (2015) on mechanical flotation cells and by Yianatos et al. (2017) on flotation columns have revealed significant deviations from perfect mixing in industrial machines. Hence, careful attention is necessary when estimating RTD for characterizing flotation kinetics in continuous systems.

2.4.4. $f(k)$ Model Structures

Equations 2.4.10 to 2.4.14 offer greater flexibility in kinetic models compared to the classical single rate constant (SRC) approach of Equation 2.4.2. Prior to the presentation of Equation 2.4.10 by Imaizumi and Inoue (1963), several alternative models were reported in literature. For instance, Kelsall (1961) described a graphical technique to illustrate the probability of flotation of two minerals and examined the impact of reagent dosage, locked mineral fractions, particle size, and flotation machine type on the probability of flotation. The size-by-size kinetic characterization used two discrete rate constants and their relative content [Equation 2.4.11].

This methodology was applied to an ore containing chalcocite and malachite at an industrial scale.

The flotation rate constant distribution can be described using several distributions, which are based on the generalizations of Equations 2.4.2 and 2.4.3. These distributions include the Exponential distribution (Dowling et al., 1985), Uniform distribution (Huber-Panu et al., 1976), Sinusoidal distribution (Diao et al., 1992), Normal distribution (Chander and Polat, 1995), Triangular distribution (Harris and Chakravarti, 1970), Weibull distribution (Yianatos et al., 2010), and Double Normal distribution (Ferreira and Loveday, 2000). Literature also includes additional model structures that have been proposed, tested, and compared. For instance, Lynch et al. (1981a) summarized different flotation rate distributions, including N discrete rate constants [Equation 2.4.12], a polynomial model, and bimodal Gamma distribution models.

In addition to the distributions proposed in Equations 2.4. and 2.4.3, there are various other model structures that have been proposed, evaluated, and compared in literature. For instance, Dowling et al. (1985) introduced additional model structures, the Gas-Solid Absorption model, Two-Stage Exponentials, and the Uniform $f\ (k)$ model analogous of a second order system proposed by Klimpel (1980). In contrast, five distinct model structures were compared by Mazumdar (1994) for the flotation rate distribution, comprising the models based on the proportionality and logarithmic proportionality laws proposed by Lai (1990). To simplify comparisons, Polat and Chander (2000) standardized the parameter definition for six $f(k)$s in terms of the variance and mean of the distributions. Ahmed (2004) compared eight model structures, including but not limited to the Rosin-Rammler, SRC, and Uniform models, which included initial time corrections to represent $R(t)$.

Vinnett et al., 2015 reports that another alternative in characterizing batch flotation kinetics is the use of fractional calculus. In this method, the generalization of Equation 2.4.1: $d^{\alpha}C/dt^{\alpha} = -k_{\alpha}(C - C_{\infty})$ is used, which involves a fractional derivative order α and a fractional rate constant k_{α}. According to Tarasov (2010), fractional kinetics have demonstrated benefits in unusual systems with nonlocal dynamics that exhibit long-term memory over time. In a study by Hassanzadeh et al. (2019) to evaluate the suitability of various kinetic models for representing flotation data, they examined 12 models, including those suggested by Hill (1910) for hemoglobin dissociation curves and Mitscherlich (1919) for plant growth, using information criteria.

The models described in literature differ based on the shape of $f(k)$ and the number of parameters they use, with more parameters providing greater flexibility to fit time-recovery data. Klimpel (1980) introduced the rectangular distributed model, which has proven to be one of the most successful methods. According to Yianatos (2007), one advantage of this function is that it follows the parsimony principle by using the least number of parameters while providing model fit that is just as good as the Gamma and Weibull distributions (illustrated in Figure 2.9(b)). However, a disadvantage of the rectangular function is that it cannot identify the maximum attainable recovery. This is because, as pointed out by Kelly and Carlson (1991), it becomes interdependent on the presence of the mineral fraction with zero rate constant.

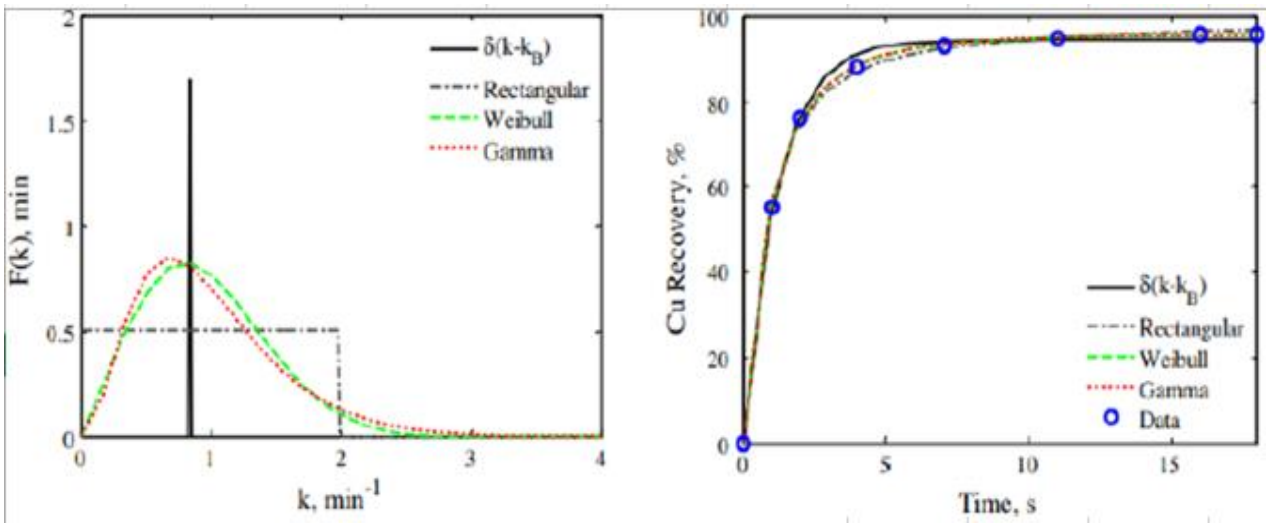

(a) (b)

Figure 2.9*:* (a) Different rate constant distributions (F(k)) for batch tests and their respective time-recovery prediction (b) (Yianatos et al., 2007).

The literature has presented a number of model structures to match experimental data and examine each model's degree of flexibility. Additionally, researchers have looked at the average rate constants and proportion of non-floatable material to compare operating techniques or different ores. Nevertheless, there hasn't been much research done on $f(k)$ forms or calculated parameters. One common approach to characterizing flotation kinetics involves using a few distinct rate constants [Equation 2.4.11] to classify the rate of the flotation process, k, such as slow, immediate, and fast rate constants, and R_∞ to determine the proportion of floatable and non-floatable materials. This method has been widely used to study flotation rate and performance in various studies (Chen et al., 1999; Braga et al., 2020; Chen et al., 2019; Harris et al., 2002; Welsby et al., 2010; Filippov et al., 2013;; Ross, 2019; Kelsall, 1961; Sutherland, 1989). However, using discrete rate constants must be approached with caution to avoid overfitting (Dowling et al., 1985; Bu et al., 2017b; Sahoo et al., 2017; Hassanzadeh et

al., 2019), particularly when the number of experimental data points is comparable to the number of fitting parameters ($w_i, R_\infty,$ and $k_{1,i}$).

2.4.4.1 Gamma Rate Constant Distribution

The Gamma flotation rate constant distribution is a robust statistical tool that is widely utilized in the field of mineral processing to quantify the rate of particle flotation in a mineral slurry within a flotation cell. The distribution is based on the Gamma probability distribution function, which represents a generalization of the exponential distribution. The distribution's suitability is grounded in its ability to conform to flotation data with a high degree of accuracy by providing a good fit. The Gamma flotation rate constant distribution is governed by two crucial parameters, the shape parameter (α) and the scale parameter (β), which regulate the curve's shape and position on the x-axis, respectively.

The Gamma flotation rate constant distribution is an indispensable modelling tool used to examine the behaviour of various particle sizes during flotation processes, and it facilitates the prediction of flotation rates for particles of specific sizes. The distribution is especially valuable for the estimation of the mean flotation rate constant for any given PSD. Its versatility and applicability have made it a go-to model in the field of mineral processing, where it plays a key role in the separation and concentration of minerals. The Gamma flotation rate constant distribution also includes a normalization constant (Γ) that ensures the distribution integrates to 1 over its support. The support of the distribution is typically defined as the range of flotation rate constants observed in a given flotation process.

The probability density function (PDF) of the Gamma flotation rate constant distribution is given by the following equation:

$$f(k) = \left(\frac{\beta^{\alpha+1}}{\Gamma(\alpha+1)}\right) \cdot k^{\alpha} \cdot e^{-\beta \cdot k} \qquad \text{(Equation 2.4.15)}$$

Where;

- k is the flotation rate constant,
- β is the scale parameter,
- α is the shape parameter, and
- $\Gamma(\alpha + 1)$ is the Gamma function evaluated at $\alpha + 1$.

The Gamma flotation rate constant distribution has a number of useful properties, including the fact that it is a continuous distribution that can take on any positive value. It is also a flexible distribution that can be adjusted to fit a wide range of experimental data as previously noted above.

2.4.4.2 Weibull Rate Constant Distribution

The Weibull flotation rate constant distribution is a widely used statistical model in mineral processing to describe the flotation kinetics of particles in a flotation cell. It is a flexible distribution that has been shown to be highly effective in fitting experimental data and modelling the complex behaviour of particles during the flotation process.

The Weibull distribution is based on the Rosin-Rammler distribution function, which was originally developed to describe the size distribution of particles in a material. The WRR distribution adds an additional Weibull factor to account for the variation in flotation rate among different particle sizes. Like the Gamma distribution, it is characterized by two parameters: the shape parameter (n), which controls the shape of the distribution curve, and the scale parameter (k_m), which represents the characteristic particle size of the distribution, unlike the Gamma distribution to which it regulates the curve's position on the x-axis.

The PDF for the Weibull flotation rate constant distribution is given by:

$$f(k) = \left(\frac{n}{k_m}\right) \cdot \left(\frac{k}{k_m}\right)^{n-1} \cdot e^{\left(-\left(\frac{k}{k_m}\right)^{n}\right)} \qquad \text{(Equation 2.4.16)}$$

Where;

- k is the flotation rate constant as in the Gamma model,
- n and k_m are the shape and scale parameters, respectively.

Compared to the Gamma flotation rate constant distribution, which assumes that all particles in the slurry have the same flotation rate constant, the Weibull distribution provides a more accurate representation of the complex behaviour of particles in a flotation cell, as it accounts for the variation in flotation rate among different particle sizes. In situations where the PSD is wide and there is significant variation in flotation rate among particles of different sizes, the Weibull distribution has been found to provide a better fit to flotation data. The Weibull distribution also allows for the accurate estimation of the cumulative recovery of particles as a function of time, which is an important parameter in the design and optimization of flotation circuits. However, the Gamma distribution has a simpler form and requires fewer parameters

to be estimated from experimental data, making it a more straightforward model to use in some cases.

In summary, the choice between the Weibull and Gamma flotation rate constant distributions will depend on the specific characteristics of the flotation system being studied, as well as the nature of the experimental data available. Both models are valuable tools for understanding the kinetics of flotation processes and optimizing mineral processing operations.

The numerical integration of Equation 2.4.10, which accounts for the range of observed recovery rates, as reported by Imaizumi and Inoue (1963), for both the Gamma and Weibull models will be executed in the Results and Discussion section. Shown below is a summary table illustrating the different kinetic models discussed in this section of the work.

Table 2.1: A summary table showing the different kinetic models discussed on section 2.4.4.

Model	$F(k)$	$R(t)$
Single rate constant	$\delta_{KGZ}(k)$	$R_\infty \cdot [1 - \mathrm{e}^{(-k \cdot t)}\ ]$
Rectangular (Klimpel)	$\frac{1}{k_{Max}} \cdot [\mu_o(k) - \mu_{k_{Max}}(k)]$	$R_\infty \cdot \left[1 - \frac{1 - \mathrm{e}^{(-k_{Max} \cdot t)}}{k_{Max} \cdot t}\right]$
Gamma	$\left(\frac{\beta^{\alpha+1}}{\Gamma(\alpha+1)}\right) \cdot k^{\alpha} \cdot e^{-\beta \cdot k}$	Evaluated on 4.5
Weibull	$\left(\frac{n}{k_m}\right) \cdot \left(\frac{k}{k_m}\right)^{n-1} \cdot e^{\left(-\left(\frac{k}{k_m}\right)^n\right)}$	Shown on 4.5
Exponential	$\frac{1}{k_{exp}} \cdot e^{-\frac{k}{k_{exp}}}$	$R_\infty \cdot [1 - \frac{1}{1 + k_{exp} \cdot t}]$

2.4.5. Estimation Methods for R_∞ and $f(k)$

2.4.5.1 Linear Regression

In the early stages of flotation research, as evidenced by the works of Garcia-Zuñiga (1935), Arbiter (1951), Gaudin et al. (1942), Horst (1958), Holland-Batt (1971), Morris (1952), Tewari and Biswas (1969), and Kelsall (1961), the most common methods used for estimating kinetic parameters were mathematical transformations or graphical techniques, such as using log-scale. To illustrate, one approach was to express Equation 2.4.2 as $-ln[1 - R(t)/R_\infty] = k\,t$, where R_∞ is a known value. To determine the rate constant, a linear regression was performed between $y = -ln[1 - R_{data}/R_\infty]$, and $x = t$, where t signifies the flotation times vector and R_{data} represents the vector of measured recoveries. Alternatively, the gradient of the graph of y versus x was used to obtain the k values. Non-linearity in this plot was indicative of a higher reaction order or the presence of multiple rate constants, as noted in works by Arbiter (1951) and Kelsall (1961).

Other model structures for $R(t)$ have also employed analogous techniques. In semi-log scale, two datasets are presented in Figure 2.10, from which it is possible to interpret a SRC in Figure 2.10(a) and two deterministic rate constants in Figure 2.10(b). Although there are now software tools available to directly estimate kinetic parameters through nonlinear regression, the conversion of time-recovery data is still commonly employed in flotation rate characterizations by researchers such as Shahbazi et al., 2017; Eskanlou et al., 2018; Bagheri et al., 2020; Nikolaev, 2019; Taguta et al., 2019. However, it is important to note that using transformations and linear regressions may not result in the most accurate parameter estimates and model fitting in the original experimental domain, as discussed by Rhinehart (2016).

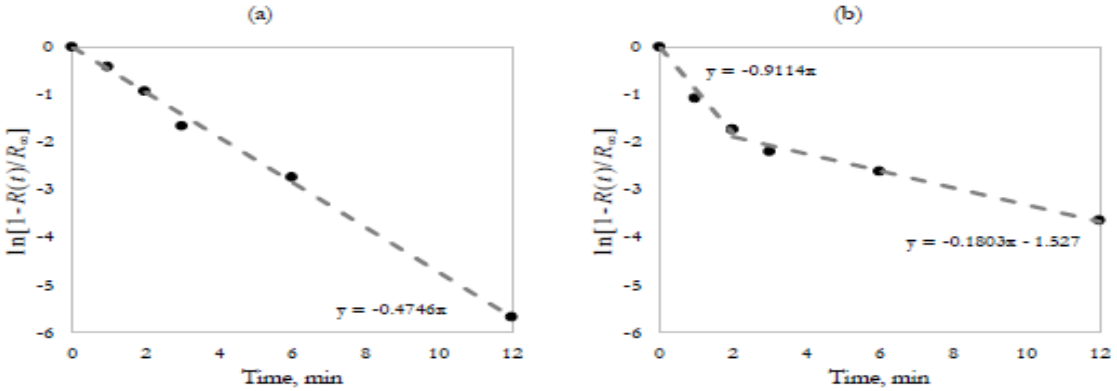

Figure 2.10*:* Examples of k estimations on semi-log plots denoted by (a) for a single rate constant and (b) two rate constants.

2.4.5.2 Nonlinear Regression

Literature has extensively reported and utilized nonlinear regression to fit batch flotation recoveries, as evidenced by works by Kelly and Carlson, 1991; Polat and Chander, 2000; Ahmed, 2004; Rubio et al., 2007; Chaves and Ruiz, 2009; Tabosa and Rubio, 2010; Sahoo et al., 2017; Bu et al., 2017b; Bahrami et al., 2019b; and Hassanzadeh et al., 2019. With this method, the sum of squared residuals (SSR) is minimized in order to estimate the model parameters as per Equation (2.4.17), and this can be done directly without requiring any mathematical transformations. In Equation 2.4.17, the variables n, R_{mod} , and $R_{data,i}$ represent the number of replicates, vector of model recoveries (from any model structure for $R(t)$), the i^{th} vector of experimental data, respectively. Several software packages, including MATLAB, MS Excel, python, and others, can be used to solve the optimization problem of Equation (2.4.15). The least-squares estimation of Equation 2.4.17 offers several advantages when normal errors are identically and independently distributed (Seber and Wild, 1989; Bates and Watts, 1988; and Allen, 1997), suggesting that the errors in the measured recoveries have a constant variance, s^2_{Rdata}. Figure 2.11 illustrates an example of the solution for R_{data} and R_{mod} for a given experimental dataset.

$$min \sum_{i=1}^{n} [R_{data,i} - R_{mod}]^T [R_{data,i} - R_{mod}] \qquad \text{(Equation 2.4.17)}$$

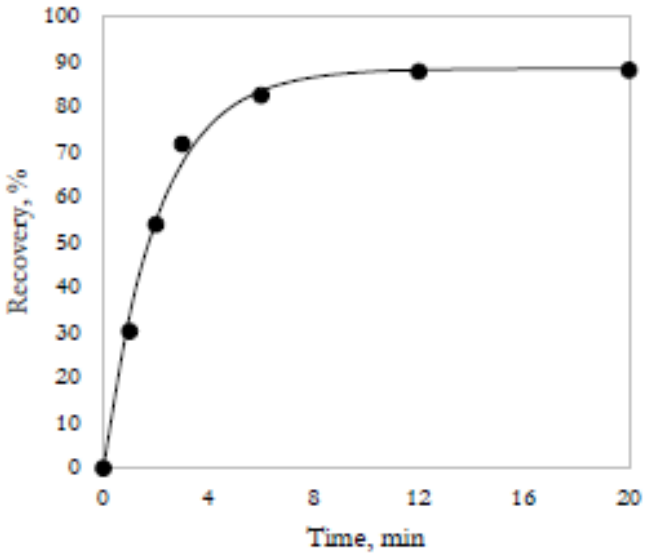

Figure 2.11*:* An illustration of the experimental recovery data, $R_{data}(t)$, and the $R(t)$ solution resulting from the minimizing Equation (2.4.17)

The evaluation and comparison of the goodness-of-fit (GOF) for kinetic models have been extensively examined in literature. Lynch et al. (1981a) comprehensively outlined various continuous and discrete distributions that can be used to define flotation rates. In their study, Lynch et al. (1981a) noted that an improved fitting is generally achieved with an increased number of parameters. However, it is crucial to balance the number of parameters with their physical significance to ensure a meaningful trade-off. Dowling et al. (1985) conducted an assessment of thirteen model structures, taking into consideration both the GOF (root-mean-square error or RMSE) and the confidence interval of the parameters. The authors noted that adding an extra parameterization often resulted in a dilution effect, causing the confidence interval of the parameters to widen. Moreover, the simplification of complex models with a higher number of parameters was done to reduce them to simpler forms. “

In a different investigation conducted by Mazumdar (1994), five distinct model structures were compared based on their statistical performance indicators related to GOF, such as random residual pattern, absolute magnitude of the residuals, and mean squared error (MSE), along with the parameter stability, encompassing the predicted residual error sum of squares (PRESS) and the confidence interval of the parameters. The findings of the study revealed that no specific model outperformed the others for the datasets examined. In a separate investigation by Polat and Chander (2000), they observed that utilizing three-parameter rate models to depict flotation kinetics leads to a substantial enhancement in model fitting. The study also involved fractioning the samples by specific gravity and size, with the flotation rate distributions approximating the conventional first-order model for each class.

Another study by Ahmed (2004) examined eight model structures for batch flotation of coal, and both MSE and PRESS were used to evaluate model fitting and stability. However, the results indicated that no single model consistently performed the best for the datasets evaluated. Nonetheless, for the examined coal flotation, two models (Rosin-Rammler and first-order with 2 rate constants under $R_\infty = 100\%$) were recommended. Bu et al. (2017b) highlighted the overfitting phenomenon that arises from an increase in the number of parameters in kinetic characterizations. As the number of terms increases, the reliability of the estimates decreases. In another investigation, Sahoo et al. (2017) investigated seven distinct model structures with regards to their GOF and model consistency using various statistical measures, including the RMSE, maximum residual, Jarque-Bera test, kurtosis and skewness of the residuals, Akaike information criterion, F-tests and confidence interval of the parameters. However, the results were consistent with those obtained by Ahmed (2004) in that none of the models performed

consistently better than the others across all the evaluated datasets. Although various kinetic models have been proposed to describe the flotation behaviour of minerals, the predictive performance of these models can be highly dependent on the mineralogical characteristics of the ores. For instance, Hassanzadeh et al. (2019) investigated the performance of twelve kinetic models, including the exponential model and the second-order reaction proposed by Arbiter (1951), in terms of both model fitting and complexity. To evaluate model fitting, the authors used statistical metrics such as the adjusted coefficient of determination R^2_{adj}, the law of iterated logarithm, the sum of squared residuals (SSR), and the Bayesian and Akaike information criteria. The results showed that the optimal model varied depending on the mineralogy of the ore.

2.4.5.3 Laplace Inversion Approaches

In order to characterize batch flotation kinetics, inversion approaches have been proposed which take into consideration certain properties of Equation 2.4.10 and its discretization. Kapur and Mehrotra (1974) made use of the integral term of Equation 2.4.10 which represents the Laplace Transform of the flotation rate distribution $\mathcal{L}[f\ (k)]$:

$$\mathcal{L}[f(k)] = \int_0^\infty e^{-kt} f(k) dk = 1 - \frac{R}{R_\infty} \qquad \text{(Equation 2.4.18)}$$

In the study by Kapur and Mehrotra (1974) and later by Mehrotra and Padmanabhan (1990), inversion approaches were proposed to characterize batch flotation kinetics. Empirical flotation data was used to evaluate the methodology under varying conditions such as particle size, changes in gas dispersion, pH, initial pulp density, impeller speed, reagent dosage, and circuit stage (rougher, scavenger, and cleaner). Saddle points in the cumulative $f(k)$s were reported by Mehrotra and Padmanabhan (1990), which indicated abrupt discontinuities in the flotation rate distribution. More recently, Pascual and Whiten (2015) developed an inversion approach using Laguerre polynomials and finely spaced discrete components to determine the Laplace Transform of $[1-R(t)/R_\infty]$ for $f(k)$, without requiring specific model structures for it. While a regularization technique was used to address the ill-conditioned solution for $f(k)$, the method still showed discontinuities in pentlandite and chalcopyrite data. Although useful in cases where no specific model structures are required, there is a need to further define a regularization criterion that can control overfitting.

3. EXPERIMENTAL PROCEDURES AND APPARATUS

The following section will cover several important subsections. First, the comminution subsection will describe the process of reducing ore samples to a suitable size for milling. Next, the sample preparation and milling curves subsection will provide details on the milling process to predict the milling duration required for a specific particle size grind. The pre-characterization and mineralogy subsection will explain the methods used to identify and analyse the mineral components of the ore. The chemical analysis methods subsection will outline the techniques used to analyse the chemical composition of the ore samples. Finally, the flotation subsection will detail the specific flotation process used in this setup and the parameters that were varied during the experiments.

3.1. Comminution

The first stage during the comminution circuit involved a jaw crusher and a vibrating screen with a 1.7 mm aperture size. The sample was initially fed into the jaw crusher, which reduced the size of the material to a more manageable size. The crushed material was then fed onto the vibrating screen, where the undersize particles were transported using a conveyor belt and collected in bags for further sample preparation. The oversize particles were cone crushed and then fed back into the vibrating screen for further sizing. This process was repeated until the entire 100 kg sample had been crushed to 100% passing through the 1.7 mm screen. Figure 3.1 below is the process flowsheet illustrating this stage.

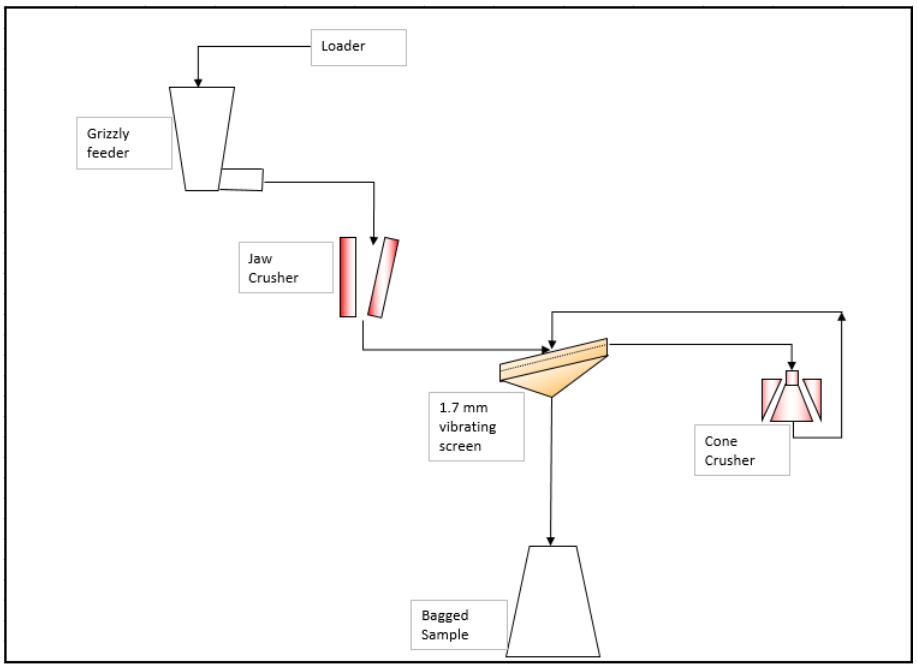

Figure 3.1: Comminution circuit.

3.2. Sample Preparation and Milling Curves

Sample preparation then commenced with the 100 kg sample that had been crushed to 100% passing 1.7 mm being riffled, blended and sub-sampled to create fifty 2kg samples that are representative of the entire sample. The sub-sampling apparatus used was a rotary splitter as depicted on Figure 3.2 below. These sub-samples were then stored in a freezer to prevent excess oxidation prior to further processing.

Figure 3.2: Rotary splitter.

Target grind sizes of 80% passing 150, 106, 75, 53, 38 µm were selected as the benchmarks for the milling process. A fixed 2kg mass of the Platreef ore sample was charged into the milling apparatus along with high chromium steel rods of sizes 10 mm, 15 mm, and 20 mm diameters. The volume of water added to the mill was based on the operating volume within the mill, which was determined beforehand. As such the slurry density was maintained at 60% solids, see

Figure 3.4 for the milling apparatus. The mill speed was maintained at 73 revolutions per minute during the entire process. The milling process was carried out for a predetermined period, during which the ore sample was reduced in size due to the impacts and abrasion caused

by the milling media. Wet and dry screening methods were employed to determine the percentage of the sample that passed through the target sieve sizes which were chosen as part of the $\sqrt{2}$ sieve stack as per Table 3.1. Wet screening was performed using a slurry made with tap water, which allowed the fine particles to pass through the sieve. The remaining sample was dried overnight in an oven and then subjected to dry screening.

Table 3.1: $\sqrt{2}$ sieve sizes.

Sieve Size (μm)
212
150
106
75
53
38
25

Figure 3.3: Sieve stack on a Paskal shaker.

The results of both the wet and dry screenings were combined to determine the final percentage passing the target sieve sizes. This process was repeated several times, varying the milling time each time, until the target grind size was achieved. The results were then used to constructs milling curves for each target grind, which provided valuable information on the relationship between milling time and particle size reduction for the Platreef ore sample. The milling curve was used to determine the optimal milling time required to achieve the desired target grind size. Additionally, this information enabled the generation of the PSD curve for each grind.

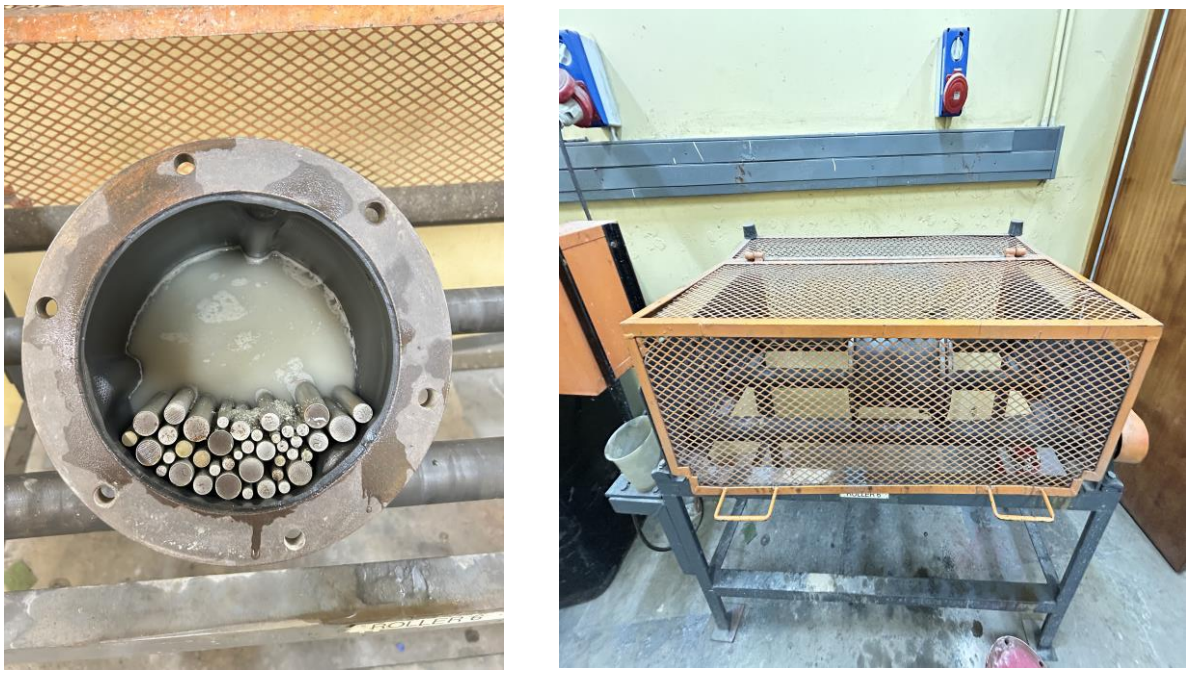

Figure 3.4: Milling Apparatus.

The milling process for the 80%-38 um fraction involved a combination of traditional tumbling milling (as depicted in Figure 3.4) and stirred milling (as illustrated in the process diagram shown in Figure 3.5). This was done to ensure that the target grind is met sooner, as the traditional tumbling mill apparatus on

Figure 3.4 would have resulted in very high milling times to achieve the grind. The apparatus used for stirred milling is presented in Figure 3.6. Ceramic balls with sizes ranging from 2 mm to 4 mm were employed as grinding media in the stirred milling. The pulp density utilized during the milling operation was set at 50% solids. See the appendices for the stirred milling conditions.

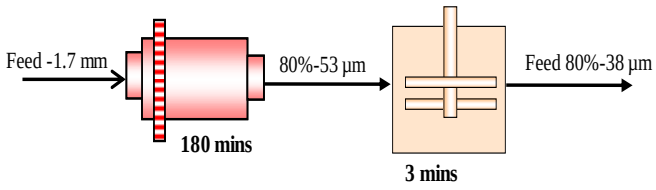

Figure 3.5: Flowsheet for the milling curve of the 80%-38 µm.

Figure 3.6: Stirred Milling Apparatus.

3.3. Mineralogical Characterisation

3.3.1. PGM Search

Polished sections that are representative of the feed samples were prepared for PGMs analysis using automated scanning electron microscopy (AutoSEM), see Figure 3.7 for the apparatus. The AutoSEM analysis relies on a bright phase search, which identifies PGMs based on their higher backscatter intensity under the electron beam, as compared to gangue minerals. The AutoSEM analysis enables the identification of all PGMs present in the sample, along with their associations with gangue, grain size distribution, and liberation characteristics.

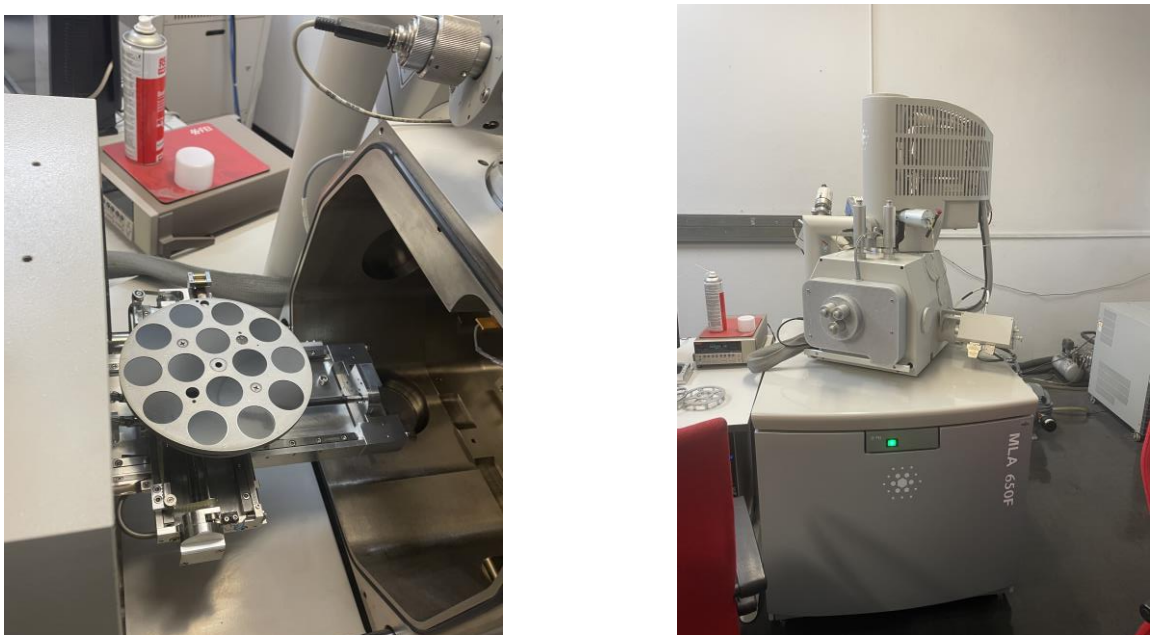

Figure 3.7: PGM search using AutoSEM apparatus.

3.3.2. Base Metal Sulphide (BMS) Search

Automated scanning electron microscopy (AutoSEM) using the MLA/QEMSCAN system was employed to perform an in-depth study of the modal mineralogy and base metal sulphide minerals present in the feed sample, see Figure 3.8 for the apparatus. The sample was subjected to screening into various size fractions before being mounted onto polished sections for MLA/QEMSCAN analysis, utilizing either the Particle Mapping Analysis (PMA) technique or the Extended BSE (XBSE) liberation analysis method. The PMA technique involves particle mapping to create false colour maps that allow for the identification and mapping of different minerals in the sample. On the other hand, the XBSE method utilizes area X-ray analysis to efficiently segment ore samples containing phases with sufficient BSE contrast.

The MLA/QEMSCAN analysis provided information on various aspects of the mineralogy of the sample, such as mineral species, grain size distribution, degree of liberation, and mineral associations. The analysis was performed on each size fraction of the sample, and the results were combined into a single result for the total sample. This combination was weighted according to the masses of the individual size fractions.

Figure 3.8: QEMSCAN machine for BMS search.

3.4. Flotation

During the investigation, flotation kinetics tests were conducted on a rougher stage using a Denver D12 flotation machine (see Figure 3.9 below) and a 5L flotation cell (Figure 3.9). After transferring the milled sample to the flotation cell, water was added to top up the cell contents to a static operating level. The impeller motor was switched on and set at an operating speed of 1200 revolutions per minute (rpm), causing the contents to form a new dynamic operating level. Reagents were added in the following order: collectors, depressants, and frothers as explained in section 2.2. A conditioning time was allowed for the reagents to function in the system. The air was then turned on to allow the froth to build up to an acceptable level for flotation.

In each kinetic test, five concentrates were collected at flotation durations of 1, 2, 4, 13, and 10 minutes, as shown in Figure 3.10. The last two concentrates were included to estimate the R_∞ and to preferentially characterize the slow-floating components. The scrapping interval during the collection of concentrates was fixed at 15 seconds. The flotation conditions employed are seen in Table 3.2.

The concentrate obtained from this scraping was collected using a tray placed below the cell launder. Throughout the test, water was added to maintain a constant dynamic operating pulp

level. The rougher flotation rate tests were conducted on 2kg feed batches made into a slurry of 30% solids by weight to generate enough sample for subsequent chemical analysis. Three reagent suites, as outlined in Table 3.4.2, were used during the tests.

Figure 3.9: Flotation apparatus including a D12 Denver machine, 5L cell, collection tray, and scrappers.

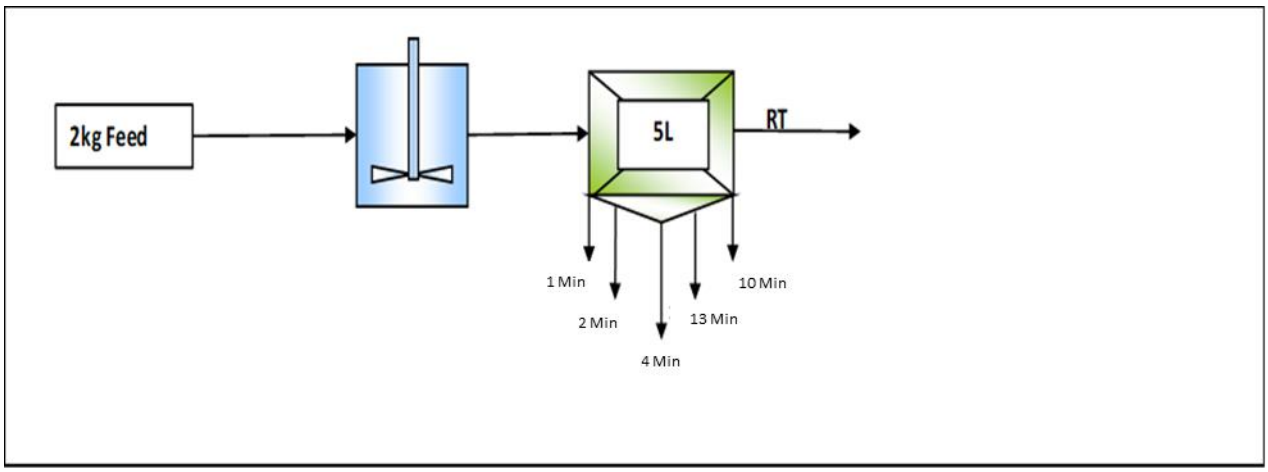

Figure 3.10: Rougher kinetic tests process flowsheet.

Table 3.2: Flotation operating conditions.

CONDITIONS												
Stage		Reagents [g/t]			Time [min]		Impeller Speed [rpm]	Air Flowrate [L/min]	pH	Eh [mV]	Cell Size [L]
		SIBX	SENDEP 30E	DOW 200	Conditioning	Float					
Grind											
Rougher Feed		80			2		1200	30			5
			250		2						
				80	1						
	RC1					1					
	RC2					2					
	RC3					4					
	RC4					13					
	RC5					10					
Total [Rougher]		80	250	80		30	1200	30			
Total [Overall]		80	250	80		30	1200	30			

The collector dosage (SIBX) was varied at three dosage levels (80, 120, 160 g/t) for each grind while maintaining the rest of the operating conditions the same. As such, three tests were done for each grind as per summary table below.

Table 3.3: Summary table for flotation test-work conditions.

Grind	Test #	Reagents [g/t] (1% solution)			Time [min]		
80% passing		SIBX	Sendep 30E	Dow 200	Mill (Min)	Condition (Min)	Float (Min)
150 µm	1	80	250	80	60	2-2-1	30
	2	120	250	80		2-2-1	30
	3	160	250	80		2-2-1	30
106 µm	1	80	250	80	80	2-2-1	30
	2	120	250	80		2-2-1	30
	3	160	250	80		2-2-1	30
75 µm	1	80	250	80	100	2-2-1	30
	2	120	250	80		2-2-1	30
	3	160	250	80		2-2-1	30
53 µm	1	80	250	80	180	2-2-1	30
	2	120	250	80		2-2-1	30
	3	160	250	80		2-2-1	30
38 µm	1	80	250	80	180 + SMD	2-2-1	30
	2	120	250	80		2-2-1	30
	3	160	250	80		2-2-1	30

After the flotation tests, the concentrates and tailings were dewatered, dried, and weighed. All 3 flotation test products for each grind were screened at 150, 75, 38 µm and samples were then sent to Mintek's Analytical Chemistry Division (ACD) for assaying of (2E) + Au and base metals (Cu and Ni) as describe in section 3.5.3. to determine the PGM recoveries across size.

3.4.1. Flotation Reagents

The following organic reagents SIBX, SENDEP 30E and DOW200 were prepared to be 1% solutions in 250 mL conical flasks during the flotation test-work programme as depicted on Figure 3.11.

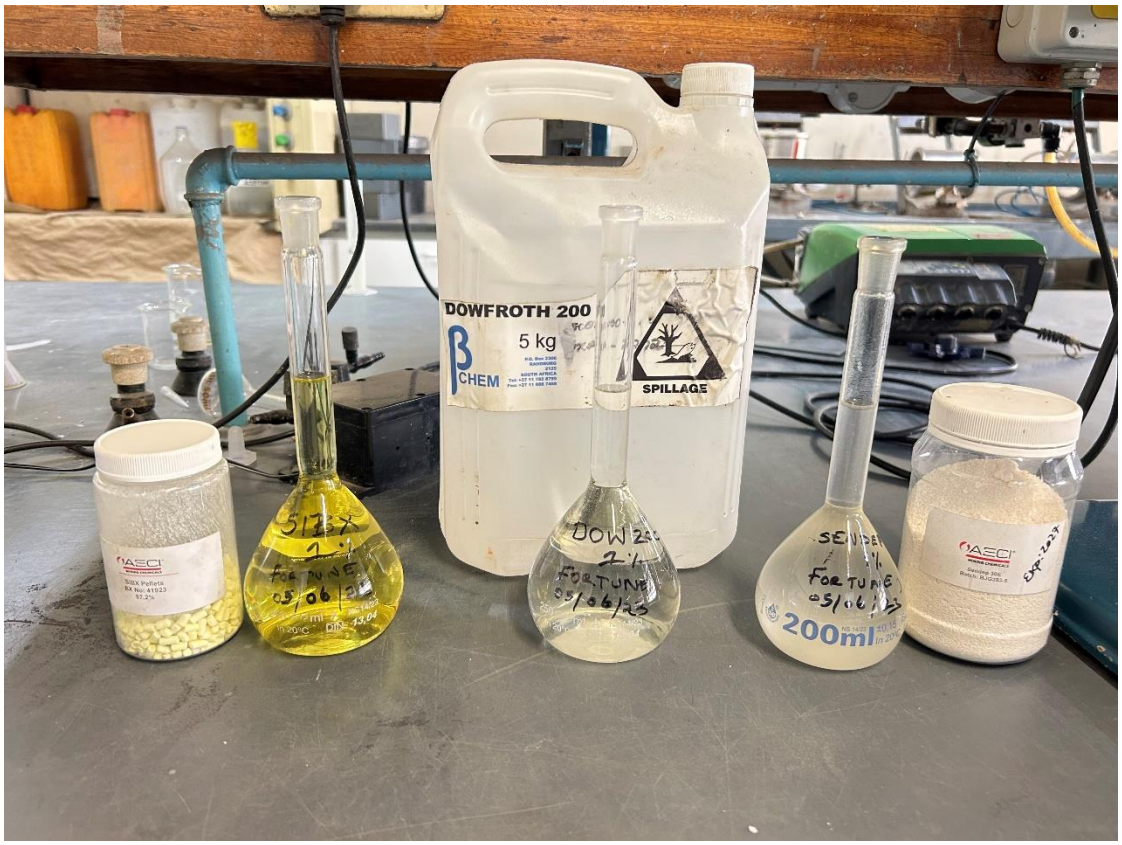

Figure 3.11: Chemical reagents used for the flotation test-work.

SIBX is a collector extensively used in mineral flotation processes, especially for sulphide minerals. It is an organic salt that preferentially adheres to the surface of sulphide minerals, inducing hydrophobicity and facilitating their separation from other minerals present in the ore. To optimize the flotation process and facilitate the extraction of the desired minerals, SIBX is usually added to the flotation pulp and conditioned for a specific duration to allow perfect mixing conditions to exist in the pulp.

SENDEP 30E is a blend of organic depressants that is frequently utilized in the flotation of sulphide ores. As a depressant, it selectively restrains the flotation of certain minerals, specifically those containing gangue like talc, serpentine, and other silicate bearing minerals. By adding SENDEP 30E to the flotation pulp, the gangue-bearing minerals can be prevented from floating, while the recovery of copper and PGM minerals can be enabled.

In flotation, DOW200 is a frother employed to improve the stability and mobility of mineralized bubbles throughout the flotation process. As discussed, the frother is added to the flotation pulp to generate a consistent foam or froth layer on the surface of the flotation cell, enabling the flotation of valuable mineral particles to the surface for recovery.

3.5. Chemical Analysis

3.5.1. Head Assays

Two 300g head sub-samples of the ore were taken for assays at Mintek's Analytical Chemistry Division (ACD). The samples were analysed as per section 3.5.3.

3.5.2. Size by Assays

To determine the (2E) + Au and base metals (Cu, Ni) deportment across size for each size fraction, size-by-assay tests were conducted on representative sub-samples of each grind sample. For each grind, a 1kg milled sample was wet screened at 25 µm, and the resulting fractions were filtered and dried. Once the +25 µm fraction was dry, the material was screened into the relevant size classes using a Pascal shaker, as outlined in Table 3.1.

3.5.3. Chemical Analysis Methods

As mentioned above, feed samples and flotation products were analysed for (2E) + Au using a standard fire assay method without high-temperature cupellation, followed by pressure dissolution of the prills using sealed glass tubes and analysed using inductively coupled plasma optical emission spectroscopy (ICP-OES) and Cu and Ni using ICP-Base_Metals. The table below illustrates the different methods and elements that each method can analyse, together with the detection limit.

Table 3.4: Chemical analysis methods

Method	Elements	Determination limit
Fire Assay: FA2	Pt, Pd, Au (2E + Au)	0.1 ppm
ICP-Base_Metals	Cu, Ni	0.05 %

The flotation products obtained from Test 3 runs, as detailed in Table 3.4, underwent wet screening with a 38 µm sieve size to assess the portion of the sample that passed through specified target sieve sizes incorporated within the √2 sieve stack. The wet screening process involved the utilization of a slurry comprising tap water, enabling the finer particles to traverse the sieve. Subsequently, the oversize sample was subjected to overnight drying in an oven,

followed by dry screening at 150 , 75 , and 38 µm. This allowed for the determination of size-specific metal recoveries, Weibull and Gamma rate distributions.

Since the fire assay method requires a substantial sample mass to accurately analyse the elemental content of Pt, Pd, and Au, Test 3 runs were performed in duplicate. The screened products were analysed using ICP exclusively for base metals as per Table 3.4. This choice the analytic method was driven by the relatively small mass of the screened samples, rendering them unsuitable for analysis via the fire assay method. To address this limitation, calibration curves derived from prior Platreef assays conducted in other projects were used. These calibration curves were constructed to establish correlations between the concentration of Cu and that of Pt, Pd, and Au. This approach allowed for the estimation of Pt, Pd, and Au contents in our screened products based on their Cu assay results.

4. RESULTS AND DISCUSSION

4.1. Milling Curves

Figure 4.1 below represents the milling curves for each targeted grind.

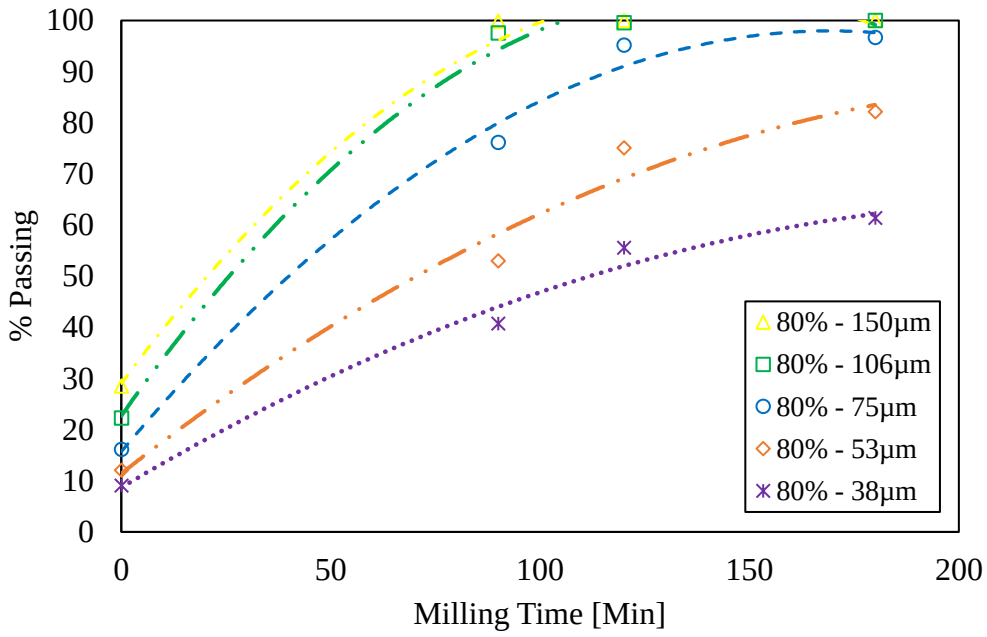

Figure 4.1: Milling curves for each grind.

Figure 4.1, shows that the milling times to achieve 80% passing 150, 106, 75, 53 µm were approximately 60, 80, 100, and 180 minutes, respectively. The 80% passing 38 µm milling test required the sample to be milled for 180 minutes to achieve a grind at a about 60% passing 38 µm and then additional milling had to be done using a stirred mill as per section 3.2. The milling time that resulted from this was an additional 3 minutes to achieve 80% passing 38 µm. These milling times were employed throughout the remainder of test work to achieve the target grinds.

4.2. Particle Size Distribution

The PSD analysis was performed on five different grinds, namely 80% passing 150, 106, 75, 53, 38 µm. The PSD analysis provides insights into the distribution of particle sizes within each grind. See Figure 4.2 below for the PSD of each grind.

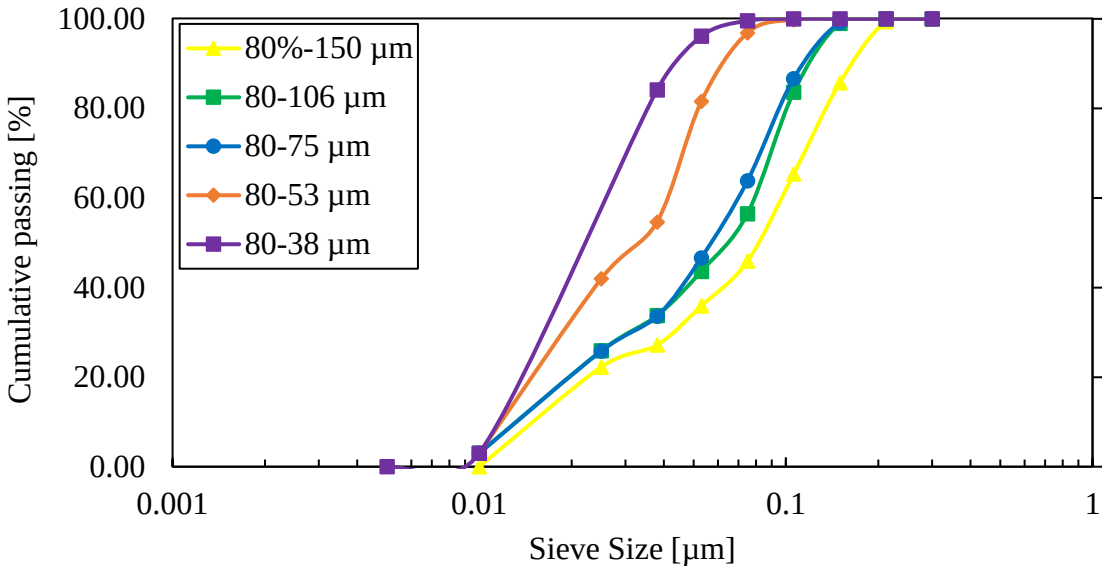

Figure 4.2: Particle size distribution for each grind.

Figure 4.2 shows that the PSD varies across the grinds as expected since each grind represents an increasing milling time from 80% passing 150 µm down to 80% passing 38 µm.

The d_{10}, d_{50}, and d_{90} values were calculated to represent the particle sizes below which 10%, 50%, and 90% of the particles are found, respectively. This data was then plotted in a form of a bar chart as depicted on Figure 4.3 below.

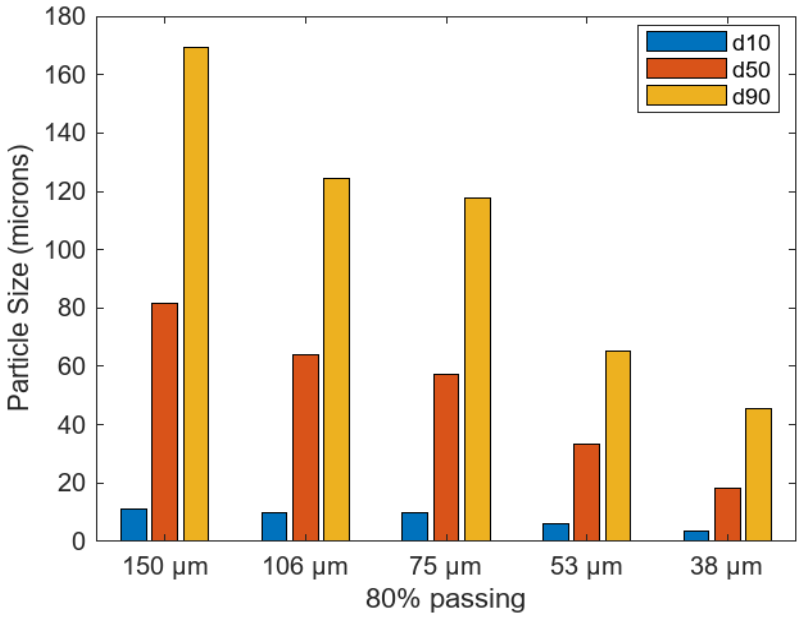

Figure 4.3: Bar chart showing d_{10}, d_{50}, and d_{90} for each grind.

Comparison of the d_{10} values show that the 80% passing 38 µm grind exhibited the smallest particle sizes with a d_{10} value of 3.6 µm, while the 80% passing 150 µm grind had the largest particle sizes with a d_{10} value of 11.2 µm. This indicates that the 80% passing 38 µm grind

contains a larger proportion of finer particles, whereas the 80% passing 150 µm grind consists of coarser particles.

Moving on to the d_{50}values, they represent the median particle size in each grind. The 80% passing 38 µm again exhibited the smallest d_{50} value, indicating a finer PSD. The 80% passing 150 µm grind, on the other hand, had the largest d_{50} value, indicating a coarser PSD.

Similarly, the d_{90} values provide insights into the upper range of particle sizes within each grind. The 80% passing 38 µm grind had the smallest d_{90} value, indicating a lower presence of larger particles. The 80% passing 150 µm grind had the largest d_{90} value, suggesting a higher occurrence of larger particles.

Overall, the PSD analysis reveals that the grinds exhibit distinct PSDs. The 80% passing 38 µm grind tends to have finer particles, while the 80% passing 150 µm contains coarser particles. This information is valuable for various applications, such as material processing, where the PSD plays a crucial role in determining the desired properties and performance of the final product. Understanding the PSD is essential for optimizing processes, milling circuit design and mill power requirements.

4.3. Head Assays and Assay by Size

The flotation feeds were characterized in terms of grades (unscreened and size-by-size). Table 4.1 below shows the unscreened feed grades from two sub-samples (A and B).

Table 4.1: Unscreened feed grades.

Sample No.	Grade						
	Pt	Pd	Au	2E+Au	Pt/Pd ratio	Cu	Ni
	g/t	g/t	g/t	g/t		(%)	(%)
Sample A	0.49	0.70	0.08	1.27	0.70	0.10	0.19
Sample B	0.54	0.69	0.31	1.54	0.78	0.09	0.19
Average	0.52	0.70	0.20	1.41	0.74	0.10	0.19

The average feed grades as per Table 4.1 are 1.41 g/t (2E)+Au, 0.10% Cu, and 0.19% Ni were used as reference checks and variance calculations for flotation calculations. Figure 4.4 presents the fluctuations in 2E (Pt and Pd) + Au feed grades as a function of particle size for different feed particle grinds (the summarised data can be seen on the appendices).

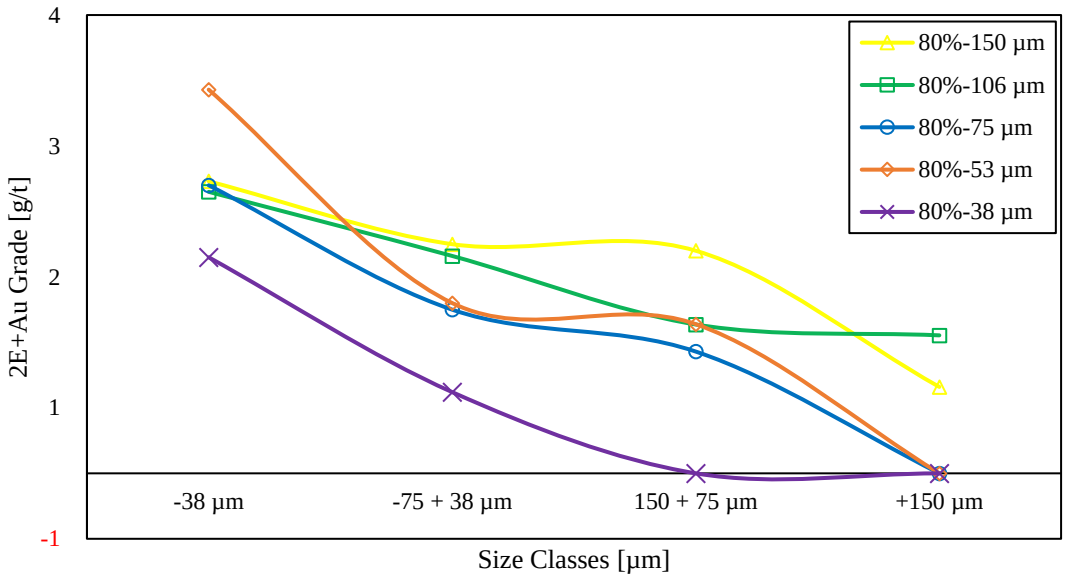

Figure 4.4: screened (2E) + Au grades by size for the Platreef ore at different feed grinds.

A discernible pattern emerges from the data, showing a gradual increase in (2E) + Au content as particle size decreases across all the grinds, reaching a notable peak in the -38 µm size category for all grinds. In the case of coarser grinds (specifically 80%-150 µm, 80%-106 µm, and 80%-75 µm), the (2E) + Au content remains relatively constant in the -38 µm fractions, hovering around approximately 2.6 g/t. Coarser size fractions in each grind generally show significantly reduced (2E) + Au content, however an elevated concentration of (2E) + Au is noticeable in the -150+75 µm size fractions for the 80%-150 µm, 80%-75 µm, and 80%-53 µm grinds. It is worth noting that in the finer grinds, reporting 0.0 g/t for the +150 µm size fraction does not indicate a complete absence of PGMs in this size range. Instead, this result stems from the lack of mass reporting to that size class due to extended grinding times, causing the 2E + Au grades to be reported as 0.0 g/t. The results seen in Figure 4.4 show that better liberation of (2E) + Au grains probably occur at -38 µm and -150+75 µm size fractions suggesting that some 2E + Au grains maybe liberated slightly coarse while others may require fine griding for liberation.

Figure 4.5 illustrate the distribution of 2E + Au in the flotation feed at different grinds, the summarised data can be seen on the appendices. Notably, all grinds exhibit high 2E + Au occurrence in the -38 µm size class, accounting for more than 30% of 2E + Au content. The finer grind, i.e 80%-38 µm, exhibited the highest distribution in the -38 µm size class, reporting nearly 94%. In contrast, the 2E + Au distribution in the +150 µm size categories are minimal.

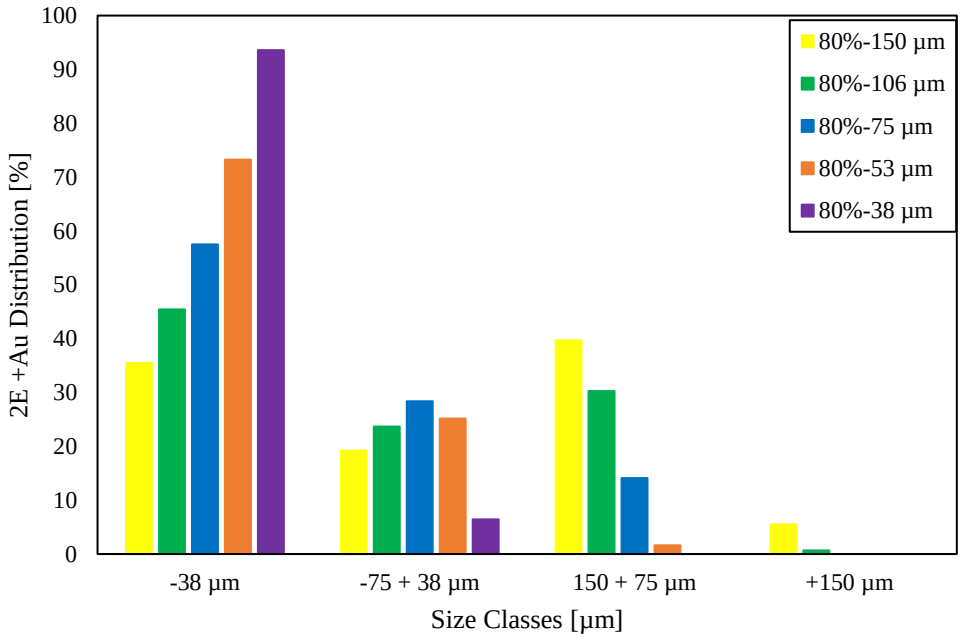

Figure 4.5: 2E + Au distribution by size for the Platreef ore at different feed grinds.

The calibration curves depicted below were used for estimating Pt, Pd, and Au contents in Test 3 flotation products for all grinds as per section 3.5.3.

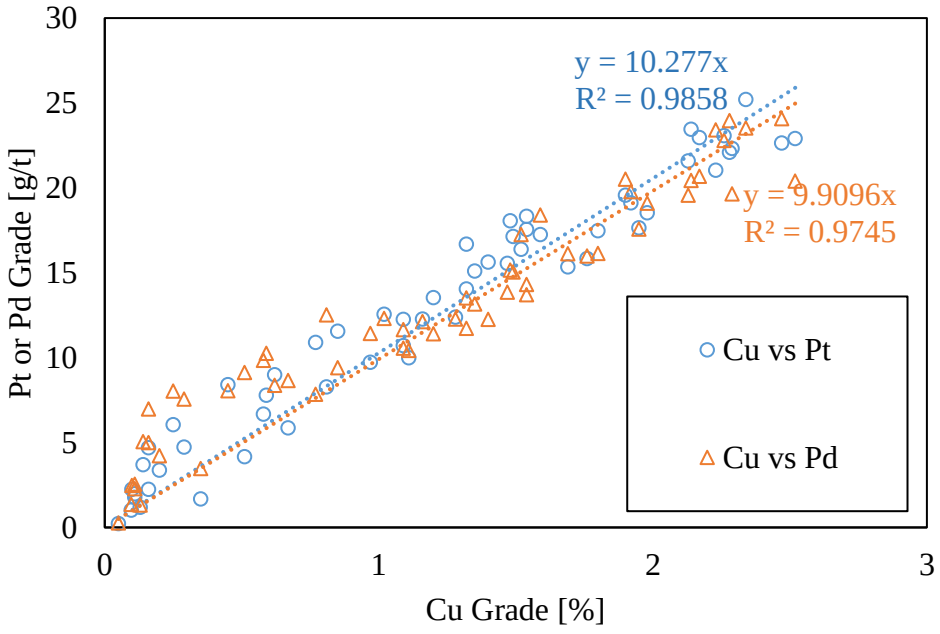

Figure 4.6: Cu vs Pt and Pd Calibration Curve.

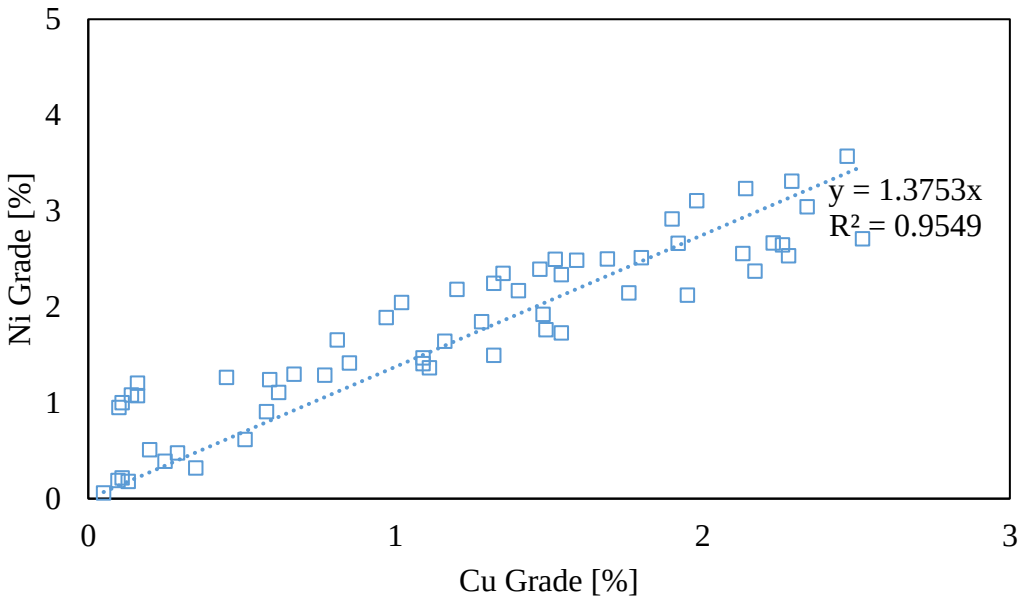

Figure 4.7: Ni vs Cu Calibration Curve.

4.4. Mineralogical Characterisation

4.4.1. PGM Search

Tables below present the distribution of PGM species per grind size;

Table 4.2: Distribution of PGM species for the 80%-150µm grind

PGM	PGM Vol %	# PGM grains	Average ECD (um)
PdBiTe	35	31	3.1
PdAs	3	3	3.5
PtPdAs	6	9	2.6
RuS	5	3	3.8
PtS	8	2	6.9
PtBiTe	4	3	3.8
PtPdBiSb	16	19	2.7
PtPdBiTe	2	4	2.4
RhIrAsS	0	1	2.4
PtAs	11	4	4.6
PdBiSb	10	2	7.9
PdSb	1	1	3.1
Total	**100**	**82**	

Distribution of PGM species for the 80%-150µm grind highlights the dominance of PdBiTe, constituting 35% of the total volume, with a relatively high abundance and average Equivalent

Circular Diameter (ECD) of 3.1 µm. Other significant species included PtPdBiSb and PtAs, with volumes of 16% and 11% respectively, indicating their importance in the sample. Additionally, variations in average ECD values among species suggested differences in grain size distribution, which could influence processing and extraction methodologies. Species with smaller grain sizes, such as PtPdBiTe and PtPdAs, may exhibit higher floatability due to their increased surface area-to-volume ratio, while those with larger grain sizes, like PtS and PdBiSb, may present challenges in achieving efficient flotation.

Table 4.3: Distribution of PGM species for the 80%-106µm grind

PGM	PGM Vol %	# PGM grains	Average ECD (um)
PdSb	2	1	5.9
PtRhAsS	6	3	4.6
PtAs	13	7	4.5
PdBiTe	20	37	2.4
PtBiTe	24	5	6.7
PtAsS	0	1	1.7
PtS	8	6	3.9
PtPdBiSb	2	2	3.9
PdBi	1	3	1.9
PtPdBiTe	21	37	2.5
PtPdAs	2	5	2.3
	100	**107**	

Distribution of PGM species for the 80%-106µm grind notably shows that PdBiTe remains a dominant species, constituting 20% of the total volume, with a significant number of grains (37) and an average ECD of 2.4 µm. However, PtBiTe emerges as a more abundant species at this grind size, comprising 24% of the volume with only 5 grains with an average ECD of 6.7 µm. This suggests a coarser liberation of PtBiTe particles compared to PdBiTe. Additionally, PtAs shows an increase in volume percentage (13%) and number of grains (7), with a slightly lower average ECD of 4.5 µm compared to PtBiTe. These variations in abundance and grain characteristics among PGM species may influence flotation behavior, with finer particles potentially exhibiting higher floatability due to increased surface area-to-volume ratio. The presence of larger PtBiTe grains could pose challenges in achieving efficient liberation and flotation at this grind size.

Table 4.4: Distribution of PGM species for the 80%-75µm grind

PGM	PGM Vol %	# PGM grains	Average ECD (um)
PdBiSb	14	16	3.8
PtS	38	15	5.7
PtPdBiSb	4	6	3.5
PtBiTe	6	5	4.6
PdBi	0	2	2.1
PdBiTe	3	16	2.1
PtPdS	20	4	9.2
PtAs	9	5	5.0
PtPdAs	2	9	2.2
PtPdBiTe	1	3	2.0
PtRhAsS	2	7	2.3
PdSb	2	2	4.1
PtRhCuS	0	2	1.4
	100	**92**	

In the 75 µm grind size data, significant differences are observed compared to the previous grind sizes. PtS emerges as the dominant species, constituting 38% of the total volume, with a substantial number of grains (15) and an average ECD of 5.7 µm. This contrasts with the dominance of PdBiTe in previous grind sizes. PtPdS also shows notable abundance, comprising 20% of the volume, with a high average ECD of 9.2 µm, indicating relatively coarse particles. PdBiSb, although present in lower abundance compared to PtS and PtPdS, exhibits a considerable number of grains (16) and an average ECD of 3.8 µm. These differences in mineralogical composition and grain characteristics suggest potential variations in flotation behavior at this grind size. PtS and PtPdS, with coarser particles, may require different flotation strategies compared to finer particles like PdBiTe observed in previous grind sizes. The abundance of PtS and PtPdS could also impact circuit design and reagent selection for optimal recovery of valuable PGM species.

Table 4.5: Distribution of PGM species for the 80%-53µm grind

PGM	PGM Vol %	# PGM grains	Average ECD (um)
PdBiTe	15	25	2.3
PtBiTe	21	6	5.0
PdBiSb	6	2	5.9
PtAs	45	6	8.1
PtPdBiSb	6	5	3.2
PtBiSb	4	1	6.7
PtPdBiTe	1	1	2.5
PtPdAs	1	2	2.1
PtRhAsS	1	1	3.0
	100	**49**	

At the 53 µm grind size, the mineralogy data indicates further shifts in PGM species distribution compared to coarser grind sizes. PtAs emerges as the dominant species, constituting 45% of the total volume, with a relatively low number of grains (6) but a high average ECD of 8.1 µm, indicating coarse particles. This contrasts with the dominance of PdBiTe and PtBiTe observed in previous grind sizes. PtBiTe and PdBiTe remain significant, comprising 21% and 15% of the volume respectively, PtBiTe has a smaller number of grains (6) compared to 25 grains of PdBiTe. PdBiSb and PtPdBiSb also show notable abundance, each comprising 6% of the total volume. These species exhibit variations in grain characteristics, with PdBiSb showing a higher average ECD (5.9 µm) compared to PtPdBiSb (3.2 µm). The prevalence of coarser particles in PtAs and PtBiTe could influence flotation behaviour, potentially requiring adjustments in processing conditions to achieve optimal recovery. Additionally, the presence of multiple PGM species with varying characteristics underscores the importance of comprehensive mineralogical analysis in optimizing flotation performance and maximizing metal recovery.

4.4.2. BMS Modal Mineralogy

The primary base metal sulfides in the ore consist predominantly of pyrrhotite, accounting for approximately 41.90% of the mass, along with pentlandite. These are accompanied by chalcopyrite, comprising around 21.24% of the mass, and minor quantities of pyrite at 2.42% mass. Additionally, other sulfides constitute a minimal proportion, totalling 0.14% by mass as depicted by Figure 4.8 below.

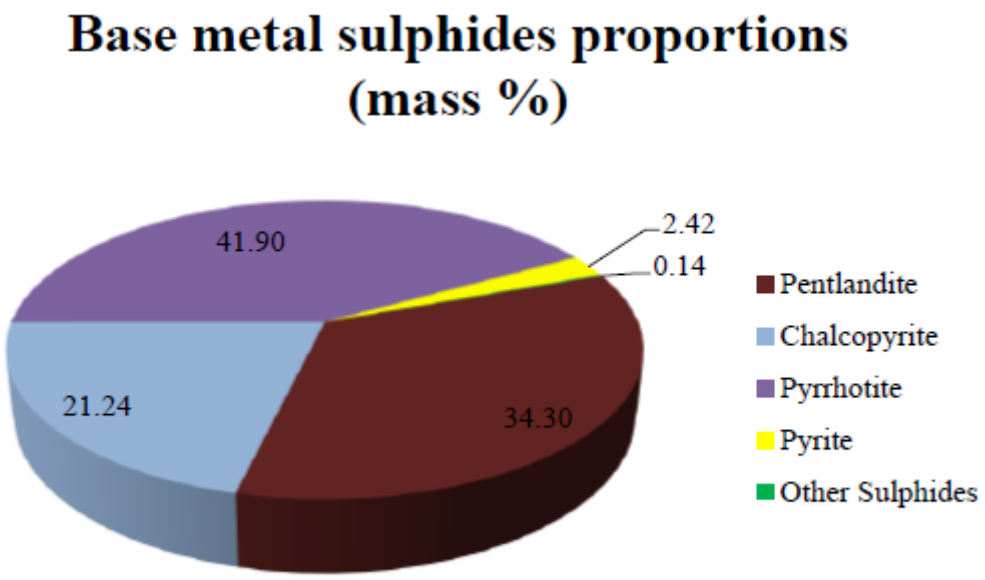

Figure 4.8: Bulk modal BMS proportions.

4.5. Numerical Integration

In the realm of characterizing flotation kinetics, the conventional approach has often relied on deterministic rate parameters and maximum recoveries. However, the inherent variability observed in flotation performance—be it due to particle size, association, liberation, or composition—necessitates a more nuanced understanding of this complex process. Pioneering works by Sutherland and Imaizumi and Inoue have underscored the impact of distributed process variables on flotation performance, paving the way for the development of mathematical models. Central to these models is the integration of the recovery function $R(t)$. In this section, we delve into the numerical integration of Equation 2.4.10 for only the Gamma model, exploring its utility in quantifying flotation rate heterogeneity. This integration, exemplified by Equation 2.4.10, offer invaluable insights into the dynamics of particle recovery, further enriching our comprehension of flotation kinetics.

We shall now re-examine Equation 2.4.10 presented below before we commence numerical integration;

$$R(t) = R_{\infty}\,(1 - \int_0^{\infty} e^{-kt} f(k)dk) \qquad \text{(Equation 2.4.10)}$$

4.5.1. Gamma Model Integration

The PDF of the Gamma flotation rate constant distribution, as expressed in Equation 2.4.15 above, has been revisited below:

$$f(k) = \left(\frac{\beta^{\alpha+1}}{\Gamma(\alpha+1)}\right) \cdot k^{\alpha} \cdot e^{-\beta \cdot k} \qquad \text{(Equation 2.4.15)}$$

Substituting Equation 2.4.15 above into Equation 2.4.10 gives;

$$R(t) = R_{\infty}\left(1 - \int_0^{\infty} e^{-kt} \cdot \left(\frac{\beta^{\alpha+1}}{\Gamma(\alpha+1)}\right) \cdot k^{\alpha} \cdot e^{-\beta \cdot k} dk\right)$$

Rewriting the above equation taking into consideration the properties of exponents and moving the constants (variables that are not a function of k) outside the integral gives;

$$R(t) = R_{\infty}\left(1 - \left(\frac{\beta^{\alpha+1}}{\Gamma(\alpha+1)}\right) \cdot \int_0^{\infty} k^{\alpha} \cdot e^{-(\beta+t) \cdot k} dk\right)$$

To solve this integral, a change of variable is needed to simplify the expression. Let name u as;

$$u = (\beta + t) \cdot k$$

This implies that;

$$du = (\beta + t) \cdot dk$$

Solving for dk;

$$dk = \frac{1}{\beta+t} \cdot du$$

Additionally, $\frac{u}{\beta+t} = k$

Substituting the previous two equations into the integral above simplifies to;

$$R(t) = R_{\infty}\left(1 - \left(\frac{\beta^{\alpha+1}}{\Gamma(\alpha+1)}\right) \cdot \frac{1}{\beta+t} \cdot \int_0^{\infty} \left(\frac{u}{\beta+t}\right)^{\alpha} \cdot e^{-u} \cdot du\right)$$

Simplification of the integral term gives;

$$R(t) = R_{\infty}\left(1 - \left(\frac{\beta^{\alpha+1}}{\Gamma(\alpha+1)}\right) \cdot \frac{1}{(\beta+t)^{\alpha+1}} \cdot \int_0^{\infty} u^{\alpha} \cdot e^{-u} \cdot du\right)$$

Employing the properties of the Gamma Function as depicted below;

$$\int_0^{\infty} u^{\alpha} \cdot e^{-u} \cdot du = \Gamma(\alpha+1)$$

Therefore, the equation simplifies to;

$$R(t) = R_\infty \left(1 - \left(\frac{\beta^{\alpha+1}}{\Gamma(\alpha+1)}\right) \cdot \frac{1}{(\beta+t)^{\alpha+1}} \cdot \Gamma(\alpha+1)\right)$$

Cancelling like-terms and simplifying further;

$$R(t) = R_\infty \left(1 - \left(\frac{\beta}{\beta+t}\right)^{\alpha+1}\right) \qquad \text{(Equation 4.1.1)}$$

The expression presented above, denoted as Equation 4.1.1, illustrates the kinetic Gamma model applied in flotation.

4.5.2. Weibull Model Integration

The PDF of the Weibull flotation rate constant distribution, as expressed in Equation 2.4.16 above, has been revisited below:

$$f(k) = \left(\frac{n}{k_m}\right) \cdot \left(\frac{k}{k_m}\right)^{n-1} \cdot e^{\left(-\left(\frac{k}{k_m}\right)^n\right)} \qquad \text{(Equation 2.4.16)}$$

Substituting Equation 2.4.16 above into Equation 2.4.10 gives;

$$R(t) = R_\infty \left(1 - \int_0^\infty e^{-kt} \cdot \left(\frac{n}{k_m}\right) \cdot \left(\frac{k}{k_m}\right)^{n-1} \cdot e^{\left(-\left(\frac{k}{k_m}\right)^n\right)} dk\right)$$

Rewriting the above equation taking into consideration the properties of exponents and moving the constants (variables that are not a function of k) outside the integral gives;

$$R(t) = R_\infty \left(1 - \left(\frac{n}{k_m}\right) \cdot \int_0^\infty \left(\frac{k}{k_m}\right)^{n-1} \cdot e^{-\left(\left(\frac{k}{k_m}\right)^n + kt\right)} dk\right)$$

The integration of the expression above gives the cumulative distribution function (CDF) for the Weibull model according to Ahmed, 1995 shown below

$$R = R_\infty \left(1 - e^{-\left(\frac{t}{k_n}\right)^n}\right) \qquad \text{(Equation 4.1.2)}$$

4.6. MATLAB Parameter Estimates

In the process of fitting flotation models to experimental data, the selection of appropriate initial parameter guesses, and the imposition of upper and lower bounds play a pivotal role in the optimization process. The choice of initial guesses is fundamental as it determines the starting point for the optimization algorithm. Poor initial guesses can lead to convergence to local minima, resulting in inaccurate parameter estimates. This is particularly significant when applying complex models such as the Gamma and Weibull models, which comprises multiple parameters. For instance, where the Gamma model is employed for fitting, the initial guesses for parameters R_∞, a, and b greatly influence the fitting process. Inaccurate initial guesses, such as those provided by the default values, can hinder the convergence of the optimization algorithm, often leading to unusually small or large values that do not represent the system's true behaviour.

Furthermore, the specification of upper and lower bounds on parameters is essential to maintain physical realism in the estimated values. In practice, these bounds prevent the optimization algorithm from exploring unrealistic regions of parameter space. While it is common to establish lower bounds to enforce non-negativity, upper bounds can also be critical, particularly when certain parameters should not take excessively large values. By setting appropriate bounds, we ensure that parameter estimates align with the physical interpretation of the parameters. This is particularly relevant in the context of flotation modelling, where parameters often carry meaningful physical interpretations. Without bounds, optimization might produce estimates that lack physical realism and may not accurately represent the underlying flotation process.

To fully understand the importance of near-accurate parameter initial guesses, the MATLAB code, as seen on the Appendices, will be used to demonstrate how changing the initial values of a and b for Gamma and n and k_m for Weibull have an effect on your model fitting. When setting the initial guesses for the shape factors, i.e a and n to be $\gg 1$, the following model fittings results;

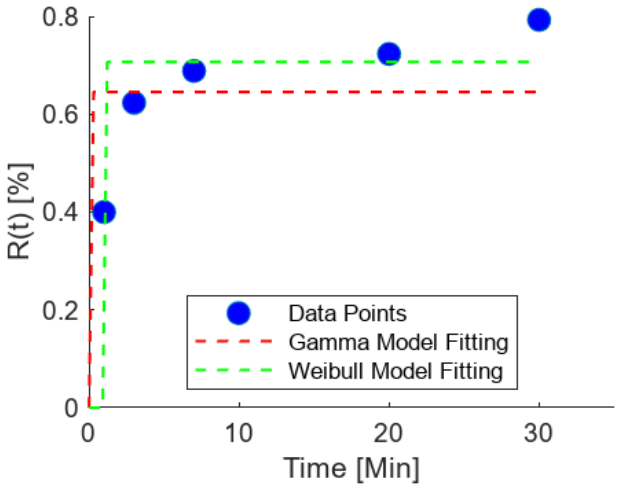

Figure 4.9: How inaccurate initial shape parameters affect model fittings, a case for a and n to be $\gg 1$.

When setting the initial guesses for the scale factors, i.e b and k_m to be $\ll 0$, the following model fittings results;

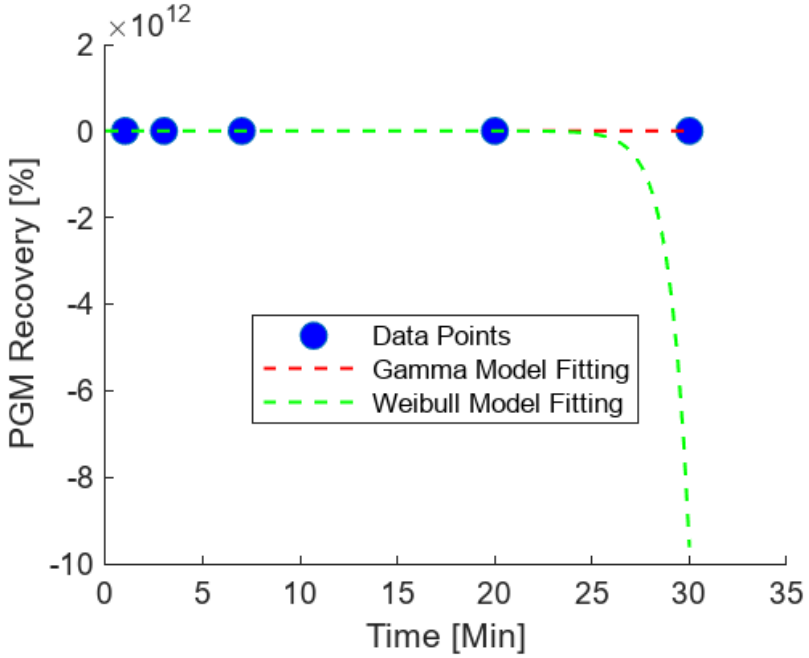

Figure 4.10: How inaccurate initial shape parameters affect model fittings, a case for b and k_m to be $\ll 0$.

In the context of this dissertation, lower bounds were defined as [0.00, 0.00] for the parameters $[a, b]$ in the Gamma model and [0.00, 0.00] for $[n, k_m]$ in the Weibull Model. These lower bounds were established to ensure that the least squares estimation method avoids selecting negative values as global minima for these parameters, thus maintaining the physical integrity of the models. To facilitate a valid comparison, the initial parameter guesses for the shape parameters were consistently held at identical values for both models. While these initial

guesses could be modified for specific analytical purposes, maintaining uniformity in the initial guesses served the purpose of facilitating a meaningful and equitable comparison between the models. The same principle applied to the scale parameters as well.

In summary, the careful consideration of initial parameter guesses and the judicious application of upper and lower bounds are essential for accurate parameter estimation in flotation modelling. In the case of our specific dataset, which involves the Gamma model, the choice of initial guesses and bounds can greatly impact the quality of the fitting results, ultimately influencing the reliability of the flotation model and its ability to describe the experimental data effectively.

4.7. Statistical Analysis

In the context of statistical evaluation, R-squared (R^2) and root mean squared error (RMSE) were employed as metrics to evaluate the performance of regression models. The formula utilized for calculating R^2 is provided as follows:

$$R^2 = 1 - \frac{RSS}{TSS} \qquad \text{(Equation 4.7.1)}$$

Here, RSS represents the sum of the squared residuals, which signifies the disparity between observed and predicted values. TSS, on the other hand, represents the total sum of squares, illustrating the variance between observed values and the mean value. The formula for calculating RMSE is presented in Equation 4.7.2 below:

$$RMSE = \sqrt{\sum_{i=1}^{N} \frac{\left(R_{actual} - R_{predicted}\right)^2}{N}} \qquad \text{(Equation 4.7.2)}$$

Where R_{actual} is the actual recovery value, $R_{predicted}$ is the model recovery value, and N is the number of observations in the dataset.

4.8. Flotation

In this dissertation, we investigated the applicability of two commonly employed distribution models, the Gamma and Weibull distributions, in fitting flotation rate data for different grind sizes of Platreef ore, specifically at 80% passing 106, 75, 53, and 38 µm. The summarised data used for plotting the figures below may be found on the appendices.

4.8.1. Gamma versus Weibull

The analysis of Figure 4.11 (a) to (e) below offers insights into the performance of these models.

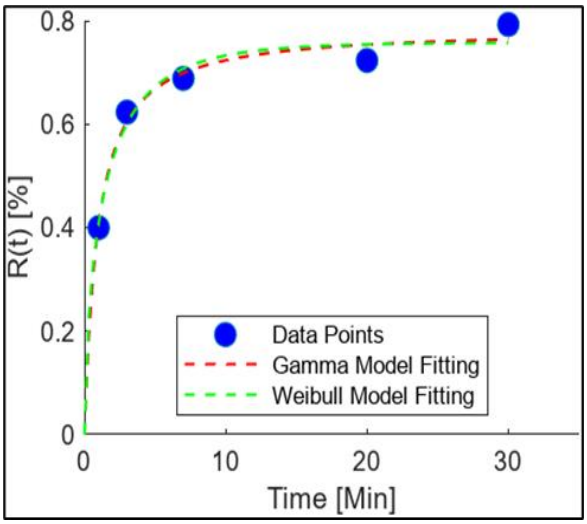

(a)

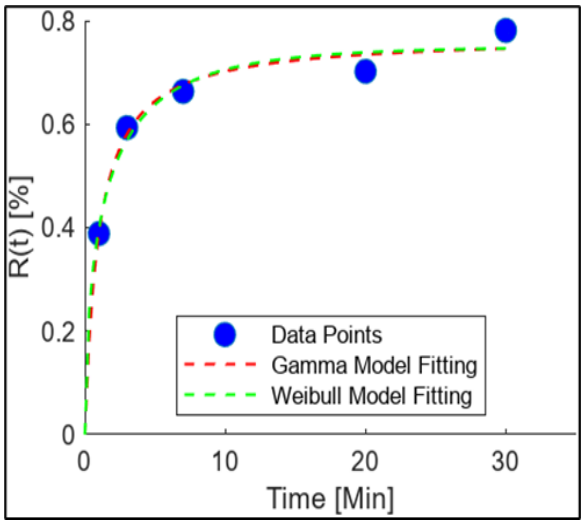

(b)

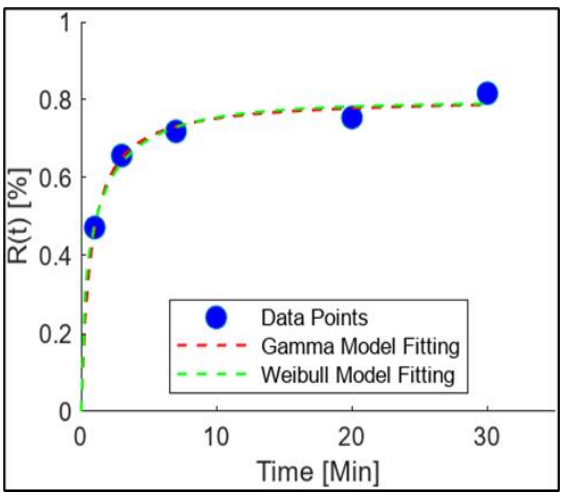

(c)

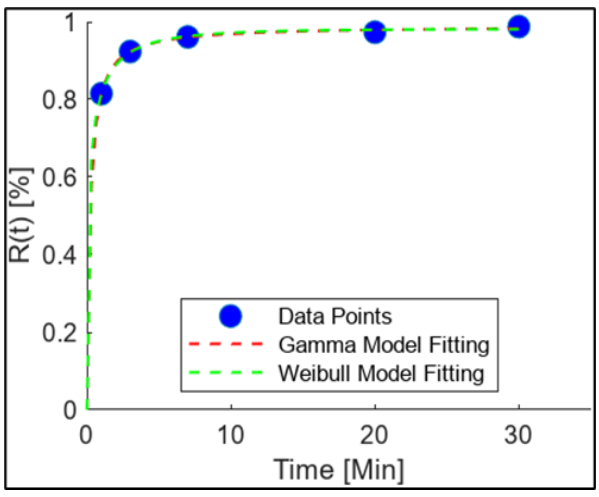

(d)

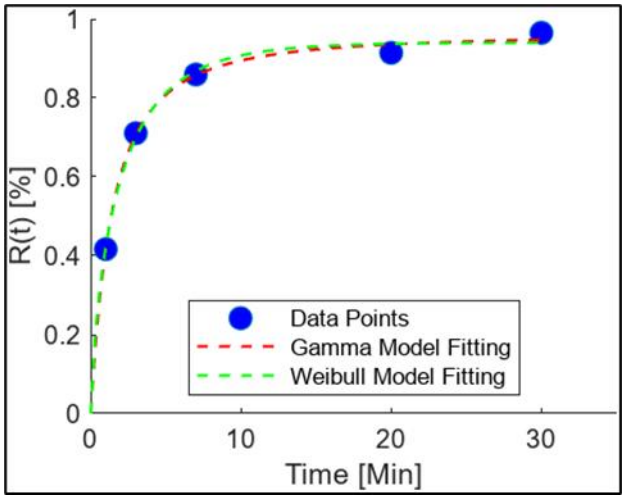

(e)

Figure 4.11: Flotation rates with Gamma and Weibull models fitted for (a) 80%-150 µm, (b)80%-106 µm, (c) 80%-75 µm, (d) 80%-53 µm, and (e) 80%-38 µm.

Both models exhibit nearly overlapping results, indicating that their fitting accuracy is comparable. Notably, the Gamma and Weibull models consistently showcase impressive proficiency in fitting flotation data across all grind sizes, underscoring their resilience and adaptability. While both models excel in efficiently fitting flotation data, looking closely at the dataset, it becomes apparent that their effectiveness slightly diminishes as grind sizes become coarser, from (e) to (a) on Figure 4.11 above, particularly in the case of the Weibull model. To explain this, we further examined the recoveries associated with each grind size.

In the case of 80%-150 µm, the Gamma model yielded an ultimate maximum recovery (R_∞) of approximately 78.35%, while the Weibull distribution produced a slightly lower recovery of approximately 75.79% compared to the actual recovery of 79.29%. In the case of 80%-106 µm grind size, the Gamma exhibited its superior predictive capabilities with R_∞ of approximately 77.03%, while the Weibull model estimated approximately 75.02% compared to the actual recovery of 78.13%. The trend persisted at 80%-75 µm, where the Gamma model achieved a $R_\infty$of roughly 80.58% surpassing the Weibull's recovery rate of approximately 79.31%. However, as we transitioned to finer grinds, the disparities became less pronounced.

At 80%-53 µm, the Gamma model maintained its efficiency with a recovery rate of about 98.95% whereas the Weibull distribution's performance, noticeably still less than the Gamma's, resulted in a recovery rate of approximately 98.19% compared to the actual recovery of 98.7%. Finally, at the 80%-38 µm grind size, the Gamma model outperformed the Weibull model yet again, with a recovery rate of around 98.19% compared to the Weibull's recovery of approximately 94.04% These results underscore the Gamma distribution's remarkable

consistency in accurately modelling flotation rate data across various grind sizes, emphasizing its potential for widespread application in the field of ore processing.

Regression analysis was employed to identify the most suitable data fitting model from the listed options, aiming to offer a quantitative comprehension of the underlying factors impacting the flotation process. The residual analysis, a statistical technique utilized to appraise the precision of the models, was utilized to assess the quality of model fitting. Table 4.6 below illustrates these parameters as calculated as per section 4.7;

Table 4.6: Summary results for Test 1s (80 g/t SIBX collector dosage) per grind.

Grind	Gamma Model				Weibull Model			
80% passing: (µm)	a	b	R^2	$RSME$	k_m	n	R^2	$RSME$
150	0.087	1.036	0.975	0.021	1.480	0.641	0.964	0.025
106	3.45×10^{-6}	0.974	0.971	0.022	1.613	0.569	0.962	0.026
75	1.23×10^{-7}	0.711	0.977	0.018	1.152	0.513	0.970	0.02
53	0.008	0.218	0.997	0.004	0.247	0.410	0.995	0.004
38	1.097	2.088	0.987	0.018	1.269	0.772	0.981	0.022

The R^2 and $RSME$ values presented are consistent with the earlier discussion, confirming the Gamma model's superior fitting performance in comparison to the Weibull model. This is evident from the higher R^2 values and lower $RSME$ values of the Gamma model, both exceeding 95% accuracy and staying within a 0.03 error margin.

This discrepancy may be attributed to the inherent differences in the nature of particle interactions at distinct grind sizes. The disparity in recovery percentages further corroborates these findings, with the Gamma model consistently outperforming the Weibull distribution in predicting recovery rates. These results underscore the importance of selecting the most appropriate distribution model based on the specific ore characteristics and grind sizes to ensure accurate and reliable flotation rate predictions. When this concept is applied within the framework of liberation, wherein longer grinding times correspond to increased liberation, it

prompts the question of whether higher liberation, regardless of specific ore characteristics, leads to improved fitting results.

To investigate this question, one may look at the overall effect of the Gamma and Weibull models as per section 4.8.2 below.

4.8.2. Effect of particle liberation on Gamma and Weibull models

The figures below depict the effect of liberation on Gamma and Weibull model's accuracy in fitting recovery data for Platreef ores. The summarised data used for plotting Figure 4.12 below may be found on the appendices.

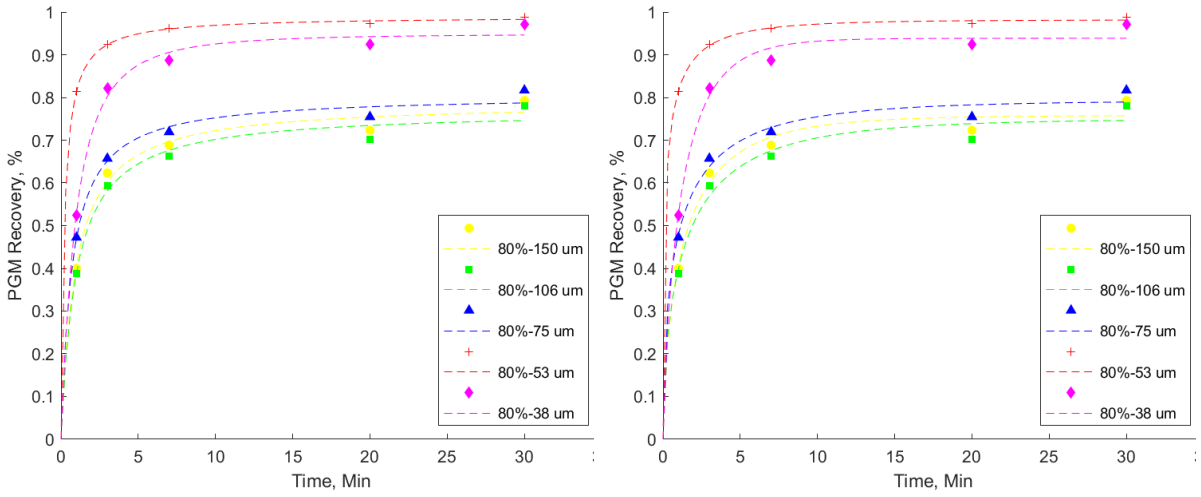

(a) (b)

Figure 4.12: Effect of liberation on (a) Gamma and (b) Weibull models accuracy in fitting recovery data.

A salient observation emerges when Figure 4.12 is carefully considered. The fitting for both Gamma and Weibull models is more accurate in the initial stages of flotation for all particle grinds i.e. first 5 minutes, and at higher flotation times the fitting becomes more accurate the finer the grind with 80%-53 µm showing the best fit. Therefore, grinding process appears to exert a discernible influence on the accuracy and goodness of fit of the models when applied to flotation recoveries. This phenomenon becomes particularly pronounced with increasing residence times, specifically those ≥ 20 minutes, wherein the model's curves exhibit conspicuous deviations from the actual dataset. This apparent sensitivity of the models to the grind parameter in the context of flotation recoveries merits a comprehensive discussion. The association between grind and model accuracy is a complex interplay of several factors. Firstly, the PSD of the ore influences the liberation and exposure of valuable minerals for flotation.

Coarser grinds may not provide the requisite level of liberation, leading to reduced recovery rates as per Figure 4.12 while excessively fine grinds can lead to excessive overgrinding, which also negatively impacts recovery by generating valuable fines that prove challenging to extract through flotation.

Secondly, the chemical analysis method may produce variability in the ore composition, with variations in mineral composition, gangue mineral content, and other ore characteristics impacting the flotation process data. Such variations can render the modelling process challenging, particularly when using fixed models like the Gamma and Weibull distribution. Furthermore, higher residence times can amplify the influence of grind due to the prolonged exposure of particles to the flotation environment. During extended residence times, variations in grind size can become more pronounced, leading to increasingly noticeable deviations in the models fit to the actual data, especially in plant or industry scale processes.

An additional noteworthy feature on Figure 4.12 (a) and (b) pertains to the superior recovery rates observed for the coarser 80%-53 µm grind in comparison to the finer 80%-38 µm grind. This phenomenon can be predominantly attributed to the concave relationship between recovery and grind size, wherein recovery rates exhibit an ascent up to a specific point, commonly termed the "optimum grind," followed by a subsequent decline. The discussion surrounding this intriguing observation is pivotal for understanding the underlying dynamics of the recovery-grind relationship. The concave shape of the recovery curve in relation to grind size is indicative of the interplay between several critical factors mentioned on section 2.

In the context of flotation rate distributions in the field of mineral processing, "$f(k)$ vs k curves" often termed “rate distributions” are used to represent the distribution of flotation rates for different particle sizes or mineral species. These curves provide valuable insights into the efficiency and selectivity of the flotation process as previously stated.

The respective rate distributions as modelled by the Gamma and Weibull models on Figure 4.12 (a) and (b) above are shown on Figure 4.13 (a) and (b).

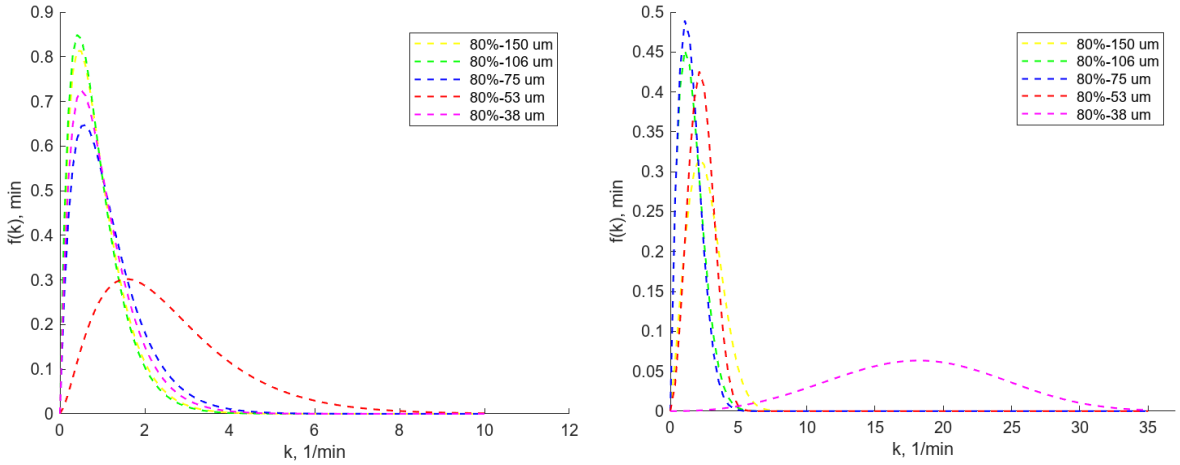

Figure 4.13: Rate distributions modelled using the (a) Gamma and (b) Weibull models based on Figure 4.12 data.

An examination of the depicted rate distributions yields valuable insights into the flotation process's efficiency. This aspect is often underexplored in the existing literature, which predominantly concentrates on rate distribution modelling rather than elucidating the information these distributions convey. Moreover, while most authors explain how altering shape and scale parameters impacts the distribution, they typically neglect to emphasize the underlying significance. This author contends that the shape of the distribution bears greater importance than what is conventionally acknowledged. Specifically, a distribution skewed towards higher k values signify the rapid and efficient recovery of a substantial portion of PGM particles as depicted by Gamma distribution for the 80%-53 μm on Figure 4.13(a). Conversely, a distribution skewed towards lower k values suggests that many particles or PGM minerals exhibit slower attachment to bubbles, resulting in less efficient recovery.

The pronounced prevalence of low k values in the Gamma distributions for other particle grinds implies that a significant portion of these particles exhibits slow flotation behavior. This phenomenon may be attributed to either inadequate liberation in the case of coarser grinds or the challenges associated with floating finer particles mixed with slimes in the 80-38 µm range. To attain more favourable outcomes, various parameters can be adjusted as follows:

- Reagent Dosages: Altering the type and quantity of reagents can reshape the curve, leading to an optimization of valuable mineral recovery.
- Pulp Density: Modifying the solid-liquid ratio of the slurry can influence the collisions and attachment of particles to bubbles, thereby affecting the curve.
- Agitation: Adjusting the agitation level within the flotation cell can enhance interactions between bubbles and particles, ultimately improving recovery rates.

A significant insight that can be gleaned from the Weibull distributions presented in Figure 4.13(b) pertains to the distribution's peak, which signifies the proportion of particles exhibiting the mean rate constant value. When examining Figure 4.13, it becomes evident that coarser grinds predominantly feature a substantial number of particles with lower rate constants. In contrast, the 80%-38 µm grind displays a relatively higher proportion of particles with higher rate constants, as evidenced by the rightward shift of the peak. This observation underscores the inherent complexity of the flotation process. Relying solely on one model for characterizing the process may lead to incomplete insights. Different models can reveal distinct facets of the process, and their combined use can provide a more comprehensive understanding. In this case, the Weibull distributions elucidate variations in rate constants among particle sizes, shedding light on the intricate interplay of factors impacting the flotation process.

4.8.3. Effect of reagent dosage on Gamma and Weibull models

As indicated in Table 3.3, the collector (SIBX) dosage was raised from 80 g/t to 120 g/t at a standard concentration of 1%, aiming to investigate whether this adjustment of collector dosage would lead to any alterations in the goodness of fits or the rate distributions for both models. The summarised data obtained from plotting Figures 4.14 and 4.15 below are found on Table 4.7 and Table 4.8.

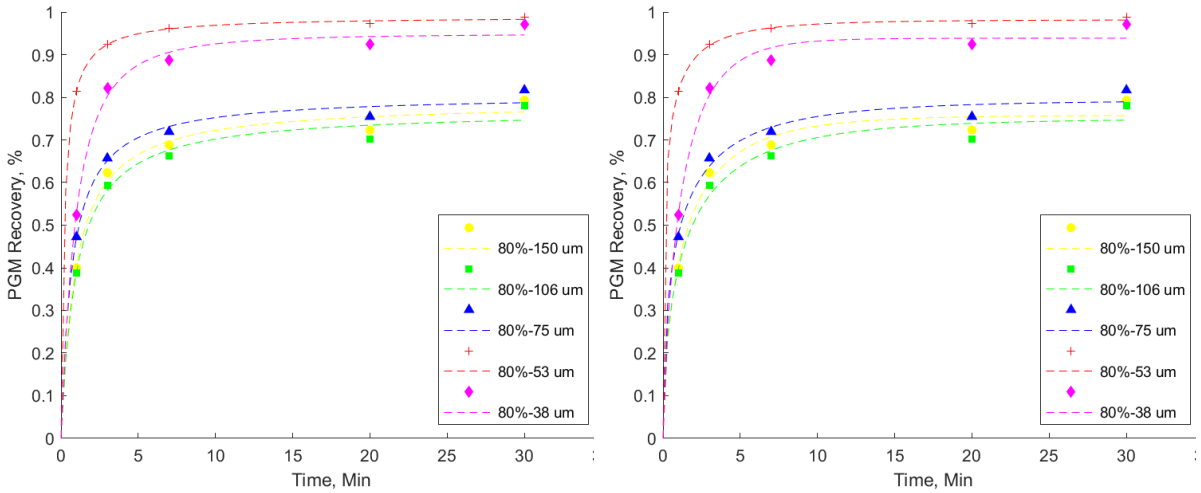

(a) (b)

Figure 4.14: Effect of collector dosage on (a) Gamma and (b) Weibull models accuracy in fitting recovery data (case for 80 g/t SIBX).

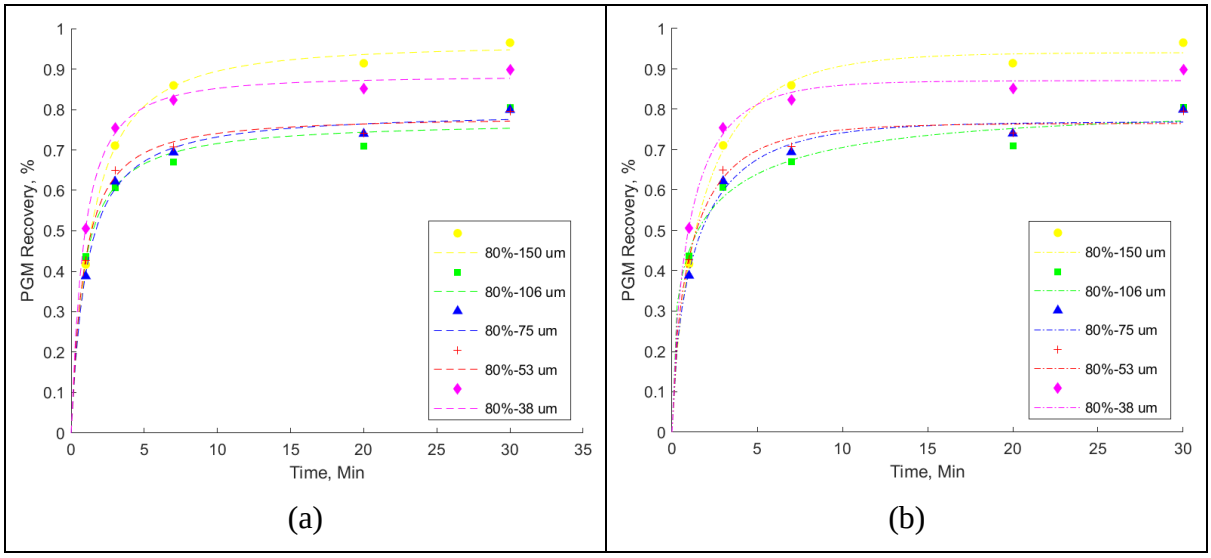

Figure 4.15: Effect of collector dosage on (a) Gamma and (b) Weibull models accuracy in fitting recovery data (case for 120 g/t SIBX)

Table 4.7: Summary data for the effect of collector dosage on the Gamma model's goodness of fit.

Grind	Gamma Model (80 g/t SIBX)				Gamma Model (120 g/t SIBX)			
80% passing: (µm)	a	b	R^2	$RSME$	a	b	R^2	$RSME$
150	0.087	1.036	0.975	0.021	0.586	2.295	0.996	0.013
106	3.45×10^{-6}	0.974	0.971	0.022	2.25×10^{-14}	0.814	0.940	0.03
75	1.23×10^{-7}	0.711	0.977	0.018	0.137	1.201	0.983	0.018
53	0.008	0.218	0.997	0.004	0.306	1.172	0.981	0.017
38	1.097	2.088	0.987	0.018	0.597	1.400	0.989	0.014

Table 4.8: Summary data for the effect of collector dosage on the Weibull model's goodness of fit

Grind	Weibull Model (80 g/t SIBX)				Weibull Model (120 g/t SIBX)			
80% passing: (µm)	k_m	n	R^2	$RSME$	k_m	n	R^2	$RSME$
150	1.480	0.641	0.964	0.025	1.991	0.750	0.993	0.017
106	1.613	0.569	0.962	0.026	1.563	0.416	0.948	0.028
75	1.152	0.513	0.970	0.020	1.615	0.660	0.974	0.023
53	0.247	0.410	0.995	0.004	1.307	0.664	0.972	0.021
38	1.269	0.772	0.981	0.022	1.200	0.693	0.983	0.018

An insightful observation can be drawn from our analysis of Figure 4.14 and Figure 4.15 and Table 4.7 and Table 4.8. It is evident that the dosage of the collector does not significantly impacts the accuracy and goodness of fit of the models in the context of flotation recoveries as seen by comparable R^2 and $RSME$ values for both Test 1 (80 g/t SIBX) and Test 2 (120 g/t SIBX). Nonetheless, PGM recoveries were affected, particularly for the 80%-53 µm and 80%-38 µm grinds where a decrease in recoveries was noted at higher collector dosages. This is most likely a result of hindered selectivity achieved with higher collector dosages. A higher dosage of SIBX proves more effective for UG2 compared to Platreef (Doubra et al, 2023). UG2 ore may necessitate a slightly higher dosage due to limited floatability of valuable mineral species when combined with a co-collector like dithiophosphate. Conversely, the complex composition of Platreef ore may include Pd minerals with a strong affinity for collectors, facilitating effective flotation at lower dosages. To mitigate higher gangue recovery, many operations have chosen to increase depressant concentrations. However, elevating the depressant dosages while maintaining the same collector and frother dosage may result in decreased Pd recovery, likely due to excessive depressant use, hindering collector attachment and froth destabilization.

The impact that alterations in collector dosages have on rate distributions is shown in Figure 4.16 and Figure 4.17. This examination provides valuable insights into process optimization

and offers strategies for managing scale and shape factors to achieve the most favourable process behaviour.

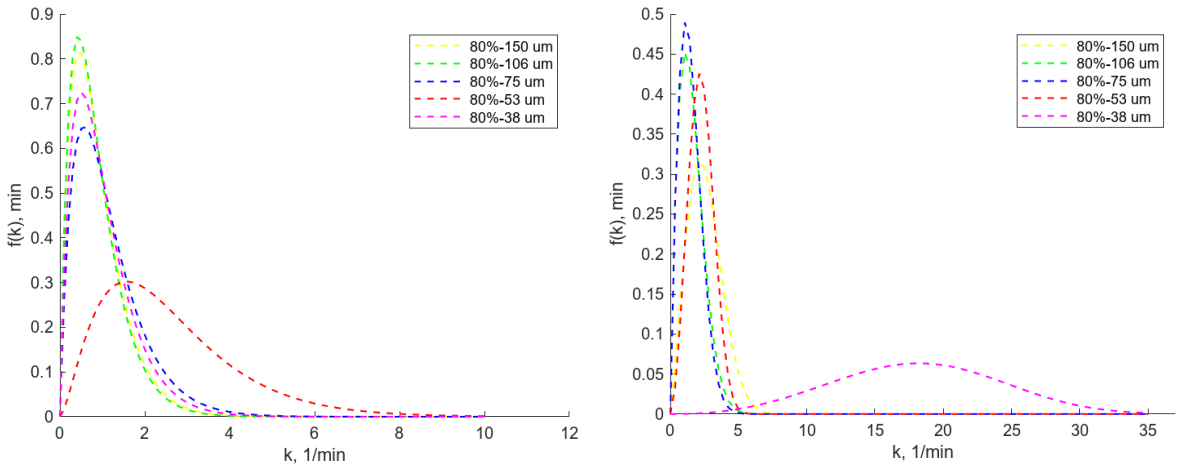

Figure 4.16: Rate distributions modelled using the (a) Gamma and (b) Weibull models based on Figure 4.14 data (case for 80 g/t SIBX).

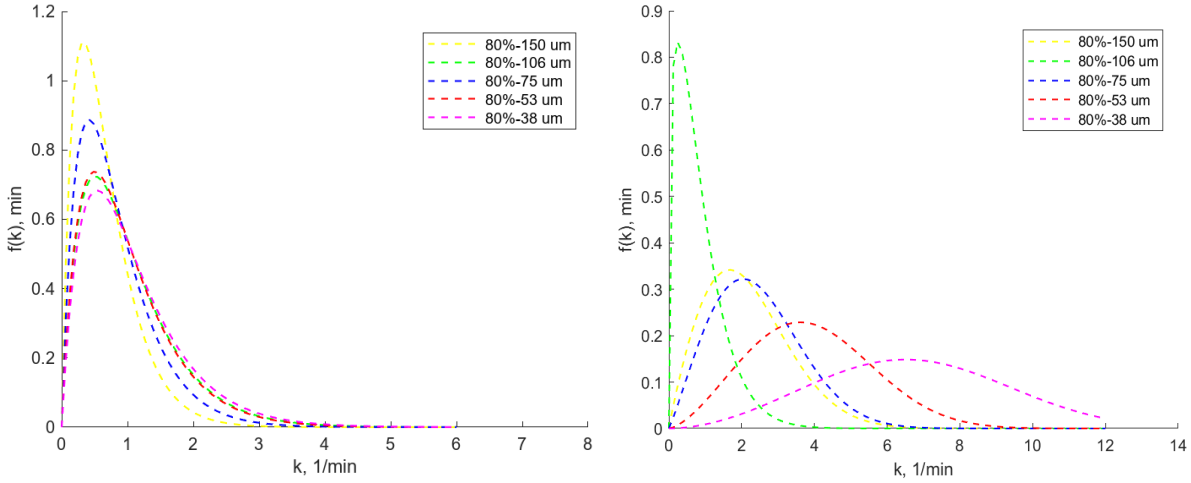

(a) (b)

Figure 4.17: Rate distributions modelled using the (a) Gamma and (b) Weibull models based on Figure 4.15 data (case for 120 g/t SIBX).

Figure 4.16 and Figure 4.17 above underscores the limitations of relying solely on a single model based on good fitting behaviour to comprehensively grasp the underlying process dynamics. Conversely, employing an excessive number of models for the analysis of a single dataset might result in overlooking crucial insights and being inundated with extraneous information, ultimately hindering process optimization. Therefore, it is imperative to exercise

caution and delineate the specific information required when selecting the most suitable models, ensuring a balanced approach that aids in effective process enhancement.

As demonstrated earlier, the Gamma model has proven to be comparatively more effective than the Weibull model in fitting time-recovery data. However, the current figure illustrates how the Gamma model may offer limited insights when process conditions undergo changes, as evidenced by the relatively consistent rate distributions when comparing Figure 4.16 (a) and Figure 4.17 (a). Notably, the primary distinction lies in the effect of increased collector dosage, which appears to enhance the fraction of particles with lower rate constants for both the 80%-150µm grind, and the 80%-38 µm grind, as evidenced by the noticeable increase in peaks, respectively.

In contrast, the Weibull model appears to offer more insightful information when examining the impact of collector dosage. The underlying chemistry suggests that higher reagent dosages support accelerated reaction rates. Consequently, it was anticipated that both the Gamma and Weibull models would reflect this effect at increased collector dosages, albeit not in a linear manner. Faster reaction rates manifest in the form of shifted rate distributions towards higher (right) rate constants, as illustrated in Figure 4.17 (b). Interestingly, this figure serves as an apt illustration of the initial expectations concerning the investigation into the effect of grind, where finer grinding correlates with swifter reaction rates.

Indeed, the initial investigation primarily centred around the interplay of the shape and scale factors, particularly how grind and collector dosages influenced these parameters. This question can now be addressed, as it appears that elevated grind levels and increased collector dosages have contributed to enhancing the scale and shape parameters in the Weibull models, as evidenced by the MATLAB code provided. This effect is manifest in the rightward shift observed on Figure 4.17 (b) and the widening of the Weibull distribution as grind becomes finer or collector dosage increases. Surprisingly, as the grind size decreases, one might anticipate reduced variability in flotation rates, implying narrower rate distribution spreads, typically associated with less variability in the PSD. However, what we observe here is the opposite phenomenon: a smaller grind results in a broader spread of the distributions.

The shift in scale and shape factors within the Weibull models as grind characteristics and collector dosages change provides a deeper understanding of the underlying processes. These factors have fundamental implications for process dynamics. The rightward shift in rate distributions seen in Figure 4.17 (b) signifies that, as grind becomes finer or collector dosage

increases, the process exhibits faster reaction rates. Furthermore, the widening of the Weibull distribution as grind gets finer or collector dosage rises indicates increased variability in the process behaviour. This increased spread reflects the complex interplay of factors influenced by grind and collector dosage, such as PSD, surface chemistry, and reaction kinetics.

Practically, these insights are invaluable for process optimization. They highlight the need for a nuanced approach to process control, emphasizing that achieving optimal behaviour may require fine-tuning collector dosages and grind conditions based on specific goals and constraints. This information can be applied in industrial settings to enhance recovery rates and efficiency in flotation processes, as well as in other areas of chemical engineering and manufacturing where understanding and manipulating process kinetics are critical.

In essence, these findings underscore the complexity of chemical processes and provide guidance for tailoring these processes to improve their efficiency and effectiveness in real-world applications. Further research and experimentation can build upon these insights and refine our ability to manage and optimize such intricate systems.

4.8.4. Model selectivity on particle size

The rate distributions yield valuable insights into the selectivity of the flotation process, which pertains to its ability to differentially recover specific minerals or particles while excluding others. By comparing curves for various particle species, one can understand which minerals possess higher k values, signifying their enhanced recoverability, while those with lower k values exhibit less efficient recovery rates. This information has paramount importance in process optimization, aimed at maximizing the retrieval of valuable minerals and minimizing the recovery of undesired gangue materials.

To illustrate this concept, let us consider Figure 4.18 (a) and (b) below, where the Weibull model is exclusively employed for our analysis of Test 3 data for the 80%-106 µm grind as per Table 3.3.

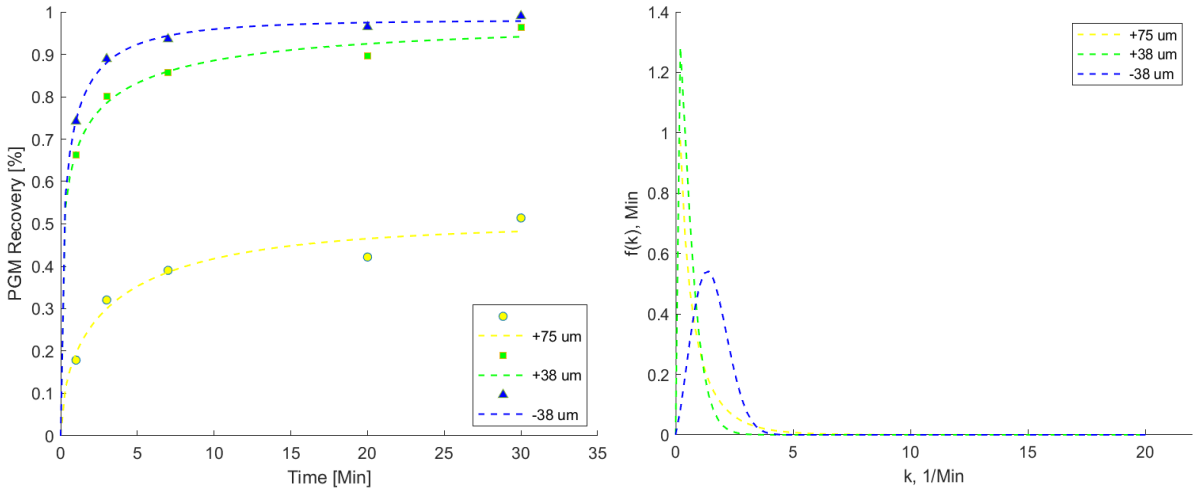

(a) (b)

Figure 4.18: Weibull model showing selectivity of particles.

Figure 4.18 shows the selectivity phenomenon, here is it clear that -38 µm particles not only exhibited the highest recoveries but also demonstrated relatively higher k values. Conversely, the coarser +75 µm particles showed lower recovery rates, attributable to their lower k values. This phenomenon can also be applied to flotation tailings whereby the $f(k)$ vs k curves can be used to reveal the distribution of un-floated particles, which make up the tailings. A long tail on the curve at low k values would signify that a significant proportion of particles or minerals have low flotation rates and remain in the tailings.

5. CONCLUSIONS

Throughout this study, the intricate interplay of milling durations, PSDs, collector dosages, and their consequential impact on flotation processes were explored. This research was prompted by the necessity to unravel the influence of processing variables on the characteristics of flotation modelling, particularly using the Gamma and Weibull models, and their applicability in laboratory settings. Through analysis and experimentation, the author has unearthed valuable insights that not only shed light on the mechanics of milling but also offer indispensable knowledge for the optimization of processes within the domains of material processing and mineral extraction. This section now presents the distilled findings from the research, encompassing critical aspects such as milling duration, PSD, reagent dosages, and their influence on rate distributions.

In this dissertation, the utility of the Gamma and Weibull distribution models in effectively fitting flotation rate data for Platreef ore across a spectrum of grind sizes was explored. The examination has encompassed their performance characteristics, their sensitivity to variations in collector dosages and grind characteristics, and the depth of insight these models provide into the intricate dynamics of the flotation process.

Objectives have been linked to overall project conclusions as below;

- **Objective 1: Conduct chemical and mineralogical analysis of Platreef ore: To gain a better understanding of this PGM ore's complex nature**
  - The chemical and mineralogical analysis revealed that Platreef ore is highly heterogeneous, containing a significant amount of pentlandite and chalcopyrite. This complexity affects the flotation performance, which was critical in fitting the flotation models used in this study.
  - Coarser grind sizes tend to exhibit shifts in dominant PGM species, with finer particles often showing higher abundance of valuable species like PtBiTe and PtPdBiTe.
- **Objective 2: Perform rougher flotation rate experiments: Collect data needed for flotation rate constants estimation**
  - The rougher flotation experiments showed that the flotation rate distributions varied significantly with particle size and collector dosage, providing essential data for fitting the Gamma and Weibull models.

- **Objective 3: Perform numerical integration to evaluate $R(t)$ for the Gamma model: Assess the time-recovery relationship using the Gamma model**
  - Numerical integration to evaluate $R(t)$ for the Gamma model demonstrated a strong fit with the experimental data, confirming the model's suitability for estimating flotation rate constant distributions.
- **Objective 4: Fit Gamma and Weibull models to time-recovery curves: Estimate rate distributions at different particle sizes and collector dosages**
  - Both Gamma and Weibull models were successfully fitted to the time-recovery curves, with the Gamma model showing a slightly better fit for all particle sizes, while the Weibull model was less accurate for coarser particles.
  - The accuracy of the models diminishes with longer residence times, particularly when collector dosages are changed.
- **Objective 5: Determine the effect of particle size and collector dosages on the Gamma and Weibull model parameters: Analyse how particle size and varying collector dosages influences the model parameters**
  - The analysis indicated that smaller particle sizes led to higher rate distribution in both models, affirming the hypothesis that particle size significantly influences the flotation rate parameters.
  - A distribution skewed towards higher k values indicate efficient recovery, while lower k values signify slower attachment to bubbles.
  - The dosage of the collector affects the shape and spread of rate distributions. Understanding this relationship is crucial for optimizing flotation processes.

6. RECOMMENDATIONS

I. Superficial air flux velocity measurements must be taken and plotted against recovery versus time graphs. This may then be used to test how this relates to the parameters of the Weibull and Gamma rate distributions.

II. Exploring rate distributions using alternative equipment such as a column cell could yield potential benefits.

III. It is also recommended that that the effect of pH be tested to show its effect on rate distributions.

7. REFERENCES

Ahmed, N., Jameson, G.J., 1989. Flotation kinetics. Mineral Processing and Extractive Metallurgy Review 5, 77-99.

Ahmed, M.M., 2004. Discrimination of different models in the flotation of Maghara coal. Mineral Processing and Extractive Metallurgy 113, 103-110.

Allen, M.P., 1997. Understanding regression analysis. Plenum Press, New York, USA.

Agante, E., Carvalho, T., Durão, F., Pinto, A., Mariano, T., 2007. Kinetic study of froth flotation for PET-PVC separation, 2004 New and Renewable Energy Technologies for Sustainable Development, Evora, pp. 117-126.

Agar, G.E., Stratton-Crawley, R., Bruce, T.J., 1980. Optimizing the design of flotation circuits. Canadian Mining and Metallurgical Bulletin 73, 173-181.

Albijanic, B., Subasinghe, N., Park, C.H., 2015b. Flotation kinetic models for fixed and variable pulp chemical conditions. Minerals Engineering 78, 66-68.

Arbiter, N., 1951. Flotation rates and flotation efficiency. Transactions of the American Institute of Mining and Metallurgical Engineers 190, 791-796.

Asghar, A., Ahmad, H., Behnam, F., 2015. Investigating the first-order flotation kinetics models for Sarcheshmeh copper sulfide ore. International Journal of Mining Science and Technology 25, 849-854.

Bagheri, B., Vazifeh Mehrabani, J., Farrokhpay, S., 2020. Recovery of sphalerite from a high zinc grade tailing. Journal of Hazardous Materials 381, 120946.

Bahrami, A., Ghorbani, Y., Hosseini, M.R., Kazemi, F., Abdollahi, M., Danesh, A., 2019a. Combined Effect of Operating Parameters on Separation Efficiency and Kinetics of Copper Flotation. Mining, Metallurgy & Exploration 36, 409-421.

Bahrami, A., Kazemi, F., Ghorbani, Y., Abdolahi Sharif, J., 2019b. The Order of Kinetic Models, Rate Constant Distribution, and Maximum Combustible Recovery in Gilsonite Flotation. Mining, Metallurgy & Exploration 36, 1101-1114.

Bates, D.M., Watts, D.G., 1988. Nonlinear regression analysis and its applications. Wiley, New York, USA.

Bu, X., Xie, G., Chen, Y., Ni, C., 2017a. The Order of Kinetic Models in Coal Fines Flotation. International Journal of Coal Preparation and Utilization 37, 113-123.

Bu, X., Xie, G., Peng, Y., Ge, L., Ni, C., 2017b. Kinetics of flotation. order of process, rate constant distribution and ultimate recovery. Physicochemical Problems of Mineral Processing 53, 342-365.

Braga, F.Y.A., Luz José, A.M., Milhomem, F.O., 2020. Size-dependent kinetics of iron ore reverse flotation. Particulate Science and Technology 4, 419-426.

Chaves, A.P., Ruiz, A.S., 2009. Considerations on the Kinetics of Froth Flotation of Ultrafine Coal Contained in Tailings. International Journal of Coal Preparation and Utilization 29, 289-297.

Chander, S., Polat, M., 1995. Flotation Kinetics: Methods For Estimating Distribution Of Rate Constants, International Mineral Processing Congress (XIX IMPC). Society for Mining, Metallurgy & Exploration, San Francisco, USA, pp. 105–111.

Chen, G., Grano, S., Sobieraj, S., Ralston, J., 1999. The effect of high intensity conditioning on the flotation of a nickel ore. Part 1: size-by-size analysis. Minerals Engineering 12, 1185-1200.

Chen, W., Chen, F., Bu, X., Zhang, G., Zhang, C., Song, Y., 2019. A significant improvement of fine scheelite flotation through rheological control of flotation pulp by using garnet. Minerals Engineering 138, 257-266.

de Bruyn, P.L., Modi, H.J., 1956. Particle Size and Flotation Rate of Quartz. The American Institute of Mining, Metallurgical, and Petroleum Engineers 205, 415-419.

Dehghani, F., Rahimi, M., Rezai, B., 2013. Influence of particle shape on the flotation of magnetite, alone and in the presence of quartz particles. Journal of the Southern African Institute of Mining and Metallurgy 113, 905-911.

Diao, J., Fuerstenau, D., Hanson, J., 1992. Kinetics of coal flotation, Society for Mining Metallurgy and Exploration-American Institute of Mining, Metallurgical, and Petroleum Engineers Annual Meeting, Phoenix, AZ, USA.

Dowling, E.C., Klimpel, R.R., Aplan, F.F., 1985. Model discrimination in the flotation of a porphyry copper ore. Minerals and Metallurgical Processing 2, 87-101.

Duan, J., Fornasiero, D., Ralston, J., 2003. Calculation of the flotation rate constant of chalcopyrite particles in an ore. International Journal of Mineral Processing 72, 227-237.

Ek, C., 1992. Flotation Kinetics, in: Mavros, P., Matis, K.A. (Eds.), Innovations in Flotation Technology. Springer Dordrecht, The Netherlands, pp. 183-210.

Eskanlou, A., Shahbazi, B., Vaziri Hassas, B., 2018. Estimation of flotation rate constant and collision efficiency using regression and artificial neural networks. Separation Science and Technology 53, 374-388.

Ferreira, J.P., Loveday, B.K., 2000. An improved model for simulation of flotation circuits. Minerals Engineering 13, 1441-1453.

Filippov, L.O., Matinin, A.S., Samiguin, V.D., Filippova, I.V., 2013. Effect of ultrasound on flotation kinetics in the reactor-separator. Journal of Physics: Conference Series 416, 012016.

Garcia-Zuñiga, H., 1935. La recuperación por flotación es una función exponencial del tiempo. Boletín Minero, Sociedad Nacional de Minería 47, 83-86.

Harris, C., Chakravarti, A., 1970. Semi-batch froth flotation kinetics: species distribution analysis. Transactions of the American Institute of Mining, Metallurgical, and Petroleum Engineers 247, 162-172.

Harris, M.C., Runge, K.C., Whiten, W.J., Morrison, R.D., 2002. JKSimFloat as a practical tool for flotation process design and optimisation, Mineral Processing Plant Design Practice and Control Conference. Society for Mining Metallurgy & Exploration, Vancouver, Canada, pp. 461-478.

Hassanzadeh, A., Huu Hoang, D., Brockmann, M., 2019. Assessment of flotation kinetics modelling using information criteria; case studies of elevated-pyritic copper sulfide and high-grade carbonaceous sedimentary apatite ores. Journal of Dispersion Science and Technology, 1-12.

Holland-Batt, A.B., 1971. Efficiency in batch separations. The Institute of Materials, Minerals and Mining 80, C12-23.

Hill, A.V., 1910. The possible effects of the aggregation of the molecules of haemoglobin on its dissociation curves. The Journal of Physiology 40, 4-7.

Huber-Panu, I., Ene-Danalache, E., Cojocariu, D.G., 1976. Mathematical models of batch and continuous flotation, Flotation--A. M. Gaudin Memorial. American Institute of Mining, Metallurgical, and Petroleum Engineers, Inc., New York, USA, pp. 675-724.

Imaizumi, T., Inoue, T., 1963. Kinetic consideration of froth flotation, in: Roberts, A. (Ed.), 6th International Mineral Processing Congress. Pergamon Press, Cannes, France, pp. 581-593.

Jameson, G.J., 2012. The effect of surface liberation and particle size on flotation rate constants. Minerals Engineering 36-38, 132-137.

Kapur, P.C., Mehrotra, S.P., 1974. Estimation of the flotation rate distributions by numerical inversion of the Laplace transform. Chemical Engineering Science 29, 411-415.

Karimi, M., Akdogan, G., Bradshaw, S.M., 2014. A computational fluid dynamics model for the flotation rate constant, Part I: Model development. Minerals Engineering 69, 214-222.

Kelly, E.G., Carlson, C.E., 1991. Two flotation models: Resolution of a conflict. Minerals Engineering 4, 1333-1338.

Kelsall, D.F., 1961. Application of probability assessment of flotation systems. Transactions of the Institution of Mining and Metallurgy 70, 191–204.

Klimpel, R.R., 1980. Selection of chemical reagents for flotation, in: Mular, A.L., Bhappu, R.B. (Eds.), Mineral processing plant design. Society for Mining, Metallurgy & Exploration-American Institute of Mining, Metallurgical, and Petroleum Engineers, New York, USA, pp. 907-934.

Laskowski, J.S., 2001. Flotation machines, Developments in Mineral Processing. Elsevier, Amsterdam, The Netherlands, pp. 225-262.

Lynch, A., Johnson, N., Manlapig, E., Thorne, C., 1981a. Mineral and coal flotation circuits: their simulation and control. Elsevier, Amsterdam, The Netherlands.

Mazumdar, M., 1994. Statistical discrimination of flotation models based on batch flotation data. International Journal of Mineral Processing 42, 53-73.

Mehrotra, S., Padmanabhan, N., 1990. Analysis of flotation kinetics of Malanjkhand copper ore, India, in terms of distributed flotation-rate constant. Transactions of the Institution of Mining and Metallurgy Section C-Mineral Processing and Extractive Metallurgy 99, C32-C42.

Morris, T., 1952. Measurement and evaluation of the rate of flotation as a function of particle size. Mining Engineering 4, 794-798.

Mendez, D.A., Gálvez, E.D., Cisternas, L.A., 2009. State of the art in the conceptual design of flotation circuits. International Journal of Mineral Processing 90, 1-15.

Ni, C., Xie, G., Jin, M., Peng, Y., Xia, W., 2016. The difference in flotation kinetics of various size fractions of bituminous coal between rougher and cleaner flotation processes. Powder Technology 292, 210-216.

Nikolaev, A.A., 2019. Flotation recovery of toner containing iron oxide from water suspension. Minerals Engineering 144, 106027.

Doubra, P., Carelse, C., Chetty, D., Manuel, M., 2023, Experimental and Modelling Study of Pt, Pd, and 2E+Au Flotation Kinetics for Platreef Ore by Exploring the Influence of Reagent Dosage Variations. Minerals. 13, 1350.

Pascual, R.L., Whiten, W.J., 2015. The determination of floatability distribution from laboratory batch cell tests. Minerals Engineering 83, 1-12.

Polat, M., Chander, S., 2000. First-order flotation kinetics models and methods for estimation of the true distribution of flotation rate constants. International Journal of Mineral Processing 58, 145–166.

Pyke, B., Fornasiero, D., Ralston, J., 2003. Bubble particle heterocoagulation under turbulent conditions. Journal of Colloid and Interface Science 265, 141-151.

Rhinehart, R.R., 2016. Nonlinear regression modeling for engineering applications: modeling, model validation, and enabling design of experiments. John Wiley & Sons, Chichester, UK.

Ross, V., 2019. Key aspects of bench flotation as a geometallurgical characterization tool. Journal of the Southern African Institute of Mining and Metallurgy 119, 361-367.

Rubio, J., Capponi, F., Rodrigues, R.T., Matiolo, E., 2007. Enhanced flotation of sulfide fines using the emulsified oil extender technique. International Journal of Mineral Processing 84, 41-50.

Runge, K.C., Franzidis, J.P., Manlapig, E.V., 2003. A study of the flotation characteristics of different mineralogical classes in different streams of an industrial circuit, in: Lorenzen, L., Bradshaw, D.J. (Eds.), XXII International Mineral Processing Congress, Cape Town, South Africa, pp. 962-972.

Sahoo, S.K., Suresh, N., Varma, A.K., 2017. Performance Evaluation of Basic Flotation Kinetic Models Using Advanced Statistical Techniques. International Journal of Coal Preparation and Utilization, 1-23.

Seber, G.A.F., Wild, C.J., 1989. Nonlinear regression. Wiley, New York, USA.

Schuhmann Jr, R., 1942. Flotation Kinetics. I. Methods for steady-state study of flotation problems. The Journal of Physical Chemistry 46, 891-902.

Shahbazi, B., Chehreh Chelgani, S., Matin, S.S., 2017. Prediction of froth flotation responses based on various conditioning parameters by Random Forest method. Colloids and Surfaces A: Physicochemical and Engineering Aspects 529, 936-941.

Sutherland, K.L., 1948. Physical chemistry of flotation. XI. Kinetics of the flotation process. The Journal of Physical Chemistry 52, 394-425.

Sutherland, D.N., 1989. Batch flotation behaviour of composite particles. Minerals Engineering 2, 351-367.

Tabosa, E., Rubio, J., 2010. Flotation of copper sulphides assisted by high intensity conditioning (HIC) and concentrate recirculation. Minerals Engineering 23, 1198-1206.

Taguta, J., McFadzean, B., O'Connor, C., 2019. The relationship between the flotation behaviour of a mineral and its surface energy properties using calorimetry. Minerals Engineering 143, 105954.

Tarasov, V.E., 2010. Fractional dynamics: applications of fractional calculus to dynamics of particles, fields and media. Springer Science & Business Media, Heidelberg, Dordrecht, London, New York.

Tewari, S.N., Biswas, A.K., 1969. Flotation kinetics for calcite in a semi-batch system. Journal of Applied Chemistry 19, 173-177.

Trahar, W.J., 1981. A rational interpretation of the role of particle size in flotation. International Journal of Mineral Processing 8, 289-327.

Trahar, W.J., Warren, L.J., 1976. The flotability of very fine particles—a review. International Journal of Mineral Processing 3, 103-131.

Van der Westhuizen, A.P., Deglon, D.A., 2007. Evaluation of solids suspension in a pilot scale mechanical flotation cell: The critical impeller speed. Minerals Engineering, 20, 233-240.

Vinnett, L., Alvarez-Silva, M., Jaques, A., Hinojosa, F., Yianatos, J., 2015. Batch flotation kinetics: Fractional calculus approach. Minerals Engineering 77, 167-171.

Welsby, S.D.D., Vianna, S.M.S.M., Franzidis, J.-P., 2010. Assigning physical significance to floatability components. International Journal of Mineral Processing 97, 59-67.

Wills, B., Napier-Munn, T., 2006. Wills' mineral processing technology: an introduction to the practical aspects of ore treatment and mineral recovery, 7th ed. Butterworth-Heinemann, Oxford.

Woodburn, E.T., Loveday, B.K., 1965. The effect of variable residence time on the performance of a flotation system. Journal of the Southern African Institute of Mining and Metallurgy 65, 612-628.

Xu, M., 1998. Modified flotation rate constant and selectivity index. Minerals Engineering 11, 271-278.

Yianatos, J., Bergh, L., Vinnett, L., Panire, I., Diaz, F., 2015. Modelling of residence time distribution of liquid and solid in mechanical flotation cells. Minerals Engineering 78, 69-73.

Yianatos, J., Vinnett, L., Panire, I., Alvarez-Silva, M., Díaz, F., 2017. Residence time distribution measurements and modelling in industrial flotation columns. Minerals Engineering 110, 139-144.

8. APPENDICES

Table 8.1: Rod milling curve data.

	As-is			90 MIN			120 MIN			180 MIN		
Sieve size(mm)	mass (g)	mass %	Cumulative % Passing	Mass(g)	Mass %	Cumulative % Passing	Mass(g)	Mass %	Cumulative % Passing	Mass(g)	Mass %	Cumulative % Passing
1.7		0.00	100.00		0.00	100.00		0.00	100.00		0.00	100.00
1.18	197.08	9.91	90.09		0.00	100.00		0.00	100.00		0.00	100.00
0.85	313.15	15.75	74.34		0.00	100.00		0.00	100.00		0.00	100.00
0.6	241.16	12.13	62.21		0.00	100.00		0.00	100.00		0.00	100.00
0.425	176.73	8.89	53.32		0.00	100.00		0.00	100.00		0.00	100.00
0.3	195.10	9.81	43.51		0.00	100.00		0.00	100.00		0.00	100.00
0.212	156.40	7.87	35.65		0.00	100.00		0.00	100.00		0.00	100.00
0.15	140.83	7.08	28.57	2.2	0.11	99.89		0.00	100.00		0.00	100.00
0.106	125.27	6.30	22.27	44.3	2.28	97.61	7.8	0.39	99.61		0.00	100.00
0.075	121.11	6.09	16.17	415.9	21.41	76.19	87.7	4.37	95.24	66.2	3.31	96.69
0.053	81.52	4.10	12.08	450.5	23.20	52.99	403.0	20.10	75.13	290.5	14.53	82.16
0.038	59.85	3.01	9.07	237.1	12.21	40.79	391.7	19.54	55.60	415.1	20.77	61.39
0.025	37.83	1.90	7.16	164.9	8.49	32.29	295.3	14.73	40.87	262.8	13.14	48.25
0	142.43	7.16	0.00	627.2	32.29	0.00	819.3	40.87	0.00	964.6	48.25	0.00
	1988.46	100.00		1942.1	100.00		2004.8	100.00		1999.2	100.00	

Table 8.2: Stirred milling conditions.

Water S.G (g/cm3)	**1.00**
Solid mass (g)	**200**
% Solids	**50**
Water mass (g)	**200**
Slurry mass (g)	**400**
solids S.G (g/cm3)	**3.20**
Slurry S.G (g/cm3)	**1.52**
Slurry volume (cm3)	**263**
Mill Dimensions	
Diameter (cm)	**18.00**
Height (cm)	**23.00**
Mill Volume (π/4 (D2/L)	**5853**
% Loading (fraction)	**0.50**
Ball bulk volume (cm3)	**2926**
Ball material volume (cm3)	**1756**
Ball S.G (g/cm3)	**4.30**
Ball Mass (g)	**7550**

Table 8.3: Stirred milling curve data.

	180			183 MIN			185 MIN			183 MIN Confirmation		
Sieve size(µm)	mass (g)	mass %	Cumulative % Passing	Mass(g)	Mass %	Cumulative % Passing	Mass(g)	Mass %	Cumulative % Passing	Mass(g)	Mass %	Cumulative % Passing
106		0.00	100.00		0.00	100.00		0.00	100.00		0.00	100.00
75	66.21	3.31	96.69	8.1	0.40	99.60	0.6	0.03	99.97	1.9	0.10	99.90
53	290.45	14.53	82.16	68.9	3.44	96.16	9.9	0.50	99.47	69.9	3.52	96.38
38	415.13	20.77	61.39	240.3	11.99	84.17	106.9	5.41	94.06	244.2	12.30	84.09
25	262.76	13.14	48.25		0.00	84.17	0.0	0.00	94.06		0.00	84.09
-25	964.60	48.25	0.00	1687.0	84.17	0.00	1858.0	94.06	0.00	1670.0	84.09	0.00
sum	1999.15	100.00		2004.3	100.00		1975.4	100.00		1986.0	100.00	

Table 8.4: Assay by Size data for 80%-150µm

				Grade							Distribution					
Screen size (µm)	Mass	Mass	Cum % passing	Pt	Pd	Au	2E+Au	Pt/Pd ratio	Cu	Ni	Pt	Pd	Au	2E+Au	Cu	Ni
	(g)	(%)	%	g/t	g/t	g/t	g/t		(%)	(%)	g/t	g/t	g/t	g/t	%	%
+150 µm	285	14.26	85.74	0.25	0.32	0.09	0.66	0.78	0.05	0.09	5.11	5.19	10.04	5.52	7.67	7.10
150 + 75 µm	796.3	39.84	45.90	0.74	0.84	0.12	1.70	0.88	0.07	0.13	42.27	38.04	37.41	39.72	29.15	27.44
-75 + 38 µm	374.6	18.74	27.16	0.77	0.81	0.17	1.75	0.95	0.10	0.21	20.69	17.26	24.93	19.24	19.36	20.85
-38 µm	542.8	27.16	0.00	0.82	1.28	0.13	2.23	0.64	0.15	0.31	31.93	39.51	27.62	35.52	43.83	44.60
Head (calc.)	**1998.70**	**100.00**		**0.70**	**0.88**	**0.13**	**1.71**	**0.81**	**0.09**	**0.19**	**100.00**	**100.00**	**100.00**	**100.00**	**100.00**	**100.00**
Head (meas.)	2000.00			0.99	0.96	0.18	2.12	0.74	0.10	0.19						
% Variance				**29.67**	**8.01**	**27.56**	**19.74**	**9.88**	**3.68**	**0.66**						

Table 8.5: Assay by Size data for 80%-106µm

				Grade							Distribution					
Screen size (µm)	Mass	Mass	Cum % passing	Pt	Pd	Au	2E+Au	Pt/Pd ratio	Cu	Ni	Pt	Pd	Au	2E+Au	Cu	Ni
	(g)	(%)	%	g/t	g/t	g/t	g/t		(%)	(%)	g/t	g/t	g/t	g/t	%	%
+150	19.8	0.99	99.01	0.51	0.32	0.22	1.05	1.61	0.05	0.09	0.72	0.42	1.65	0.65	0.19	0.48
-150 + 75	854.0	42.50	56.52	0.62	0.44	0.08	1.14	1.40	0.06	0.12	37.02	24.67	25.94	30.25	9.81	26.27
-75 + 38	457.6	22.77	33.74	0.75	0.76	0.15	1.66	0.99	0.82	0.18	24.13	22.83	26.06	23.67	71.83	21.11
-38	678.0	33.74	0.00	0.80	1.17	0.18	2.15	0.68	0.14	0.30	38.13	52.08	46.34	45.43	18.17	52.14
Head (calc.)	**2009.45**	**100.00**		**0.71**	**0.76**	**0.13**	**1.60**	**1.07**	**0.26**	**0.19**	**100.00**	**100.00**	**100.00**	**100.00**	**100.00**	**100.00**
Head (meas.)	2000.00			0.99	0.96	0.18	2.12	0.74	0.10	0.19						
% Variance				**28.62**	**20.73**	**25.72**	**24.83**	**43.92**	**169.41**	**2.18**						

Table 8.6: Assay by Size data for 80%-75 µm

				Grade							Distribution					
Screen size (µm)	Mass	Mass	Cum % passing	Pt	Pd	Au	2E+Au	Pt/Pd ratio	Cu	Ni	Pt	Pd	Au	2E+Au	Cu	Ni
	(g)	(%)	%	g/t	g/t	g/t	g/t		(%)	(%)	g/t	g/t	g/t	g/t	%	%
+150	0	0.00	100.00	0.00	0.00	0.00	0.00	-	0.00	0.00	0.00	0.00	0.00	0.00	0.00	0.00
-150 + 75	460.0	23.72	76.28	0.35	0.45	0.13	0.93	0.78	0.60	0.12	14.06	12.58	24.97	14.12	61.45	13.98
-75 + 38	687.6	35.45	40.83	0.51	0.64	0.10	1.25	0.80	0.08	0.16	30.62	26.75	28.72	28.37	12.09	27.86
-38	792.0	40.83	0.00	0.80	1.26	0.14	2.20	0.63	0.15	0.29	55.32	60.66	46.31	57.51	26.45	58.16
Head (calc.)	**1939.60**	**100.00**		**0.59**	**0.85**	**0.12**	**1.56**	**0.73**	**0.23**	**0.20**	**100.00**	**100.00**	**100.00**	**100.00**	**100.00**	**100.00**
Head (meas.)	2000.00			0.52	0.70	0.20	1.41	0.74	0.10	0.19						
% Variance				**14.65**	**22.03**	**36.69**	**11.18**	**2.04**	**139.95**	**7.16**						

Table 8.7: Assay by Size data for 80%-53µm

				Grade							Distribution					
Screen size (µm)	Mass	Mass	Cum % passing	Pt	Pd	Au	2E+Au	Pt/Pd ratio	Cu	Ni	Pt	Pd	Au	2E+Au	Cu	Ni
	(g)	(%)	%	g/t	g/t	g/t	g/t		(%)	(%)	g/t	g/t	g/t	g/t	%	%
+150	0	0.00	100.00	0.00	0.00	0.00	0.00	-	0.00	0.00	0.00	0.00	0.00	0.00	0.00	0.00
-150 + 75	62.1	3.07	96.93	0.51	0.50	0.13	1.14	1.04	0.05	0.11	1.81	1.33	2.32	1.60	1.81	2.12
-75 + 38	855.5	42.29	54.64	0.57	0.55	0.19	1.30	1.04	0.06	0.11	27.40	20.19	46.78	25.16	27.40	29.23
-38	1105.2	54.64	0.00	1.13	1.64	0.16	2.93	0.69	0.11	0.20	70.79	78.48	50.89	73.24	70.79	68.65
Head (calc.)	**2022.9**	**100.0**		**0.87**	**1.14**	**0.17**	**2.19**	**0.85**	**0.08**	**0.16**	**100.00**	**100.00**	**100.00**	**100.00**	**100.00**	**100.00**
Head (meas.)	2000.0			0.99	0.96	0.18	2.12	0.74	0.10	0.19						
% Variance				**12.02**	**19.40**	**2.65**	**2.90**	**14.27**	**12.02**	**16.22**						

Table 8.8: Assay by Size data for 80%-38µm

				Grade							Distribution					
Screen size (µm)	Mass	Mass	Cum % passing	Pt	Pd	Au	2E+Au	Pt/Pd ratio	Cu	Ni	Pt	Pd	Au	2E+Au	Cu	Ni
	(g)	(%)	%	g/t	g/t	g/t	g/t		(%)	(%)	g/t	g/t	g/t	g/t	%	%
+150	0	0.00	100.00	0.00	0.00	0.00	0.00	-	0.00	0.00	0.00	0.00	0.00	0.00	0.00	0.00
-150 + 75	8.1	0.40	99.60	0.00	0.00	0.00	0.00	-	0.00	0.00	0.00	0.00	0.00	0.00	0.00	0.00
-75 + 38	309.2	15.43	84.17	0.28	0.28	0.06	0.62	1.00	0.05	0.09	7.32	5.45	9.09	6.44	8.39	7.28
-38	1687.0	84.17	0.00	0.65	0.89	0.11	1.65	0.73	0.10	0.21	92.68	94.55	90.91	93.56	91.61	92.72
Head (calc.)	**2004.3**	100.00		**0.59**	**0.79**	**0.10**	**1.48**	**0.77**	**0.09**	**0.19**	**100.00**	**100.00**	**100.00**	**100.00**	**100.00**	**100.00**
Head (meas.)	2000.0			0.52	0.70	0.20	1.41	0.74	0.10	0.19						
% Variance				**14.62**	**14.00**	**47.77**	**5.65**	**3.73**	**4.79**	**0.34**						

Table 8.9: PSD data for 80%-150µm

Screen size (µm)	Mass	Mass	Cum % passing
	(g)	(%)	
300	0.00	0.00	100.00
212	12.90	0.65	99.35
150	272.10	13.61	85.74
106	408.00	20.41	65.33
75	388.30	19.43	45.90
53	200.00	10.01	35.89
38	174.60	8.74	27.16
25	98.30	4.92	22.24
-25	444.50	22.24	
Head (calc.)	**1998.70**	**100.00**	
Head (meas.)	2000.00		

Table 8.10: PSD data for 80%-106µm

Screen size (µm)	Mass	Mass	Cum % passing
	(g)	(%)	
300	0.00	0.00	100.00
212	0.00	0.00	100.00
150	19.80	0.99	99.01
106	309.05	15.38	83.63
75	544.90	27.12	56.52
53	258.30	12.85	43.66
38	199.33	9.92	33.74
25	158.20	7.87	25.87
-25	519.82	25.87	3.00
Head (calc.)	**2009.40**	**100.00**	
Head (meas.)	2000.00		

Table 8.11: PSD data for 80%-75µm

Screen size (µm)	Mass	Mass	Cum % passing
	(g)	(%)	
300	0.00	0.00	100.00
212	0.00	0.00	100.00
150	17.10	0.86	99.14
106	247.90	12.48	86.66
75	453.10	22.80	63.86
53	341.80	17.20	46.66
38	259.30	13.05	33.61
25	154.90	7.80	25.81
-25	512.90	25.81	3.00
Head (calc.)	**1987.00**	**100.00**	
Head (meas.)	2000.00		

Table 8.12: PSD data for 80%-53µm

Screen size (µm)	Mass	Mass	Cum % passing
	(g)	(%)	
300	0.00	0.00	100.00
212	0.16	0.01	99.99
150	0.40	0.02	99.97
106	3.42	0.17	99.80
75	58.73	2.90	96.90
53	310.63	15.35	81.55
38	544.90	26.93	54.62
25	256.10	12.66	41.96
-25	849.14	41.96	3.00
Head (calc.)	**2023.5**	**100.0**	
Head (meas.)	2000.0		

Table 8.13: PSD data for 80%-38µm

Screen size (µm)	Mass	Mass	Cum % passing
	(g)	(%)	
300	0.00	0.00	100.00
212	0.00	0.00	100.00
150	0.00	0.00	100.00
106	0.00	0.00	100.00
75	8.10	0.41	99.59
53	68.90	3.45	96.15
38	240.30	12.02	84.12
25	0.00	0.00	84.12
-25	1687.00	84.40	0.00
Head (calc.)	**2004.30**	**100.28**	
Head (meas.)	2000.00		

Table 8.14: Calibration curve data.

	ACD Assays				
	Cu	Ni	Pt	Pd	Au
	%	%	g/t	g/t	g/t
Volspriut Platreef	1.98	3.95	18.52	19.10	3.11
	1.28	2.51	12.38	12.27	1.85
	0.14	0.69	3.70	5.05	1.08
	1.59	3.06	17.24	18.39	2.49
	1.90	3.10	19.56	20.51	2.92
	0.25	0.74	6.05	8.02	0.39
	1.80	3.12	17.48	16.14	2.51
	2.47	4.51	22.64	24.06	3.57
	0.16	1.40	2.25	6.97	1.08
	1.95	3.01	17.65	17.57	2.12
	2.14	3.26	23.44	20.44	3.24
	1.11	1.94	10.00	10.42	1.37
	0.11	0.74	1.77	2.29	1.00
	2.23	3.87	21.04	23.41	2.67
	2.17	4.05	22.96	20.68	2.38
	0.11	0.82	1.98	2.55	0.22
	2.29	4.22	22.31	19.64	3.31
	0.59	1.85	7.78	10.24	1.24
	1.02	2.11	12.56	12.30	2.05
	1.16	2.62	12.28	12.11	1.64
	2.34	3.78	25.20	23.52	3.05
	0.20	1.11	3.37	4.23	0.51
	0.97	2.29	9.73	11.42	1.89
	0.67	1.89	5.86	8.65	1.30
	2.26	3.67	23.08	22.78	2.65
	1.48	3.29	18.06	15.15	1.92
	1.32	3.07	16.67	13.51	2.25
	1.54	2.50	18.31	14.31	1.73
	0.58	1.38	6.67	9.84	0.91
	1.09	2.57	12.26	10.56	1.47
	1.49	2.72	17.14	15.04	1.76
	0.16	1.03	4.69	5.00	1.21
	1.47	2.46	15.56	13.86	2.40
	1.52	2.91	16.38	17.25	2.50
	0.45	1.14	8.40	8.04	1.27
	0.81	2.28	8.28	12.51	1.66
	2.28	4.03	22.09	23.96	2.54
	1.69	2.71	15.35	16.11	2.50
	0.29	1.18	4.73	7.56	0.48
	0.62	1.41	8.99	8.36	1.11
	1.54	2.73	17.54	13.70	2.34
	1.09	2.71	10.70	11.64	1.41
	1.40	2.80	15.62	12.25	2.17
	1.32	2.09	14.04	11.73	1.50
	2.13	3.45	21.57	19.56	2.56
	1.92	3.44	19.12	19.77	2.67
	1.76	3.36	15.84	15.97	2.15
	0.10	0.96	2.24	2.46	0.95
	0.77	2.13	10.89	7.85	1.29
	0.85	2.23	11.54	9.40	1.42
	1.20	2.45	13.54	11.40	2.18
	1.35	2.94	15.10	13.16	2.35

Table 8.15: Flotation time - recovery data for Test 1 on the 80%-150µm grind.

				Grade							Recovery					
Products	**Time**	**Mass**	**Mass**	**Pt**	**Pd**	**Au**	**3E**	**Pt/Pd**	**Cu**	**Ni**	**Pt**	**Pd**	**Au**	**3E**	**Cu**	**Ni**
	(min)	**(g)**	**(%)**	**g/t**	**g/t**	**g/t**	**g/t**		**%**	**%**	**%**	**%**	**%**	**%**	**%**	**%**
RC1	1	32.02	1.62	13.50	19.10	1.85	**34.45**	**0.71**	1.28	2.49	41.65	42.65	20.67	39.99	27.73	35.12
RC2	2	59.35	3.00	3.52	6.34	0.53	**10.39**	**0.55**	0.21	0.96	20.10	26.24	10.98	22.35	8.29	24.98
RC3	4	52.93	2.68	1.34	1.87	0.18	**3.39**	**0.72**	0.15	0.10	6.83	6.90	3.33	6.51	6.46	3.50
RC4	13	45.28	2.29	0.85	1.12	0.14	**2.11**	**0.76**	0.09	0.10	3.71	3.54	2.21	3.46	4.60	2.00
RC5	10	108.87	5.50	0.79	0.87	0.11	**1.77**	**0.91**	0.07	0.05	8.29	6.61	4.18	6.99	7.38	4.80
RT		1680.00	84.91	0.12	0.12	0.10	**0.34**	**1.00**	0.05	0.05	19.42	14.06	58.63	20.71	45.54	29.61
Head (calc.)		**1978.45**	**100.00**	**0.52**	**0.72**	**0.14**	**1.39**	**0.72**	**0.07**	**0.11**	**100.00**	**100.00**	**100.00**	**100.00**	**100.00**	**100.00**
Head (meas)		2000.00		0.52	0.70	0.20	1.41	0.74	0.10	0.19						
Variance		**0.01**		**0.02**	**0.04**	**0.26**	**0.01**	**0.02**	**0.23**	**0.40**						

CUMULATIVE RESULTS	**Flotation Time [min]**	**Mass [g]**	**Mass [%]**	**Cumulative Grade [g/t]**							**Cumulative Recovery [%]**					
				Pt	**Pd**	**Au**	**3E**	**Pt/Pd**	**Cu**	**Ni**	**Pt**	**Pd**	**Au**	**3E**	**Cu**	**Ni**
RC1	1	32.02	1.62	13.50	19.10	1.85	34.45	0.71	1.28	2.49	41.65	42.65	20.67	39.99	27.73	35.12
RC1+RC2	3	91.37	4.62	7.01	10.81	0.99	18.82	0.61	0.58	1.49	61.75	68.89	31.65	62.34	36.02	60.10
RC1+RC2+RC3	7	144.30	7.29	4.93	7.53	0.69	13.16	0.65	0.43	1.00	68.58	75.80	34.98	68.84	42.48	63.59
RC1+RC2+RC3+RC4	20	189.58	9.58	3.96	6.00	0.56	10.52	0.67	0.37	0.79	72.29	79.33	37.19	72.31	47.08	65.59
RC1+RC2+RC3+RC4+RC5	30	298.45	15.09	2.80	4.13	0.40	7.33	0.76	0.27	0.54	80.58	85.94	41.37	79.29	54.46	70.39
RC1+RC2+RC3+RC4+RC5+RT		1978.45	100.00	0.52	0.72	0.14	1.39	0.96	0.07	0.11	100.00	100.00	100.00	100.00	100.00	100.00

Table 8.16: Flotation time - recovery data for Test 2 on the 80%-150µm grind.

				Grade							Recovery					
Products	**Time**	**Mass**	**Mass**	**Pt**	**Pd**	**Au**	**3E**	**Pt/Pd**	**Cu**	**Ni**	**Pt**	**Pd**	**Au**	**3E**	**Cu**	**Ni**
	(min)	**(g)**	**(%)**	**g/t**	**g/t**	**g/t**	**g/t**		**%**	**%**	**%**	**%**	**%**	**%**	**%**	**%**
RC1	1	37.90	1.90	13.40	18.60	1.96	**33.96**	**0.72**	1.27	2.47	46.24	47.15	20.92	43.65	31.57	33.49
RC2	2	65.92	3.31	2.29	4.53	0.81	**7.63**	**0.51**	0.10	0.80	13.74	19.97	15.04	17.06	4.33	18.91
RC3	4	61.92	3.11	1.15	1.73	0.16	**3.04**	**0.66**	0.08	0.10	6.48	7.16	2.79	6.38	3.26	2.21
RC4	13	57.48	2.88	0.75	1.01	0.17	**1.93**	**0.74**	0.07	0.10	3.93	3.88	2.75	3.76	2.65	2.05
RC5	10	126.93	6.37	0.62	0.76	0.86	**2.24**	**0.82**	0.05	0.05	7.17	6.45	30.74	9.64	4.17	2.27
RT		1643.00	82.43	0.15	0.14	0.06	**0.35**	**1.07**	0.05	0.07	22.44	15.38	27.76	19.50	54.02	41.08
Head (calc.)		**1993.15**	**100.00**	**0.55**	**0.75**	**0.18**	**1.48**	**0.73**	**0.08**	**0.14**	**100.00**	**100.00**	**100.00**	**100.00**	**100.00**	**100.00**
Head (meas)		2000.00		0.52	0.70	0.20	1.41	0.74	0.10	0.19						
Variance		**0.00**		**7%**	**8%**	**9%**	**5%**	**1%**	**21%**	**26%**						

CUMULATIVE RESULTS	**Flotation Time [min]**	**Mass [g]**	**Mass [%]**	**Cumulative Grade [g/t]**							**Cumulative Recovery [%]**					
				Pt	**Pd**	**Au**	**3E**	**Pt/Pd**	**Cu**	**Ni**	**Pt**	**Pd**	**Au**	**3E**	**Cu**	**Ni**
RC1	1	37.90	1.90	13.40	18.60	1.96	33.96	0.72	1.27	2.47	46.24	47.15	20.92	43.65	31.57	33.49
RC1+RC2	3	103.82	5.21	6.35	9.67	1.23	17.24	0.58	0.53	1.41	59.99	67.12	35.96	60.71	35.91	52.39
RC1+RC2+RC3	7	165.74	8.32	4.40	6.70	0.83	11.94	0.61	0.36	0.92	66.47	74.28	38.75	67.09	39.17	54.60
RC1+RC2+RC3+RC4	20	223.22	11.20	3.46	5.24	0.66	9.36	0.65	0.28	0.71	70.39	78.16	41.50	70.85	41.81	56.66
RC1+RC2+RC3+RC4+RC5	30	350.15	17.57	2.43	3.61	0.73	6.78	0.71	0.20	0.47	77.56	84.62	72.24	80.50	45.98	58.92
RC1+RC2+RC3+RC4+RC5+RT		1993.15	100.00	0.55	0.75	0.18	1.48	1.01	0.08	0.14	100.00	100.00	100.00	100.00	100.00	100.00

Table 8.17: Flotation time - recovery data for Test 3 on the 80%-150µm grind.

					Grade						Recovery					
Products	**Time**	**Mass**	**Mass wrt Size**	**Mass wrt Feed**	**Pt**	**Pd**	**Au**	**3E**	**Cu**	**Ni**	**Pt**	**Pd**	**Au**	**3E**	**Cu**	**Ni**
	(min)	**(g)**	**(%)**	**(%)**	**g/t**	**g/t**	**g/t**	**g/t**	**%**	**%**	**%**	**%**	**%**	**%**	**%**	**%**
RC1	1	0.0	0.0	0.00	0.00	0.00	0.00	0.00	0.00	0.00	0.00	0.00	0.00	0.00	0.00	0.00
RC2	2	0.0	0.0	0.00	0.00	0.00	0.00	0.00	0.00	0.00	0.00	0.00	0.00	0.00	0.00	0.00
RC3	4	0.0	0.0	0.00	0.00	0.00	0.00	0.00	0.00	0.00	0.00	0.00	0.00	0.00	0.00	0.00
RC4	13	0.0	0.0	0.00	0.00	0.00	0.00	0.00	0.00	0.00	0.00	0.00	0.00	0.00	0.00	0.00
RC5	10	0.0	0.0	0.00	0.00	0.00	0.00	0.00	0.00	0.00	0.00	0.00	0.00	0.00	0.00	0.00
RT		525.8	100.0	13.44	0.00	0.00	0.00	0.00	0.02	0.07	0.00	0.00	0.00	0.00	0.00	0.00
+150 um		525.8	13.44	13.44	0.00	0.00	0.00	0.00	0.00	0.00	0.00	0.00	0.00	0.00	0.00	0.00
RC1	1	13.4	0.85	0.34	29.39	28.34	5.23	62.96	2.86	2.04	43.86	43.86	43.86	43.86	43.86	19.08
RC2	2	17.8	1.12	0.46	7.39	7.13	1.31	15.83	0.72	0.74	14.65	14.65	14.65	14.65	14.65	9.21
RC3	4	8.1	0.51	0.21	1.52	1.47	0.27	3.26	0.15	0.16	1.37	1.37	1.37	1.37	1.37	0.93
RC4	13	6.7	0.42	0.17	1.10	1.06	0.20	2.35	0.11	0.13	0.82	0.82	0.82	0.82	0.82	0.60
RC5	10	22.1	1.39	0.57	2.65	2.55	0.47	5.67	0.26	0.33	6.51	6.51	6.51	6.51	6.51	5.09
RT		1516.2	95.70	38.77	0.19	0.19	0.03	0.42	0.02	0.06	32.79	32.79	32.79	32.79	32.79	65.09
-150 + 75		1584.3	40.51	40.51	0.57	0.55	0.10	1.21	0.06	0.09	29.30	28.94	27.41	28.97	27.41	26.11
RC1	1	11.4	1.75	0.29	32.78	31.61	5.83	70.23	3.19	3.26	73.55	71.22	61.60	71.35	61.60	38.25
RC2	2	16.7	2.56	0.43	4.71	4.54	0.84	10.08	0.46	1.00	15.47	14.98	12.96	15.01	12.96	17.26
RC3	4	10.0	1.53	0.26	1.72	1.66	0.31	3.69	0.17	0.28	3.39	3.28	2.84	3.29	2.84	2.83
RC4	13	7.8	1.20	0.20	1.00	0.97	0.18	2.15	0.10	0.15	1.54	1.49	1.29	1.49	1.29	1.18
RC5	10	22.0	3.37	0.56	0.94	1.17	0.22	2.33	0.12	0.20	4.08	5.08	4.39	4.56	4.39	4.58
RT		584.2	89.59	14.94	0.02	0.03	0.03	0.08	0.02	0.06	1.97	3.95	16.92	4.30	16.92	35.90
-75 + 38		652.1	16.67	16.67	0.78	0.78	0.17	1.72	0.09	0.15	16.58	16.91	18.52	16.90	18.52	17.71
RC1	1	52.3	4.55	1.34	22.61	21.80	4.02	48.43	2.20	2.35	71.29	70.38	66.76	70.48	66.76	39.88
RC2	2	117.3	10.21	3.00	2.42	2.33	0.43	5.17	0.24	0.68	17.08	16.86	15.99	16.89	15.99	25.84
RC3	4	84.9	7.39	2.17	1.16	1.12	0.21	2.49	0.11	0.31	5.96	5.88	5.58	5.89	5.58	8.48
RC4	13	61.4	5.35	1.57	0.80	0.77	0.14	1.71	0.08	0.22	2.95	2.91	2.76	2.91	2.76	4.41
RC5	10	72.5	6.31	1.85	0.47	0.58	0.11	1.16	0.06	0.14	2.05	2.60	2.47	2.33	2.47	3.35
RT		760.3	66.19	19.44	0.01	0.03	0.03	0.07	0.01	0.07	0.67	1.37	6.44	1.49	6.44	18.03
-38		1148.7	29.37	29.37	1.44	1.41	0.27	3.13	0.15	0.27	54.12	54.15	54.07	54.13	54.07	56.18
Head (calc.)		**3910.9**	**100.0**	**100.0**	**0.78**	**0.77**	**0.15**	**1.70**	**0.08**	**0.14**	**100.00**	**100.00**	**100.00**	**100.00**	**100.00**	**100.00**
Head (meas)		4000.0			0.99	0.96	0.18	2.12	0.10	0.19						
Variance		**2%**			**21%**	**20%**	**16%**	**20%**	**16%**	**26%**						

Table 8.18: Flotation time - recovery data for Test 1 on the 80%-106µm grind.

				Grade							Recovery					
Products	Time	Mass	Mass	Pt	Pd	Au	3E	Pt/Pd	Cu	Ni	Pt	Pd	Au	3E	Cu	Ni
	(min)	(g)	%	g/t	g/t	g/t	g/t		%	%	%	%	%	%	%	%
RC1	1	41.78	2.10	9.80	13.80	1.88	**25.48**	**0.71**	1.50	2.81	40.31	40.17	27.16	38.85	37.80	36.38
RC2	2	72.98	3.67	2.45	4.96	0.28	**7.69**	**0.49**	0.10	0.80	17.60	25.22	7.07	20.48	4.40	18.18
RC3	4	68.86	3.46	1.14	1.53	0.12	**2.79**	**0.75**	0.08	0.77	7.73	7.34	2.86	7.01	3.32	16.54
RC4	13	56.95	2.86	0.73	1.03	0.10	**1.86**	**0.71**	0.05	0.10	4.09	4.09	1.97	3.87	1.72	1.77
RC5	10	129.17	6.49	0.75	0.82	0.11	**1.68**	**0.91**	0.05	0.05	9.54	7.38	4.91	7.92	3.90	2.00
RT		1620.00	81.42	0.13	0.14	0.10	**0.37**	**0.93**	0.05	0.05	20.73	15.80	56.03	21.87	48.86	25.12
Head (calc.)		**1989.74**	**100.00**	**0.51**	**0.72**	**0.15**	**1.38**	**0.71**	**0.08**	**0.16**	**100.00**	**100.00**	**100.00**	**100.00**	**100.00**	**100.00**
Head (meas)		2000.00		0.52	0.70	0.20	1.41	0.74	0.10	0.19						
Variance		**0.01**		**1%**	**4%**	**25%**	**2%**	**5%**	**14%**	**15%**						

CUMULATIVE RESULTS	Flotation Time [min]	Mass [g]	Mass [%]	Cumulative Grade [g/t]							Cumulative Recovery [%]					
				Pt	Pd	Au	3E	Pt/Pd	Cu	Ni	Pt	Pd	Au	3E	Cu	Ni
RC1	1	41.78	2.10	9.80	13.80	1.88	25.48	0.71	1.50	2.81	40.31	40.17	27.16	38.85	37.80	36.38
RC1+RC2	3	114.76	5.77	5.13	8.18	0.86	14.17	0.57	0.61	1.53	57.91	65.39	34.23	59.33	42.20	54.56
RC1+RC2+RC3	7	183.62	9.23	3.63	5.69	0.58	9.90	0.64	0.41	1.25	65.64	72.73	37.09	66.34	45.53	71.11
RC1+RC2+RC3+RC4	20	240.57	12.09	2.94	4.58	0.47	8.00	0.65	0.33	0.98	69.73	76.82	39.06	70.21	47.25	72.87
RC1+RC2+RC3+RC4+RC5	30	369.74	18.58	2.18	3.27	0.34	5.79	0.75	0.23	0.65	79.27	84.20	43.97	78.13	51.14	74.88
RC1+RC2+RC3+RC4+RC5+RT		1989.74	100.00	0.51	0.72	0.15	1.38	0.89	0.08	0.16	100.00	100.00	100.00	100.00	100.00	100.00

Table 8.19: Flotation time - recovery data for Test 2 on the 80%-106µm grind.

				Grade							Recovery					
Products	Time	Mass	Mass	Pt	Pd	Au	3E	Pt/Pd	Cu	Ni	Pt	Pd	Au	3E	Cu	Ni
	(min)	(g)	(%)	g/t	g/t	g/t	g/t		%	%	%	%	%	%	%	%
RC1	1	38.57	1.94	11.80	14.10	2.11	**28.01**	**0.84**	1.43	2.63	42.97	37.99	27.59	38.78	33.48	22.42
RC2	2	86.35	4.35	2.42	4.84	0.29	**7.55**	**0.50**	0.12	0.83	19.73	29.20	8.49	23.40	6.29	15.88
RC3	4	74.58	3.76	1.05	1.53	0.11	**2.69**	**0.69**	0.10	0.80	7.39	7.97	2.78	7.20	4.53	13.24
RC4	13	65.52	3.30	0.88	0.97	0.11	**1.96**	**0.91**	0.07	0.76	5.44	4.44	2.44	4.61	2.78	11.01
RC5	10	119.90	6.04	0.56	0.70	0.11	**1.37**	**0.80**	0.06	0.75	6.34	5.86	4.47	5.90	4.37	19.77
RT		1600.00	80.61	0.12	0.13	0.10	**0.35**	**0.92**	0.05	0.05	18.13	14.53	54.23	20.10	48.56	17.68
Head (calc.)		**1984.92**	**100.00**	**0.53**	**0.72**	**0.15**	**1.40**	**0.74**	**0.08**	**0.23**	**100.00**	**100.00**	**100.00**	**100.00**	**100.00**	**100.00**
Head (meas)		2000.00		0.52	0.70	0.20	1.41	0.74	0.10	0.19						
Variance		**0.01**		**4%**	**4%**	**24%**	**0%**	**0%**	**14%**	**20%**						

CUMULATIVE RESULTS	Flotation Time [min]	Mass [g]	Mass [%]	Cumulative Grade [g/t]							Cumulative Recovery [%]					
				Pt	Pd	Au	3E	Pt/Pd	Cu	Ni	Pt	Pd	Au	3E	Cu	Ni
RC1	1	38.57	1.94	11.80	14.10	2.11	28.01	0.84	1.43	2.63	42.97	37.99	27.59	38.78	33.48	22.42
RC1+RC2	3	124.92	6.29	5.32	7.70	0.85	13.87	0.60	0.52	1.39	62.70	67.19	36.07	62.19	39.77	38.30
RC1+RC2+RC3	7	199.50	10.05	3.72	5.39	0.57	9.69	0.63	0.37	1.17	70.09	75.16	38.85	69.39	44.29	51.54
RC1+RC2+RC3+RC4	20	265.02	13.35	3.02	4.30	0.46	7.78	0.70	0.29	1.07	75.53	79.60	41.30	74.00	47.08	62.55
RC1+RC2+RC3+RC4+RC5	30	384.92	19.39	2.25	3.18	0.35	5.78	0.73	0.22	0.97	81.87	85.47	45.77	79.90	51.44	82.32
RC1+RC2+RC3+RC4+RC5+RT		1984.92	100.00	0.53	0.72	0.15	1.40	0.89	0.08	0.23	100.00	100.00	100.00	100.00	100.00	100.00

Table 8.20: Flotation time - recovery data for Test 3 on the 80%-106µm grind.

					Grade						Recovery					
Products	Time	Mass	Mass wrt Size	Mass wrt Feed	Pt	Pd	Au	3E	Cu	Ni	Pt	Pd	Au	3E	Cu	Ni
	(min)	(g)	(%)	(%)	g/t	g/t	g/t	g/t	%	%	%	%	%	%	%	%
RC1	1	0.0	0.0	0.00	0.00	0.00	0.00	0.00	0.00	0.00	0.00	0.00	0.00	0.00	0.00	0.00
RC2	2	0.0	0.0	0.00	0.00	0.00	0.00	0.00	0.00	0.00	0.00	0.00	0.00	0.00	0.00	0.00
RC3	4	0.0	0.0	0.00	0.00	0.00	0.00	0.00	0.00	0.00	0.00	0.00	0.00	0.00	0.00	0.00
RC4	13	0.0	0.0	0.00	0.00	0.00	0.00	0.00	0.00	0.00	0.00	0.00	0.00	0.00	0.00	0.00
RC5	10	0.0	0.0	0.00	0.00	0.00	0.00	0.00	0.00	0.00	0.00	0.00	0.00	0.00	0.00	0.00
RT		43.1	100.0	1.13	0.00	0.00	0.00	0.00	0.00	0.00	0.00	0.00	0.00	0.00	0.00	0.00
+150 um		43.1	1.13	1.13	0.00	0.00	0.00	0.00	0.00	0.00	0.00	0.00	0.00	0.00	0.00	0.00
RC1	1	5.4	0.37	0.14	13.57	13.08	2.41	29.06	1.32	0.57	17.87	17.87	17.87	17.87	17.87	2.92
RC2	2	9.5	0.66	0.25	6.13	5.91	1.09	13.12	0.60	0.55	14.19	14.19	14.19	14.19	14.19	5.02
RC3	4	10.1	0.70	0.26	2.84	2.74	0.50	6.08	0.28	0.36	6.99	6.99	6.99	6.99	6.99	3.49
RC4	13	9.5	0.66	0.25	1.36	1.31	0.24	2.91	0.13	0.19	3.15	3.15	3.15	3.15	3.15	1.68
RC5	10	24.7	1.71	0.65	1.53	1.47	0.27	3.28	0.15	0.25	9.21	9.21	9.21	9.21	9.21	5.84
RT		1384.8	95.90	36.31	0.14	0.14	0.03	0.31	0.01	0.06	48.60	48.60	48.60	48.60	48.60	81.06
-150 + 75		1444.0	37.86	37.86	0.28	0.27	0.05	0.61	0.03	0.07	12.75	12.57	11.96	12.60	11.96	16.51
RC1	1	14.2	1.47	0.37	31.45	30.32	5.59	67.37	3.06	2.56	68.19	65.89	58.23	66.21	58.23	28.43
RC2	2	20.4	2.11	0.53	4.60	4.44	0.82	9.86	0.45	1.03	14.34	13.86	12.25	13.93	12.25	16.44
RC3	4	19.9	2.06	0.52	1.87	1.80	0.33	4.01	0.18	0.31	5.69	5.50	4.86	5.52	4.86	4.76
RC4	13	18.9	1.96	0.50	1.42	1.37	0.25	3.05	0.14	0.25	4.11	3.97	3.51	3.99	3.51	3.71
RC5	10	54.9	5.69	1.44	0.72	0.89	0.16	1.77	0.09	0.21	6.00	7.45	6.58	6.71	6.58	8.98
RT		836.3	86.70	21.93	0.01	0.03	0.02	0.06	0.01	0.06	1.66	3.33	14.57	3.63	14.57	37.68
-75 + 38		964.6	25.29	25.29	0.68	0.68	0.14	1.50	0.08	0.13	20.36	20.77	22.37	20.73	22.37	20.18
RC1	1	67.5	4.95	1.77	23.84	22.99	4.24	51.07	2.32	2.27	74.83	74.02	71.50	74.18	71.50	38.21
RC2	2	145.1	10.65	3.80	2.20	2.13	0.39	4.72	0.21	0.84	14.87	14.71	14.21	14.74	14.21	30.32
RC3	4	129.6	9.51	3.40	0.78	0.75	0.14	1.67	0.08	0.27	4.71	4.66	4.50	4.67	4.50	8.82
RC4	13	98.4	7.22	2.58	0.64	0.61	0.11	1.36	0.06	0.20	2.91	2.88	2.78	2.89	2.78	4.79
RC5	10	176.3	12.94	4.62	0.27	0.34	0.06	0.68	0.03	0.13	2.24	2.85	2.75	2.56	2.75	5.67
RT		745.4	54.72	19.54	0.01	0.03	0.02	0.06	0.01	0.07	0.43	0.89	4.25	0.97	4.25	12.19
-38		1362.3	35.72	35.72	1.58	1.54	0.29	3.41	0.16	0.29	66.88	66.66	65.67	66.67	65.67	63.31
Head (calc.)		**3814.0**	**100.0**	**100.0**	**0.84**	**0.82**	**0.16**	**1.83**	**0.09**	**0.17**	**100.00**	**100.00**	**100.00**	**100.00**	**100.00**	**100.00**
Head (meas)		4000.0			0.99	0.96	0.18	2.12	0.10	0.19						
Variance		**5%**			**15%**	**14%**	**9%**	**14%**	**9%**	**13%**						

Table 8.21: Flotation time - recovery data for Test 1 on the 80%-75µm grind.

				Grade							Recovery					
Products	**Time**	**Mass**	**Mass**	**Pt**	**Pd**	**Au**	**3E**	**Pt/Pd**	**Cu**	**Ni**	**Pt**	**Pd**	**Au**	**3E**	**Cu**	**Ni**
	(min)	**(g)**	**(%)**	**g/t**	**g/t**	**g/t**	**g/t**		**%**	**%**	**%**	**%**	**%**	**%**	**%**	**%**
RC1	1	58.87	2.93	9.05	12.70	2.00	**23.75**	**0.71**	1.20	1.78	47.30	49.63	35.94	47.23	40.20	34.05
RC2	2	84.39	4.19	2.13	4.11	0.24	**6.48**	**0.52**	0.10	0.21	15.96	23.02	6.18	18.47	4.80	5.72
RC3	4	70.98	3.53	0.98	1.50	0.11	**2.59**	**0.65**	0.07	0.17	6.18	7.07	2.38	6.21	2.87	3.86
RC4	13	61.40	3.05	0.71	0.89	0.11	**1.71**	**0.80**	0.06	0.14	3.87	3.63	2.06	3.55	1.92	2.88
RC5	10	140.50	6.98	0.55	0.65	0.11	**1.31**	**0.85**	0.06	0.15	6.86	6.06	4.72	6.22	4.80	6.92
RT		1596.00	79.32	0.14	0.10	0.10	**0.34**	**1.40**	0.05	0.09	19.84	10.59	48.72	18.33	45.41	46.57
Head (calc.)		**2012.1**	**100.00**	**0.56**	**0.75**	**0.16**	**1.47**	**0.75**	**0.09**	**0.15**	**100.00**	**100.00**	**100.00**	**100.00**	**100.00**	**100.00**
Head (meas)		2000.0		0.52	0.70	0.20	1.41	0.74	0.10	0.19						
Variance		**1%**		**9%**	**8%**	**17%**	**5%**	**1%**	**9%**	**19%**						

CUMULATIVE RESULTS	**Flotation Time [min]**	**Mass [g]**	**Mass [%]**	**Cumulative Grade [g/t]**							**Cumulative Recovery [%]**					
				Pt	**Pd**	**Au**	**3E**	**Pt/Pd**	**Cu**	**Ni**	**Pt**	**Pd**	**Au**	**3E**	**Cu**	**Ni**
RC1	1	58.87	2.93	9.05	12.70	2.00	23.75	0.71	1.20	1.78	47.30	49.63	35.94	47.23	40.20	34.05
RC1+RC2	3	143.26	7.12	4.97	7.64	0.96	13.58	0.60	0.55	0.86	63.26	72.65	42.12	65.70	45.00	39.77
RC1+RC2+RC3	7	214.24	10.65	3.65	5.61	0.68	9.94	0.62	0.39	0.63	69.43	79.72	44.50	71.91	47.87	43.63
RC1+RC2+RC3+RC4	20	275.64	13.70	3.00	4.56	0.55	8.10	0.66	0.32	0.52	73.30	83.34	46.57	75.45	49.79	46.51
RC1+RC2+RC3+RC4+RC5	30	416.14	20.68	2.17	3.24	0.40	5.81	0.72	0.23	0.40	80.16	89.41	51.28	81.67	54.59	53.43
RC1+RC2+RC3+RC4+RC5+RT		2012.14	100.00	0.56	0.75	0.16	1.47	1.26	0.09	0.15	100.00	100.00	100.00	100.00	100.00	100.00

Table 8.22: Flotation time - recovery data for Test 2 on the 80%-75µm grind.

				Grade							Recovery					
Products	**Time**	**Mass**	**Mass**	**Pt**	**Pd**	**Au**	**3E**	**Pt/Pd**	**Cu**	**Ni**	**Pt**	**Pd**	**Au**	**3E**	**Cu**	**Ni**
	(min)	**(g)**	**(%)**	**g/t**	**g/t**	**g/t**	**g/t**		**%**	**%**	**%**	**%**	**%**	**%**	**%**	**%**
RC1	1	46.28	2.32	10.50	13.30	1.93	**25.73**	**0.79**	1.02	1.87	47.45	41.89	29.80	42.63	27.54	22.00
RC2	2	95.60	4.79	2.01	4.26	0.27	**6.54**	**0.47**	0.11	0.22	18.76	27.72	8.61	22.38	6.13	5.43
RC3	4	70.99	3.56	0.79	1.34	0.11	**2.24**	**0.59**	0.09	0.19	5.48	6.47	2.60	5.69	3.72	3.52
RC4	13	63.75	3.20	0.59	0.84	0.10	**1.53**	**0.70**	0.07	0.17	3.67	3.64	2.13	3.49	2.60	2.70
RC5	10	125.14	6.28	0.49	0.60	0.09	**1.18**	**0.82**	0.06	0.15	5.99	5.11	3.76	5.29	4.37	4.84
RT		1592.00	79.85	0.12	0.14	0.10	**0.36**	**0.86**	0.06	0.15	18.65	15.17	53.11	20.52	55.64	61.52
Head (calc.)		**1993.76**	**100.00**	**0.51**	**0.74**	**0.15**	**1.40**	**0.70**	**0.09**	**0.20**	**100.00**	**100.00**	**100.00**	**100.00**	**100.00**	**100.00**
Head (meas)		2000.00		0.52	0.70	0.20	1.41	0.74	0.10	0.19						
Variance		**0%**		**0%**	**6%**	**23%**	**0%**	**6%**	**11%**	**4%**						

CUMULATIVE RESULTS	**Flotation Time [min]**	**Mass [g]**	**Mass [%]**	**Cumulative Grade [g/t]**							**Cumulative Recovery [%]**					
				Pt	**Pd**	**Au**	**3E**	**Pt/Pd**	**Cu**	**Ni**	**Pt**	**Pd**	**Au**	**3E**	**Cu**	**Ni**
RC1	1	46.28	2.32	10.50	13.30	1.93	25.73	0.79	1.02	1.87	47.45	41.89	29.80	42.63	27.54	22.00
RC1+RC2	3	141.88	7.12	4.78	7.21	0.81	12.80	0.58	0.41	0.76	66.21	69.60	38.41	65.01	33.67	27.43
RC1+RC2+RC3	7	212.87	10.68	3.45	5.25	0.58	9.28	0.58	0.30	0.57	71.69	76.08	41.01	70.70	37.39	30.95
RC1+RC2+RC3+RC4	20	276.62	13.87	2.79	4.23	0.47	7.49	0.61	0.25	0.48	75.36	79.72	43.14	74.20	39.99	33.65
RC1+RC2+RC3+RC4+RC5	30	401.76	20.15	2.07	3.10	0.35	5.53	0.67	0.19	0.38	81.35	84.83	46.89	79.48	44.36	38.48
RC1+RC2+RC3+RC4+RC5+RT		1993.76	100.00	0.51	0.74	0.15	1.40	0.82	0.09	0.20	100.00	100.00	100.00	100.00	100.00	100.00

Table 8.23: Flotation time - recovery data for Test 3 on the 80%-75µm grind.

					Grade						Recovery					
Products	**Time**	**Mass**	**Mass wrt Size**	**Mass wrt Feed**	**Pt**	**Pd**	**Au**	**3E**	**Cu**	**Ni**	**Pt**	**Pd**	**Au**	**3E**	**Cu**	**Ni**
	(min)	**(g)**	**(%)**	**(%)**	**g/t**	**g/t**	**g/t**	**g/t**	**%**	**%**	**%**	**%**	**%**	**%**	**%**	**%**
RC1	1	0.0	0.0	0.00	0.00	0.00	0.00	0.00	0.00	0.00	0.00	0.00	0.00	0.00	0.00	0.00
RC2	2	0.0	0.0	0.00	0.00	0.00	0.00	0.00	0.00	0.00	0.00	0.00	0.00	0.00	0.00	0.00
RC3	4	0.0	0.0	0.00	0.00	0.00	0.00	0.00	0.00	0.00	0.00	0.00	0.00	0.00	0.00	0.00
RC4	13	0.0	0.0	0.00	0.00	0.00	0.00	0.00	0.00	0.00	0.00	0.00	0.00	0.00	0.00	0.00
RC5	10	0.0	0.0	0.00	0.00	0.00	0.00	0.00	0.00	0.00	0.00	0.00	0.00	0.00	0.00	0.00
RT		0.0	0.0	0.00	0.00	0.00	0.00	0.00	0.00	0.00	0.00	0.00	0.00	0.00	0.00	0.00
+150 um		0.0	0.00	0.00	0.00	0.00	0.00	0.00	0.00	0.00	0.00	0.00	0.00	0.00	0.00	0.00
RC1	1	6.7	0.74	0.17	16.75	16.15	2.98	35.89	1.63	0.63	29.28	29.26	29.19	29.26	29.25	5.91
RC2	2	9.6	1.06	0.25	4.30	4.14	0.76	9.20	0.42	0.42	10.76	10.75	10.72	10.75	10.75	5.66
RC3	4	8.2	0.91	0.21	2.25	2.17	0.40	4.83	0.22	0.31	4.82	4.82	4.81	4.82	4.82	3.53
RC4	13	7.3	0.81	0.19	1.86	1.79	0.33	3.98	0.18	0.27	3.53	3.53	3.52	3.53	3.53	2.75
RC5	10	16.8	1.86	0.44	1.53	1.48	0.27	3.28	0.15	0.25	6.70	6.70	6.68	6.70	6.70	5.85
RT		856.5	94.63	22.22	0.20	0.19	0.04	0.43	0.02	0.06	44.91	44.93	45.08	44.93	44.96	76.31
-150 + 75		905.1	23.48	23.48	0.42	0.41	0.08	0.91	0.04	0.08	19.00	18.22	15.54	18.31	15.52	15.62
RC1	1	17.7	1.71	0.46	5.97	5.76	1.06	12.79	0.58	0.58	44.34	40.54	27.52	40.57	27.52	22.08
RC2	2	28.9	2.80	0.75	1.74	1.68	0.31	3.73	0.17	0.32	21.14	19.32	13.12	19.34	13.12	19.64
RC3	4	23.5	2.28	0.61	1.29	1.25	0.23	2.77	0.13	0.25	12.77	11.67	7.92	11.68	7.92	12.34
RC4	13	18.8	1.82	0.49	0.79	0.76	0.14	1.69	0.08	0.14	6.23	5.70	3.87	5.70	3.87	5.64
RC5	10	38.6	3.74	1.00	0.57	0.70	0.13	1.40	0.07	0.12	9.21	10.82	7.35	9.71	7.35	9.56
RT		905.3	87.65	23.48	0.02	0.03	0.03	0.08	0.02	0.02	6.31	11.96	40.22	13.00	40.22	30.74
-75 + 38		1032.8	26.79	26.79	0.23	0.24	0.07	0.54	0.04	0.05	11.81	12.39	15.52	12.44	15.53	10.31
RC1	1	84.7	4.42	2.20	7.94	7.66	1.41	17.02	0.77	0.94	48.18	46.08	39.46	46.38	39.46	23.55
RC2	2	178.4	9.30	4.63	2.15	2.07	0.38	4.61	0.21	0.54	27.46	26.27	22.49	26.44	22.49	28.70
RC3	4	137.2	7.16	3.56	0.95	0.92	0.17	2.04	0.09	0.28	9.37	8.96	7.67	9.02	7.67	11.27
RC4	13	111.6	5.82	2.89	0.61	0.59	0.11	1.31	0.06	0.15	4.89	4.67	4.00	4.70	4.00	4.90
RC5	10	176.8	9.22	4.59	0.63	0.78	0.14	1.55	0.08	0.13	7.96	9.78	8.38	8.83	8.38	7.03
RT		1228.7	64.08	31.87	0.02	0.05	0.04	0.12	0.02	0.07	2.14	4.24	18.00	4.64	18.00	24.55
-38		1917.4	49.73	49.73	0.73	0.73	0.16	1.62	0.09	0.18	69.20	69.39	68.93	69.26	68.95	74.07
Head (calc.)		**3855.3**	**100.0**	**100.0**	**0.52**	**0.53**	**0.11**	**1.16**	**0.06**	**0.12**	**100.00**	**100.00**	**100.00**	**100.00**	**100.00**	**100.00**
Head (meas)		4000.0			0.52	0.70	0.20	1.41	0.10	0.19						
Variance		**4%**			**2%**	**24%**	**41%**	**17%**	**35%**	**38%**						

Table 8.24: Flotation time - recovery data for Test 1 on the 80%-53µm grind.

				Grade							Recovery					
Products	**Time**	**Mass**	**Mass**	**Pt**	**Pd**	**Au**	**3E**	**Pt/Pd**	**Cu**	**Ni**	**Pt**	**Pd**	**Au**	**3E**	**Cu**	**Ni**
	(min)	**(g)**	**(%)**	**g/t**	**g/t**	**g/t**	**g/t**		**%**	**%**	**%**	**%**	**%**	**%**	**%**	**%**
RC1	1	59.86	3.01	23.20	23.60	2.99	**49.79**	**0.98**	2.26	4.13	85.90	78.30	75.72	81.49	85.73	85.73
RC2	2	105.37	5.30	1.36	2.20	0.21	**3.77**	**0.62**	0.13	0.24	8.86	12.85	9.36	10.86	8.85	8.85
RC3	4	98.62	4.96	0.50	0.81	0.08	**1.39**	**0.62**	0.05	0.09	3.05	4.43	3.34	3.75	3.04	3.04
RC4	13	62.06	3.12	0.25	0.40	0.07	**0.72**	**0.63**	0.02	0.04	0.96	1.38	1.84	1.22	0.96	0.96
RC5	10	159.90	8.04	0.05	0.25	0.05	**0.33**	**0.12**	0.00	0.01	0.30	2.22	3.38	1.44	0.49	0.49
RT		1503.00	75.57	0.01	0.02	0.02	**0.03**	**1.00**	0.00	0.00	0.93	0.83	6.36	1.23	0.93	0.93
Head (calc.)		**1988.81**	**100.00**	**0.81**	**0.91**	**0.12**	**1.84**	**0.90**	**0.08**	**0.14**	**100.00**	**100.00**	**100.00**	**100.00**	**100.00**	**100.00**
Head (meas)		2000.00		0.99	0.96	0.18	2.12	0.74	0.10	0.19						
Variance		**0.01**		**18%**	**5%**	**33%**	**13%**	**21%**	**18%**	**24%**						
									0.04							

CUMULATIVE RESULTS	**Flotation Time (min)**	**Mass [g]**	**Mass [%]**	**Cumulative Grade [g/t]**							**Cumulative Recovery [%]**					
				Pt	**Pd**	**Au**	**3E**	**Pt/Pd**	**Cu**	**Ni**	**Pt**	**Pd**	**Au**	**3E**	**Cu**	**Ni**
RC1	1	59.86	3.01	23.20	23.60	2.99	49.79	0.98	2.26	4.13	85.90	78.30	75.72	81.49	85.73	85.73
RC1+RC2	3	165.23	8.31	9.27	9.95	1.22	20.44	0.75	0.90	1.65	94.76	91.15	85.08	92.35	94.58	94.58
RC1+RC2+RC3	7	263.85	13.27	5.99	6.54	0.79	13.32	0.70	0.58	1.07	97.81	95.58	88.42	96.10	97.62	97.62
RC1+RC2+RC3+RC4	20	325.91	16.39	4.90	5.37	0.65	10.92	0.69	0.48	0.87	98.77	96.95	90.26	97.32	98.58	98.58
RC1+RC2+RC3+RC4+RC5	30	485.81	24.43	3.30	3.68	0.46	7.44	0.50	0.32	0.59	99.07	99.17	93.64	98.77	99.07	99.07
RC1+RC2+RC3+RC4+RC5+RT		1988.81	100.00	0.81	0.91	0.12	1.84	0.88	0.08	0.14	100.00	100.00	100.00	100.00	100.00	100.00

Table 8.25: Flotation time - recovery data for Test 2 on the 80%-53µm grind.

				Grade							Recovery					
Products	**Time**	**Mass**	**Mass**	**Pt**	**Pd**	**Au**	**3E**	**Pt/Pd**	**Cu**	**Ni**	**Pt**	**Pd**	**Au**	**3E**	**Cu**	**Ni**
	(min)	**(g)**	**(%)**	**g/t**	**g/t**	**g/t**	**g/t**		**%**	**%**	**%**	**%**	**%**	**%**	**%**	**%**
RC1	1	58.10	2.91	21.20	19.20	3.78	**44.18**	**1.10**	2.06	3.77	57.22	43.22	63.93	50.56	57.22	57.22
RC2	2	107.32	5.38	4.19	7.14	0.39	**11.72**	**0.59**	0.41	0.75	20.89	29.69	12.18	24.77	20.89	20.89
RC3	4	80.00	4.01	1.68	2.56	0.18	**4.42**	**0.66**	0.16	0.30	6.24	7.94	4.19	6.96	6.24	6.24
RC4	13	69.72	3.49	0.86	1.16	0.11	**2.13**	**0.74**	0.08	0.15	2.79	3.13	2.23	2.93	2.79	2.79
RC5	10	159.38	7.98	0.59	0.78	0.09	**1.46**	**0.76**	0.06	0.10	4.37	4.82	4.18	4.58	4.37	4.37
RT		1522.00	76.23	0.12	0.19	0.03	**0.34**	**0.63**	0.01	0.02	8.49	11.20	13.29	10.19	8.49	8.49
Head (calc.)		**1996.52**	**100.00**	**1.08**	**1.29**	**0.17**	**2.54**	**0.83**	**0.10**	**0.19**	**100.00**	**100.00**	**100.00**	**100.00**	**100.00**	**100.00**
Head (meas)		2000.00		0.99	0.96	0.18	2.12	0.74	0.10	0.19						
Variance		**0.00**		**9%**	**35%**	**2%**	**20%**	**12%**	**9%**	**1%**						

CUMULATIVE RESULTS	**Flotation Time**	**Mass [g]**	**Mass [%]**	**Cumulative Grade [g/t]**							**Cumulative Recovery [%]**					
				Pt	**Pd**	**Au**	**3E**	**Pt/Pd**	**Cu**	**Ni**	**Pt**	**Pd**	**Au**	**3E**	**Cu**	**Ni**
RC1	1	58.10	2.91	21.20	19.20	3.78	44.18	1.10	2.06	3.77	57.22	43.22	63.93	50.56	57.22	57.22
RC1+RC2	3	165.42	8.29	10.16	11.38	1.58	23.12	0.77	0.99	1.81	78.12	72.91	76.11	75.33	78.12	78.12
RC1+RC2+RC3	7	245.42	12.29	7.40	8.50	1.12	17.02	0.73	0.72	1.32	84.36	80.85	80.30	82.30	84.36	84.36
RC1+RC2+RC3+RC4	20	315.14	15.78	5.95	6.88	0.90	13.73	0.73	0.58	1.06	87.15	83.98	82.53	85.22	87.15	87.15
RC1+RC2+RC3+RC4+RC5	30	474.52	23.77	4.15	4.83	0.63	9.61	0.74	0.40	0.74	91.51	88.80	86.71	89.81	91.51	91.51
RC1+RC2+RC3+RC4+RC5+RT		1996.52	100.00	1.08	1.29	0.17	2.54	0.66	0.10	0.19	100.00	100.00	100.00	100.00	100.00	100.00

Table 8.26: Flotation time - recovery data for Test 3 on the 80%-53µm grind.

					Grade						Recovery					
Products	**Time**	**Mass**	**Mass wrt Size**	**Mass wrt Feed**	**Pt**	**Pd**	**Au**	**3E**	**Cu**	**Ni**	**Pt**	**Pd**	**Au**	**3E**	**Cu**	**Ni**
	(min)	**(g)**	**(%)**	**(%)**	**g/t**	**g/t**	**g/t**	**g/t**	**%**	**%**	**%**	**%**	**%**	**%**	**%**	**%**
RC1	1	0.0	0.0	0.00	0.00	0.00	0.00	0.00	0.00	0.00	0.00	0.00	0.00	0.00	0.00	0.00
RC2	2	0.0	0.0	0.00	0.00	0.00	0.00	0.00	0.00	0.00	0.00	0.00	0.00	0.00	0.00	0.00
RC3	4	0.0	0.0	0.00	0.00	0.00	0.00	0.00	0.00	0.00	0.00	0.00	0.00	0.00	0.00	0.00
RC4	13	0.0	0.0	0.00	0.00	0.00	0.00	0.00	0.00	0.00	0.00	0.00	0.00	0.00	0.00	0.00
RC5	10	0.0	0.0	0.00	0.00	0.00	0.00	0.00	0.00	0.00	0.00	0.00	0.00	0.00	0.00	0.00
RT		0.0	0.0	0.00	0.00	0.00	0.00	0.00	0.00	0.00	0.00	0.00	0.00	0.00	0.00	0.00
+150 um		0.0	0.00	0.00	0.00	0.00	0.00	0.00	0.00	0.00	0.00	0.00	0.00	0.00	0.00	0.00
RC1	1	0.0	0.00	0.00	0.00	0.00	0.00	0.00	0.00	0.00	0.00	0.00	0.00	0.00	0.00	0.00
RC2	2	0.0	0.00	0.00	0.00	0.00	0.00	0.00	0.00	0.00	0.00	0.00	0.00	0.00	0.00	0.00
RC3	4	0.0	0.00	0.00	0.00	0.00	0.00	0.00	0.00	0.00	0.00	0.00	0.00	0.00	0.00	0.00
RC4	13	0.0	0.00	0.00	0.00	0.00	0.00	0.00	0.00	0.00	0.00	0.00	0.00	0.00	0.00	0.00
RC5	10	0.0	0.00	0.00	0.00	0.00	0.00	0.00	0.00	0.00	0.00	0.00	0.00	0.00	0.00	0.00
RT		30.5	100.00	0.80	0.03	0.05	0.05	0.13	0.03	0.09	100.00	100.00	100.00	100.00	100.00	100.00
-150 + 75		30.5	0.80	0.80	0.03	0.05	0.05	0.13	0.03	0.09	0.03	0.06	0.26	0.07	0.26	0.51
RC1	1	43.3	4.86	1.13	5.97	5.76	1.06	12.79	0.58	0.58	63.02	59.84	48.80	60.12	48.80	40.19
RC2	2	45.8	5.14	1.20	1.74	1.68	0.31	3.73	0.17	0.32	19.46	18.48	15.07	18.56	15.07	23.15
RC3	4	10.7	1.20	0.28	1.29	1.25	0.23	2.77	0.13	0.25	3.38	3.21	2.62	3.22	2.62	4.18
RC4	13	18.2	2.04	0.48	0.79	0.76	0.14	1.69	0.08	0.14	3.51	3.33	2.72	3.34	2.72	4.06
RC5	10	55.8	6.26	1.46	0.57	0.70	0.13	1.40	0.07	0.12	7.74	9.44	7.70	8.50	7.70	10.29
RT		717.4	80.50	18.78	0.02	0.03	0.03	0.08	0.02	0.02	2.90	5.72	23.10	6.24	23.10	18.13
-75 + 38		891.2	23.33	23.33	0.46	0.47	0.11	1.03	0.06	0.07	16.11	16.21	16.57	16.20	16.57	11.97
RC1	1	192.2	6.63	5.03	7.94	7.66	1.41	17.02	0.77	0.94	71.49	68.42	57.43	68.71	57.43	39.07
RC2	2	118.9	4.10	3.11	2.15	2.07	0.38	4.61	0.21	0.54	11.97	11.45	9.61	11.50	9.61	13.98
RC3	4	73.7	2.54	1.93	0.95	0.92	0.17	2.04	0.09	0.28	3.29	3.15	2.64	3.16	2.64	4.43
RC4	13	147.0	5.07	3.85	0.61	0.59	0.11	1.31	0.06	0.15	4.21	4.03	3.38	4.04	3.38	4.72
RC5	10	224.2	7.74	5.87	0.63	0.78	0.14	1.55	0.08	0.13	6.60	8.12	6.81	7.31	6.81	6.52
RT		2141.6	73.91	56.07	0.02	0.05	0.04	0.12	0.02	0.07	2.44	4.84	20.12	5.28	20.12	31.29
-38		2897.6	75.87	75.87	0.74	0.74	0.16	1.64	0.09	0.16	83.86	83.73	83.17	83.73	83.17	87.51
Head (calc.)		**3819.4**	**100.0**	**100.0**	**0.67**	**0.67**	**0.15**	**1.49**	**0.08**	**0.14**	**100.00**	**100.00**	**100.00**	**100.00**	**100.00**	**100.00**
Head (meas)		4000.0			0.52	0.70	0.20	1.41	0.10	0.19						
Variance		**5%**			**29%**	**3%**	**24%**	**6%**	**16%**	**28%**						

Table 8.27: Flotation time - recovery data for Test 1 on the 80%-38µm grind.

				Grade							Recovery					
Products	**Time**	**Mass**	**Mass**	**Pt**	**Pd**	**Au**	**3E**	**Pt/Pd**	**Cu**	**Ni**	**Pt**	**Pd**	**Au**	**3E**	**Cu**	**Ni**
	(min)	**(g)**	**(%)**	**g/t**	**g/t**	**g/t**	**g/t**		**%**	**%**	**%**	**%**	**%**	**%**	**%**	**%**
RC1	1	57.26	2.85	2.84	3.69	0.19	**26.72**	**0.94**	0.28	0.51	46.03	43.69	3.88	41.67	8.07	8.07
RC2	2	150.91	7.51	4.62	7.09	1.50	**7.15**	**0.88**	0.45	0.82	24.94	25.32	80.71	29.39	34.60	34.60
RC3	4	107.14	5.33	2.24	2.73	0.13	**5.10**	**0.82**	0.22	0.40	15.03	16.30	4.97	14.88	11.91	11.91
RC4	13	87.57	4.36	1.05	1.18	0.07	**2.30**	**0.89**	0.10	0.19	5.76	5.76	2.19	5.49	4.56	4.56
RC5	10	177.45	8.83	0.50	0.50	0.05	**1.05**	**1.00**	0.05	0.09	5.56	4.95	3.16	5.07	4.40	4.40
RT		1429.00	71.12	0.03	0.05	0.01	**0.09**	**0.60**	0.05	0.09	2.68	3.98	5.10	3.50	36.45	36.45
Head (calc.)		**2009.33**	**100.00**	**0.79**	**0.89**	**0.14**	**1.83**	**0.89**	**0.10**	**0.18**	**100.00**	**100.00**	**100.00**	**100.00**	**100.00**	**100.00**
Head (meas)		2000.00		0.99	0.96	0.18	2.12	0.74	0.10	0.19						
Variance		**0.00**		**20%**	**7%**	**21%**	**14%**	**20%**	**1%**	**6%**						

CUMULATIVE RESULTS	**Flotation Time [min]**	**Mass [g]**	**Mass [%]**	**Cumulative Grade [g/t]**							**Cumulative Recovery [%]**					
				Pt	**Pd**	**Au**	**3E**	**Pt/Pd**	**Cu**	**Ni**	**Pt**	**Pd**	**Au**	**3E**	**Cu**	**Ni**
RC1	1	57.26	2.85	12.84	13.69	0.19	26.72	0.94	0.28	0.51	46.03	43.69	3.88	41.67	8.07	8.07
RC1+RC2	3	208.17	10.36	5.45	5.95	1.14	12.53	0.89	0.40	0.73	70.98	69.01	84.59	71.06	42.68	42.68
RC1+RC2+RC3	7	315.31	15.69	4.36	4.85	0.80	10.01	0.87	0.34	0.62	86.00	85.31	89.56	85.94	54.59	54.59
RC1+RC2+RC3+RC4	20	402.88	20.05	3.64	4.06	0.64	8.33	0.87	0.29	0.53	91.76	91.07	91.74	91.42	59.15	59.15
RC1+RC2+RC3+RC4+RC5	30	580.33	28.88	2.68	2.97	0.46	6.11	0.91	0.21	0.39	97.32	96.02	94.90	96.50	63.55	63.55
RC1+RC2+RC3+RC4+RC5+RT		2009.33	100.00	0.79	0.89	0.14	1.83	0.69	0.10	0.18	100.00	100.00	100.00	100.00	100.00	100.00

Table 8.28: Flotation time - recovery data for Test 2 on the 80%-38µm grind.

				Grade							Recovery					
Products	**Time**	**Mass**	**Mass**	**Pt**	**Pd**	**Au**	**3E**	**Pt/Pd**	**Cu**	**Ni**	**Pt**	**Pd**	**Au**	**3E**	**Cu**	**Ni**
	(min)	**(g)**	**(%)**	**g/t**	**g/t**	**g/t**	**g/t**		**%**	**%**	**%**	**%**	**%**	**%**	**%**	**%**
RC1	1	87.54	4.37	12.50	15.20	1.84	**29.54**	**0.82**	1.22	2.22	53.10	51.22	59.25	52.45	53.10	53.10
RC2	2	110.94	5.54	5.39	7.46	0.33	**13.18**	**0.72**	0.52	0.96	29.02	31.86	13.47	29.65	29.02	29.02
RC3	4	76.00	3.79	1.64	2.48	0.13	**4.25**	**0.66**	0.16	0.29	6.05	7.25	3.63	6.55	6.05	6.05
RC4	13	70.29	3.51	1.10	1.42	0.12	**2.64**	**0.77**	0.11	0.20	3.75	3.84	3.10	3.76	3.75	3.75
RC5	10	204.10	10.19	0.46	0.60	0.06	**1.12**	**0.77**	0.04	0.08	4.56	4.71	4.50	4.64	4.56	4.56
RT		1454.00	72.60	0.05	0.02	0.03	**0.10**	**2.50**	0.00	0.01	3.53	1.12	16.04	2.95	3.53	3.53
Head (calc.)		**2002.87**	**100.00**	**1.03**	**1.30**	**0.14**	**2.46**	**0.79**	**0.10**	**0.18**	**100.00**	**100.00**	**100.00**	**100.00**	**100.00**	**100.00**
Head (meas)		2000.00		0.99	0.96	0.18	2.12	0.74	0.10	0.19						
Variance		**0.00**		**4%**	**36%**	**23%**	**16%**	**7%**	**4%**	**4%**						

CUMULATIVE RESULTS	**Flotation Time [min]**	**Mass [g]**	**Mass [%]**	**Cumulative Grade [g/t]**							**Cumulative Recovery [%]**					
				Pt	**Pd**	**Au**	**3E**	**Pt/Pd**	**Cu**	**Ni**	**Pt**	**Pd**	**Au**	**3E**	**Cu**	**Ni**
RC1	1	87.54	4.37	12.50	15.20	1.84	29.54	0.82	1.22	2.22	53.10	51.22	59.25	52.45	53.10	53.10
RC1+RC2	3	198.48	9.91	8.53	10.87	1.00	20.40	0.77	0.83	1.52	82.12	83.07	72.71	82.10	82.12	82.12
RC1+RC2+RC3	7	274.48	13.70	6.62	8.55	0.76	15.93	0.74	0.64	1.18	88.16	90.33	76.35	88.65	88.16	88.16
RC1+RC2+RC3+RC4	20	344.77	17.21	5.49	7.10	0.63	13.22	0.75	0.53	0.98	91.92	94.17	79.45	92.41	91.92	91.92
RC1+RC2+RC3+RC4+RC5	30	548.87	27.40	3.62	4.68	0.42	8.72	0.75	0.35	0.64	96.47	98.88	83.96	97.05	96.47	96.47
RC1+RC2+RC3+RC4+RC5+RT		2002.87	100.00	1.03	1.30	0.14	2.46	2.02	0.10	0.18	100.00	100.00	100.00	100.00	100.00	100.00

Table 8.29: Flotation time - recovery data for Test 3 on the 80%-38µm grind.

					Grade						Recovery					
Products	**Time**	**Mass**	**Mass wrt Size**	**Mass wrt Feed**	**Pt**	**Pd**	**Au**	**3E**	**Cu**	**Ni**	**Pt**	**Pd**	**Au**	**3E**	**Cu**	**Ni**
	(min)	**(g)**	**(%)**	**(%)**	**g/t**	**g/t**	**g/t**	**g/t**	**%**	**%**	**%**	**%**	**%**	**%**	**%**	**%**
RC1	1	0.0	0.0	0.00	0.00	0.00	0.00	0.00	0.00	0.00	0.00	0.00	0.00	0.00	0.00	0.00
RC2	2	0.0	0.0	0.00	0.00	0.00	0.00	0.00	0.00	0.00	0.00	0.00	0.00	0.00	0.00	0.00
RC3	4	0.0	0.0	0.00	0.00	0.00	0.00	0.00	0.00	0.00	0.00	0.00	0.00	0.00	0.00	0.00
RC4	13	0.0	0.0	0.00	0.00	0.00	0.00	0.00	0.00	0.00	0.00	0.00	0.00	0.00	0.00	0.00
RC5	10	0.0	0.0	0.00	0.00	0.00	0.00	0.00	0.00	0.00	0.00	0.00	0.00	0.00	0.00	0.00
RT		0.0	0.0	0.00	0.00	0.00	0.00	0.00	0.00	0.00	0.00	0.00	0.00	0.00	0.00	0.00
+150 um		0.00	0.00	0.00	0.00	0.00	0.00	0.00	0.00	0.00	0.00	0.00	0.00	0.00	0.00	0.00
RC1	1	0.0	0.00	0.00	0.00	0.00	0.00	0.00	0.00	0.00	0.00	0.00	0.00	0.00	0.00	0.00
RC2	2	0.0	0.00	0.00	0.00	0.00	0.00	0.00	0.00	0.00	0.00	0.00	0.00	0.00	0.00	0.00
RC3	4	0.0	0.00	0.00	0.00	0.00	0.00	0.00	0.00	0.00	0.00	0.00	0.00	0.00	0.00	0.00
RC4	13	0.0	0.00	0.00	0.00	0.00	0.00	0.00	0.00	0.00	0.00	0.00	0.00	0.00	0.00	0.00
RC5	10	0.0	0.00	0.00	0.00	0.00	0.00	0.00	0.00	0.00	0.00	0.00	0.00	0.00	0.00	0.00
RT		9.1	100.00	0.23	0.04	0.08	0.07	0.19	0.04	0.07	100.00	100.00	100.00	100.00	100.00	100.00
-150 + 75		9.09	0.23	0.23	0.04	0.08	0.07	0.19	0.04	0.07	0.01	0.02	0.10	0.03	0.10	0.10
RC1	1	8.2	1.53	0.21	8.12	7.83	1.44	17.39	0.79	0.44	47.82	43.65	29.19	43.63	29.19	7.73
RC2	2	13.6	2.54	0.35	2.16	2.08	0.38	4.62	0.21	0.50	21.08	19.24	12.87	19.24	12.87	14.57
RC3	4	9.4	1.75	0.24	1.23	1.19	0.22	2.64	0.12	0.32	8.33	7.60	5.08	7.60	5.08	6.44
RC4	13	14.6	2.72	0.37	0.72	0.69	0.13	1.54	0.07	0.14	7.54	6.89	4.61	6.88	4.61	4.38
RC5	10	30.0	5.60	0.76	0.40	0.50	0.09	0.99	0.05	0.12	8.62	10.11	6.76	9.06	6.76	7.71
RT		460.3	85.86	11.73	0.02	0.04	0.04	0.10	0.02	0.06	6.61	12.52	41.49	13.60	41.49	59.17
-75 + 38		536.07	13.66	13.66	0.26	0.27	0.08	0.61	0.04	0.09	4.37	4.66	6.12	4.66	6.12	7.42
RC1	1	171.0	5.06	4.36	12.33	11.89	2.19	26.42	1.20	0.93	69.21	67.52	60.36	67.62	60.36	27.35
RC2	2	272.0	8.05	6.93	1.95	1.88	0.35	4.18	0.19	0.62	17.43	17.00	15.20	17.03	15.20	29.00
RC3	4	167.0	4.94	4.25	0.82	0.79	0.15	1.76	0.08	0.31	4.51	4.40	3.93	4.40	3.93	8.90
RC4	13	206.0	6.09	5.25	0.62	0.59	0.11	1.32	0.06	0.16	4.17	4.07	3.64	4.07	3.64	5.67
RC5	10	305.0	9.02	7.77	0.32	0.40	0.07	0.79	0.04	0.11	3.20	4.01	3.59	3.60	3.59	5.77
RT		2259.4	66.84	57.56	0.02	0.04	0.04	0.10	0.02	0.06	1.48	3.00	13.29	3.27	13.29	23.31
-38		3380.39	86.11	86.11	0.90	0.89	0.18	1.98	0.10	0.17	95.62	95.32	93.78	95.31	93.78	92.48
Head (calc.)		**3925.5**	**100.0**	**100.0**	**0.81**	**0.80**	**0.17**	**1.79**	**0.09**	**0.16**	**100.00**	**100.00**	**100.00**	**100.00**	**100.00**	**100.00**
Head (meas)		4000.0				0.96	0.18	2.12	0.10	0.19						
Variance		**2%**			**#VALUE!**	**16%**	**4%**	**16%**	**4%**	**16%**						